NTNU

Norwegian University of
Science and Technology

Pressure Pulsation and Stresses in a Francis Turbine Operating at Variable Speed

Daniel Braathen Sannes

Master of Science in Mechanical Engineering
Submission date: June 2018
Supervisor: Ole Gunnar Dahlhaug, EPT
Co-supervisor: Igor Iliev, EPT
Einar Agnalt, EPT

Norwegian University of Science and Technology
Department of Energy and Process Engineering

NTNU
Norwegian University
of Science and Technology

Department of Energy
and Process Engineering

EPT-M-2018-76

MASTER THESIS

for

Student Daniel Sannes

Spring 2018

Pressure pulsations in a Francis turbine

Trykkpulsasjoner i en Francis turbin

Background

The average age of Norwegian hydropower plants is 45 years, and many show sign of fatigue and needs to be constantly maintained or refurbished. Additionally, some power plants in Norway has experienced failures on new Francis runners. The main problem is the formation of cracks in the turbine runner.

The main challenges for the numerical analysis of the Fluid-Structure Interaction (FSI) on high head Francis turbines originates in the natural frequency of the turbine runner and the fluid properties of the existing pressure oscillations.

Researchers in the Waterpower Laboratory at the Norwegian University of Science and Technology (NTNU), designed their own high head Francis turbine and published both geometry and model performance data in order to provide other researchers with a relevant case to work with and to promote the Francis-99 workshops. The Francis-99 workshops aim to determine the state of the art of high head Francis turbine simulations (flow and structure) under steady and transient operating conditions as well as promote their development and knowledge dissemination openly.

One of the challenges in this work is to correlate the pressure pulsations with the fatigue loads of the turbine. This would be very interesting data for variable speed operation.

Objective

Find the operating range for the Francis-99 turbine with variable speed which give the lowest material stresses in the turbine runner.

The following tasks are to be considered:

1. Literature study
   a. Pressure pulsations of a Francis turbine
   b. Fatigue loads on a Francis turbine
2. Software knowledge
   a. Labview will be used for the measurements
   b. Matlab will be used for the evaluation of the measurements
   c. ANSYS can be used for stress analysis
3. Laboratory preparations
   a. Dynamic and static calibration of the instruments used in the test rig.
4. Measurements in the Waterpower laboratory:
   a. Complete hill diagram for a Francis-99 turbine.
   b. Pressure pulsation measurements for all operating points of the Francis-99 turbine.
   c. Correlation between pressure measurements and material stress in the turbine runner.
5. If the student will go to Nepal for a excursion, earlier and further work will be presented as a publication and presented at the conference; 8th International symposium on Current Research in Hydraulic Turbines (CRHT-VIII) at Kathmandu University in March 2018.

Within 14 days of receiving the written text on the master thesis, the candidate shall submit a research plan for his project to the department.

When the thesis is evaluated, emphasis is put on processing of the results, and that they are presented in tabular and/or graphic form in a clear manner, and that they are analyzed carefully.

The thesis should be formulated as a research report with summary both in English and Norwegian, conclusion, literature references, table of contents etc. During the preparation of the text, the candidate should make an effort to produce a well-structured and easily readable report. In order to ease the evaluation of the thesis, it is important that the cross-references are correct. In the making of the report, strong emphasis should be placed on both a thorough discussion of the results and an orderly presentation.

The candidate is requested to initiate and keep close contact with his/her academic supervisor(s) throughout the working period. The candidate must follow the rules and regulations of NTNU as well as passive directions given by the Department of Energy and Process Engineering.

Risk assessment of the candidate's work shall be carried out according to the department's procedures. The risk assessment must be documented and included as part of the final report. Events related to the candidate's work adversely affecting the health, safety or security, must be documented and included as part of the final report. If the documentation on risk assessment represents a large number of pages, the full version is to be submitted electronically to the supervisor and an excerpt is included in the report.

Pursuant to “Regulations concerning the supplementary provisions to the technology study program/Master of Science” at NTNU §20, the Department reserves the permission to utilize all the results and data for teaching and research purposes as well as in future publications.

The final report is to be submitted digitally in DAIM. An executive summary of the thesis including title, student’s name, supervisor's name, year, department name, and NTNU's logo and name, shall be submitted to the department as a separate pdf file. Based on an agreement with the supervisor, the final report and other material and documents may be given to the supervisor in digital format.

☒ Work to be done in the Waterpower laboratory
☐ Field work

Department of Energy and Process Engineering, 15. January 2017

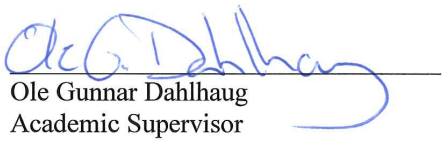

Ole Gunnar Dahlhaug
Academic Supervisor

Co-Supervisors:

- Igor Iliev
- Einar Agnalt

Preface

This Master Thesis is written at the Waterpower Laboratory at the Norwegian University of Science and Technology during the spring of 2018. It has been a fun and interesting semester with a steep learning curve. In addition to writing this thesis, I had the opportunity to travel to Nepal and participate on CRHT-VIII'18 Conference at Kathmandu University and exploring the Himalayas, which I will never forget.

I would like to take this opportunity to thank my supervisor, Ole G. Dahlhaug, who have been helping me throughout my master, and the project-work the previous semester. I also wish to thank my co-supervisors Igor Iliev and Einar Agnalt, who I have had several enlightening conversations with, helped me with my measurement and all of my questions.

I hope you enjoy your reading!

Daniel B. Sannes

Trondheim, June 8, 2018

Abstract

The introduction of new intermittent energy sources on the electrical grid increases the need of regulated power to ensure stability of grid frequency. Hydropower has the unique possibility to deliver both stability and flexibility in energy production. Due to this, turbines is operating tougher, with more starts and stops and operations outside BEP. In addition, there are more fluctuations on the grid and the turbines is experience more dynamical loading, which can increase damages on the turbine structure. Today, the industry is facing problems with both new and old high head Francis units and the main problem is the formation of cracks in the runner due to pressure fluctuations. It is therefore important to develop new methods for reducing dynamical effects and thereby reducing the fatigue load on the Francis runner. In the latest years, the focus on flexibility have increased and turbines with variable speed capabilities of more interest. Variable speed operations gives the opportunity to change the operation pattern and operate at different speeds. The main objective of this work is to find the operating range for the Francis turbine at the Waterpower Laboratory at NTNU, with variable speed, which gives the lowest material stresses.

To approach this objective, measurements of both efficiency and pressure pulsations for the whole operating range of the Francis turbine has been conducted. Peak-peak values from pressure pulsations have been presented in pressure pulsation diagrams, which is inspired by the Hill Chart. One diagram was made for each pressure sensor. By analyzing these diagrams, it is possible to find out where the turbine can be operated in order to minimize the effect of pressure pulsations. Frequency analysis was conducted for a total of eighteen operation points, for synchronous speed and for reduced speed. The guide vane passing frequency was identified as the most significant in the runner for all operation points.

Structure analysis of the turbine runner was conducted in ANSYS Mechanical, to calculate the stresses due to the pressure pulsations. A flow analysis was conducted in order to calculate the pressure distribution that was applied on the runner blades. Stresses was calculated for BEP, PL and ML for synchronous speed and reduced speed. The stresses at synchronous speed was compared to the once were the speed was reduced to investigate the relative change. Stresses was further used in a fatigue assessment, where accumulated damage was calculated. The results are showing that by reducing the speed the stresses are reduced for part load operations. Fatigue assessment showed that by reducing the speed for part load operation, the accumulated damage drastically dropped.

Sammendrag

Innføringen av nye ikke-regulerbare energikilder på el-nettet stiller høyere krav til stabilitet av nettfrekvensen. Vannkraften har den unike egenskapen at den kan tilby både stabilitet og fleksibilitet gjennom høy grad av regulering. Dette gjør at turbinene i dag kjøres tøffere, med hyppigere start og stop og kjøring utenfor beste driftspunkt. Dette resulterer i en økning av dynamisk belastning som kan føre til høyere skadefrekvens på turbinene. Spesielt høytrykks Francis turbinene har utfordringer knyttet til dette, og flere enheter har opplevd driftstekniske problemer. Hovedutfordringen er sprekkdannelse i løpehjulet på grunn av trykkpulsasjoner, og industrien har problemer med både nye og eldre enheter. Det er derfor viktig å utvikle metoder for skadebegrensing. Med dagens økte fokus på fleksibilitet har variabel turtallskjøring blitt sett på som en mulighet for å redusere trykkpulsasjoner og dermed spenningene i løpehjulet. Hovedmålet for denne oppgaven er finne ut hvordan Francis-turbinen ved Vannkraftlaboratoriet ved NTNU kan kjøres, med variabelt turtall, for å redusere spenningene på løpehjulet.

Trykk- og virkningsgradsmålinger av Francis turbinen ble gjennomført for å kartlegge trykk pulsasjoner for hele operasjons området. Peak-peak verdiene til trykk pulsasjonene ble presentert i diagrammer som er inspirert av Hill diagrammet, men istedenfor konstante virkningsgradskurver er det konstante peak-peak kurver. Et diagram ble laget per trykksensor. Ved å analysere disse diagrammene kan man finne ut hvor man kan operere turbinen for å minimere trykk pulsasjoner. Frekvensanalyse ble gjennomført for atten driftspunkter ved synkron hastighet og redusert hastighet. Ledeskovls passeringsfrekvensen ble identifisert som den mest signifikante i løpehjulet for samtlige driftspunkt.

Strukturanalyse av løpehjulet ble gjennomført i ANSYS Mechanical, for å beregne trykk pulsasjons induserte spenninger. En strømningsanalyse ble gjort for å beregne trykk distribusjonen på løpehjuls bladene, bassert på måledata. Spenningene ble beregnet for BEP, PL og ML, for synkron turtall og redusert turtall. Relativ endringen av spenningsamplituder mellom synkron turtal og redusert turtall ble analysert for å se på spenningsendring ved redusering av hastighet. Spenningene ble brukt videre i utmattingsanalyse, der det ble beregnet akkumulert skade. Resulatene viser at spenningene reduseres ved redusert hastighet, spesielt for lavlast kjøring. Utmattingsanalysen viste at ved å redusere hastigheten ved dellast så ble den akkumulerte skaden drastisk redusert.

Contents

1 Introduction **1**
- 1.1 Objective . . . 2
- 1.2 Previous and ongoing work . . . 2

2 Theoretical Background **5**
- 2.1 Pressure pulsations in a Francis turbine . . . 5
  - 2.1.1 Rotor-stator interaction . . . 5
  - 2.1.2 Draft tube pressure pulsations . . . 6
  - 2.1.3 Vortex shedding . . . 7
  - 2.1.4 System dynamics oscillations . . . 8
- 2.2 Hill chart and hydraulic efficiency . . . 8
- 2.3 Variable speed operation . . . 10
- 2.4 Mechanical properties and fatigue assessment . . . 10
  - 2.4.1 Stress and strain . . . 10
  - 2.4.2 Fatigue . . . 11
  - 2.4.3 Fatigue analysis for a Francis runner . . . 14

3 Analysis Methods **17**
- 3.1 Histogram method - Amplitude of pressure pulsations . . . 17
- 3.2 Post processing of measured data . . . 19
  - 3.2.1 Sampling rate . . . 19
  - 3.2.2 Spectral analysis . . . 19
  - 3.2.3 Filtering data . . . 20
- 3.3 Structural analysis . . . 20

4 Experimental Setup, Instruments and Measurements **23**
- 4.1 Francis model test rig . . . 23
- 4.2 Instrumentation . . . 24
- 4.3 Data logging and measurement procedure . . . 26
- 4.4 Calibration . . . 28
- 4.5 Uncertainty . . . 28

5 Structural Analysis **31**
- 5.1 ANSYS Mechanical - Setup and model . . . 31

6 Results **35**
6.1 Experimental results 35
6.2 Structural results and validation 41
6.3 Fatigue assessment 45

7 Discussion **47**
7.1 Experimental measurements 47
7.1.1 Change in pressure pulsation amplitudes 47
7.1.2 Frequency analysis 48
7.2 Structural analysis 50
7.2.1 Known errors 50
7.2.2 Stress results 51
7.3 Fatigue 52

8 Conclusion **55**

9 Further Work **57**

Refrences **58**

Appendix **A1**

A Paper for CRHT-VIII'18 **A1**

B Procedure for calculating pressure distribution on runner blades **B1**

C Start up, shut down and measurements procedure **C1**

D Pressure Pulsation Diagram and Frequency analysis **D1**

E MatLab scripts for calculation **E1**

List of Tables

4.1 Instrumentation and sensors used during measurements 25
4.2 Expanded uncertainties for pressure sensors. Long time stability is estimated based on zero-flow measurements while repeatability is estimated based on BEP measurements. 30
4.3 Expanded uncertainties for the operation sensors. Long time stability is estimated based on zero-flow measurements while repeatability is estimated based on BEP measurements. 30

5.1 Material Properties of JM3 Alloy 32
5.2 Mesh independence test, with TET10-elements. Stress value taken from the suction side of the trailing edge near the hub. 33

6.1 Detailed information on operational points used in further analysis 37
6.2 Peak-peak values for PTDT17, 97% confidence level. The last two columns show the change in value relative to the synchronous speed. All values are in kPa. 37
6.3 Peak-peak values for PTR1, 97% confidence level. The last two columns show the change in value relative to the synchronous speed. All values are in kPa. 37
6.4 Peak-peak values for PTR2, 97% confidence level. The last two columns show the change in value relative to the synchronous speed. All values are in kPa. 38
6.5 Peak-peak values for PTR4, 97% confidence level. The last two columns show the change in value relative to the synchronous speed. All values are in kPa. 38
6.6 Peak-peak values for PTGV4, 97% confidence level. The last two columns show the change in value relative to the synchronous speed. All values are in kPa. 38
6.7 Operation point used in structural analysis 42
6.8 Stress and torque results from structural simulations. Max stress value is from suction side of trailing edge near the hub. $\Delta\sigma_A$ shows the increase in stress when the pressure pulsation effect is added to the mean pressure. Comparing of torque is used for validation. 44
6.9 Curve constants for S-N curves for 13Cr-4Ni, taken from [21]. . . 45

6.10 Stress amplitudes form structural analysis converted to effective stress for stress ratio R=-1, using Goodman method. All values are in MPa. 46
6.11 Accumulated damage per 1000 operation hours. Stress amplitudes from Table 6.10 is used to find the number of cycles to failure. Number of cycles per 1000 operating hours is found based on the guide vane passing frequency. 46

List of Figures

2.1 Velocity field at the runner inlet, [17] 6
2.2 Left: part load vortex rope. Right: high load vortex core [10]. . . . 7
2.3 Illustration of a Hill Chart, taken from IEC60193 [1]. 9
2.4 Stress-strain curve for a typical steel alloy [4]. 11
2.5 S-N curves, for both CAL and VAL, for a typical steel alloy [31]. . 12
2.6 Goodman mean stress correction [6]. 13

3.1 Illustration of the Histogram method, where the peak-peak values is the difference between the upper and lower bound. This results is from sensor PTGV4 at BEP. 18
3.2 Pressure-time data with upper and lower bound. Between the two straight lines is 97% of all pressure data. From sensor PTGV4 at BEP. 18
3.3 Illustration of Welch method with overlapping segments [12]. . . . 20

4.1 Illustration of the open loop system in the laboratory. (1) centrifugal pump, (2) open channel inlet, (3) open channel outlet, (4) upstream pressure tank, (5) flowmeter, (6) generator, (7) Francis turbine, (8) downstream pressure tank, (9) water outlet. 24
4.2 Pressure sensors used for measuring pressure pulsations. Sensors along guide vanes, GV1-GV6, and on-board sensors, R1-R4. . . . 26
4.3 Pressure sensors used for measuring pressure pulsations. On-board sensors, R1-R4, and draft tube sensors DT13 and DT17. . . 26
4.4 Operation point sensors for the Francis rig. 27
4.5 Picture showing the DAQ system. 27

5.1 Mesh quality for the mesh used for all simulations. 33
5.2 1/15 part of the runner. The runner blades is split into segments. Pressure loading and boundary condition is applied at mechanical model. 34

6.1 Hill Chart for the Francis-99 turbine for the whole operating range. 36
6.2 Peak-peak values are normalized based on BEP value (2.29kPa) . 39
6.3 Peak-peak values are normalized based on BEP value (3.67kPa) . 39
6.4 Peak-peak values are normalized based on BEP value (2.37kPa) . 40

6.5 Frequency analysis for PL operation point. Frequency is normalized based on the runner frequency. 40
6.6 Frequency analysis for HL operation point. Frequency is normalized based on the runner frequency. 41
6.7 Stress distribution in the runner at PL operation. It shows that the highest stresses at the inlet is found at the pressure side of the leading edge near the shroud, with a stress value of 3.62MPa. The stress at the pressure side of leading edge near the hub is 1.01MPa. 43
6.8 Stress distribution at the suction side of one full length blade at PL operation. Maximum stress is found in the sharp corner where the blade is not fastened towards the shroud anymore, with a value of 14.67MPa. Because of stress singularity, this value is strongly depended on mesh resolution. The other point with high stresses are at the trailing edge near the hub, with a stress value of 5.13MPa. 44
6.9 S-N curve created in MatLab from the constants in Table 6.9. S-N curve is for a smooth butt weld for 13Cr-4Ni steel. Curves are created with a failure probability of: $P_f \leq 5\%$ 46

Nomenclature

Symbol	Description	Unit
z_r	Number of runner blade	[-]
z_{gv}	Number of guide vanes	[-]
z_p	Number of pole pairs	[-]
n	Rotational speed of the runner	[rpm]
f_n	Runner frequency	[Hz]
f_s	Rheingans frequency	[Hz]
f_{bp}	Blade passing frequency	[Hz]
f_{gv}	Guide vane frequency	[Hz]
f_{sd}	System dynamics oscillations	[Hz]
f_{samp}	Sampling frequency	[Hz]
f_m	Highest frequency of interest	[Hz]
f_{vs}	Vortex shedding frequency	[Hz]
f_{grid}	Grid frequency	[Hz]
v	Water velocity	[m/s]
L	Characteristic length	[m]
a	Speed of sound	[m/s]
ρ_w	Density of water	$[kg/m^3]$
K_w	Bulk modulus of water	[Pa]
D	Diameter	[m]
t	Thickness of pipe	[m]
E	Modulus of elasticity	[Pa]
Re_x	Reynolds number	[-]
D_A	Accumulated damage	[-]
R	Stress ratio	[-]
Q	Volumetric flow	$[m^3/s]$
E_h	Specific hydraulic energy	$[m^2/s^2]$
g	Gravitational constant	$[m/s^2]$
H	Pressure head	[m]
η_h	Hydraulic efficiency	[-]
ω	Angular velocity	[rad/s]
T	Torque	[Nm]
σ	Stress	[Pa]
ϵ	Strain	[-]
ν	Poisson's ratio	[-]
N	Number of cycles	[-]

Abbreviations

Symbol	Description
FFT	Fast Fourier Transform
DFT	Discrete Fourier Transform
RSI	Rotor-Stator Interaction
BEP	Best Efficiency Point
SNL	Speed-No-Load
ML	Minimum Load
PL	Part Load
HL	High Load
FL	Full Load
cdf	Cumulative Density Function
LCF	Low Cycle Fatigue
HCF	High Cycle Fatigue
VHCF	Very High Cycle Fatigue
CAL	Constant Amplitude Loading
VAL	Variable Amplitude Loading
CFD	Computational Fluid Dynamics
FEM	Finite Element Method
FEA	Finite Element Analysis
FSI	Fluid Structure Interactions
DAQ	Data Acquisition
UTS	Ultimate Tensile Strength

Chapter 1

Introduction

The electrical grid is an interconnected network where different energy sources is supplying energy that can be used by consumers. In Norway, 2014, hydropower production contributed with 136.6TWh which is 96% of the total energy production [27], while wind and thermal energy production was covering the rest. Today, intermittent power system, such as wind and solar are growing, which also increases the need for stability of the grid frequency. Hydropower has the unique possibility to deliver both flexibility in energy production together with stability to the grid, and researches from Sintef are saying that hydropower is essential when installing new wind turbines [35]. Hydro turbines uses speed droop as the primary governing of the grid, which enables fast response to changes in grid frequency. Today, there are more fluctuations on the grid and the turbines is experience more dynamical loading due to this, which can increase damages on the turbine structure [38]. Hydropower production companies are more often peaking, which means to produce energy when the electrical price is high. This results in more operation at off-design conditions with more rapid load changes, and flow phenomena such as power swings, rotating vortex rope and stochastic pulsations which can drastically shorten the life of the turbine runner [9].

Today, the industry is facing problems with both new and old Francis runners and the main problem is the formation of cracks in the runner due to pressure fluctuations [13]. Earlier design had higher safety factors, which resulted in thicker turbine runners. Today, runner designs have been improved by using numerical methods together with better steel quality which gives higher hydraulic efficiency and lighter runners. The runner is therefore less stiff, and pressure pulsations can cause larger movements than before which eventually can cause cracks due to fatigue [24] [40]. It is therefore essential to understand the fluid structure interaction (FSI) in the runner since the dynamical loads in the turbine, which is mainly caused pressure fluctuation, induces fluctuating stresses. This can eventually cause crack growth and fatigue.

It is therefore important to develop new methods for reducing dynamical effects and thereby reducing the fatigue load on the Francis runner. In the latest years, the focus on flexibility have increased and turbines with variable speed capabilities

are of more interest. This work will focus on how variable speed can be used to minimize pressure pulsation and stresses in the turbine runner to avoid crack-growth and fatigue.

1.1 Objective

The overall objective of this work is to find the operating range for the Francis turbine, at the Waterpower Laboratory at NTNU, with variable speed which give the lowest material stresses in the turbine. To approach this objective, measurements of the Francis turbine will be conducted, followed by structural analysis of the runner and fatigue assessment.

Measurements will be done for the whole operation range of the Francis turbine, i.e. from 1 degree opening until full opening of 14 degrees, for both efficiency and pressure pulsations. Pressure pulsation will be measured throughout the whole turbine, from the guide vanes, on-board the runner and in the draft tube cone. Results from pressure pulsation will be presented in pressure pulsation diagrams which illustrates the intensity of the pulsations for the whole operating range.

Structural analysis will be performed in ANSYS Mechanical, by using static structural analysis. A flow analysis based on experimental results will be used to calculate the pressure distribution to apply on the structural model. The results will be compared with the pressure pulsation to try to find a correlation between the pressure pulsation diagrams and the stresses. Then the results will be interpreted for use in fatigue assessment.

In addition to this, a paper of the early result from measurement is written and presented at 8th International Symposium on Current Research in Hydraulic Turbines (CRHT-VIII'18) at Kathmandu University in March 2018. The title of the paper is *Pressure Pulsations in a High Head Francis Turbines Operating a Variable Speed*, and can be found in Appendix A. After the conference, the paper was accepted for publishing in IOP conference series.

1.2 Previous and ongoing work

Unsteady flow and pressure pulsations have been investigated for a many years, and already in 1940, Rheingans proved that power swings was caused by draft tube surges [44]. Since then, there have been a lot of research regarding the topic of dynamical loads such as the draft tube pressure pulsation, rotor-stator interaction and vortex shedding. In the latest years, dynamical loads have caused problems for several high head Francis turbines, and the topic has been of major interest.

Numerical and experimental methods have been vital in the prediction of pressure pulsations and stresses induced by them. Seidel et al. (2012) worked on *evaluation of RSI-induced stresses in Francis runners* [33]. Strain gauge measurements from a prototype were used to validate a method for calculating the dynamic stresses by combining CFD and harmonic response analysis. The results showed that RSI-induced stresses from the analysis was in good agreement with the measured data, and the method can be used to predict the performance of new runners. In 2014, Seidel et al. published *Dynamic loads in Francis runners and their impact on fatigue life* [33], where he summarized recent findings regarding fatigue life. Different operation conditions were compared and he showed that transient, SNL and RSI are the main fatigue contributors for a high head Francis turbine. Several other papers have been published regarding fatigue loads on Francis prototypes, and Huang et al. [22], Wang et al. [45] and Paquette et al. [30], among others, should be mentioned. All of them used the same procedure as Seidel, where stresses was calculated based on CFD results, and stresses was validated based on strain measurements from a prototype turbine. Stress results was further used to perform a fatigue assessment of the prototype runner, by using the local-stress method.

Researchers from NTNU have been working with pressure pulsations and mitigation techniques for reducing the fatigue load on Francis turbines for several years. Kobro finished his doctoral thesis in 2010; *Measurements of Pressure Pulsations in Francis Turbines* [26]. He investigated dynamical pressure and strain by conducting measurements in a model and a full scale prototype turbine. The results showed that the guide vane passing frequency was the most significant for the high head Francis turbine, for both the model and prototype. In 2017, Gogstad finished his doctoral thesis *Experimental investigation and mitigation of pressure pulsation in Francis turbines* [19] where he investigated different methods for reducing pressure pulsations. He proved that air injection can be used to reduce the pulsation at part load operation without effecting the efficiency. A runner extension cone was also tested and resulted in lower pulsation, but the efficiency dropped at high load operation.

Fatigue predictions is of great importance when designing a new runner or are evaluating one that is already in operation. In 2005, Hans-Jörg Huth finished his doctoral theses at NTNU; *Fatigue Design of Hydraulic turbine runners* [23]. He investigated crack growths in the T-joint between blade and hub/shroud, and optimized the shape of this T-joint to reduce stresses and fatigue. In 2007, Anders Wormsen published a PhD on *A Fatigue Assessment Methodology for Notched Components Containing Defects* [47], where he used different methods to predict fatigue life of turbines. He developed a software called P•FAT, which could use

results from FEA directly to predict fatigue. This software is still being developed at the Department of Mechanical and Industrial Engineering at NTNU.

There are several on-going projects at the Waterpower Laboratory today. HiFrancis, is one them, which primary goal is to secure reliable operation and lifetime for high head Francis turbines operation in the future energy market [13]. The main work will consist of numerical and experimental work, and understanding fatigue loads during all operation conditions. Numerical simulations is used to calculated natural frequencies of the turbine runner, and harmonic response analysis are used to find the stresses induced by the pressure pulsations. In the end of the project, they hope to develop a better method for designing high head Francis runner that can withstand today's operation patterns. Flexibility in hydro turbines is important to meet the future need for the energymarket. PhD. Candidate Igor Iliev is currently working on a research project called Variable speed operation, where he is developing a high head Francis turbine that can be used for variable speed operation. The main goal is to design a new runner with increased efficiency at part load and high load operation. In addition to this, variable speed operation gives to opportunity of faster ramping and having a wider operation range [25].

Chapter 2

Theoretical Background

2.1 Pressure pulsations in a Francis turbine

The theory presented is based on the authors project thesis during fall of 2017; Pressure Pulsation in a Francis Turbine [15].

Damages and operational problems in hydro turbines are caused mainly by cavitation, sand erosion, material defects and fatigue [2]. Vibrations, that can result in fatigue, is due to pressure pulsations or mechanical unbalance. Pressure pulsations is a flow phenomena that is happening inside the turbine. It happens at all operation conditions, and can be both stochastic and periodic. Operation outside BEP can result in pressure pulsation such as vortex breakdown and part load vortex rope with high amplitudes that can cause serious damage to the turbine runner [42]. For a high head Francis turbine, RSI is considered at the main fatigue contributor at steady state operation [34]. Below is a description of the most common pressure pulsation phenomena.

2.1.1 Rotor-stator interaction

Rotor-Stator Interaction (RSI) is pressure pulsations that occurs due to the interaction of the rotating runner and the stationary parts. The pressure difference between the suction and pressure side of the blade causes the runner to rotate, which results in a rotating pressure field. When the flow is leaving the guide vanes, the flowfield will be nonuniform, as illustrated in Figure 2.1. When the runner blade is moving in this nonuniform velocity field, it will create a pressure pulsation each time it passes a guide vane. RSI can be divided into two phenomena, depended on the reference system; blade passing frequency and guide vane passing frequency.

Blade passing frequency

Each time a runner blade is passing a guide vane, an impulse will occur. This can be explained as each time a runner blade moves toward a guide vane the there will be an increase in local pressure. When the blade moves away from the guide vane the local pressure will decrease. Pressure waves will propagate from the vaneless space through the guide vanes and into the spiral casing. The frequency will be depended of the number of runner blade, z_r, and can be calculated by using equation 2.1. The amplitude depends on the distance between the rotating

and stationary parts and decreases with increasing distance [16].

$$f_{bp} = z_r \cdot f_n \tag{2.1}$$

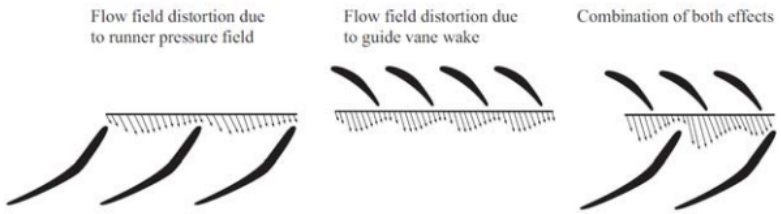

Figure 2.1: Velocity field at the runner inlet, [17]

Guide vane frequency
From the reference system of the runner, a pressure impulse occur when the runner blade passes a guide vane. This is due to the non-uniform pressure and velocity field leaving the guide vane. Therefore, the frequency will be depended on the number of guide vanes in the turbine, and can be calculated by equation 2.2. This pressure wave will propagate through the runner. The amplitude will depended on the distance between the rotating and stationary part, and decreases with increasing distance [16].

$$f_{gv} = z_{gv} \cdot f_n \tag{2.2}$$

2.1.2 Draft tube pressure pulsations

When operating outside BEP a swirling component will occur in the draft tube. At part load, the tangential direction of the flow will be the same as the runner direction, while at full load, the opposite direction.

At loads below BEP, i.e. part load, the swirling component will move in the same direction as the runner. At some operation points a vortex rope will appear in the draft tube, as seen in Figure 2.2 (left side of the figure). The high velocities in the core of the vortex can decrease the static pressure to the vapor pressure, resulting in a vapor-filled cavity core. This will typically occur at loads between 50% and 85% of the flow at best efficiency [16]. The frequency of this pulsation is called Rheingans frequency, and can be approximated by use of equation 2.3 [29]. The amplitude of this pulsations will be at its highest when the vortex rope is visible.

$$f_s = f_n \cdot 0.36 \pm 20\% \tag{2.3}$$

At higher loads than BEP, a cavitated vortex core can appear in the draft tube, as seen in Figure 2.2 (right side of the figure). This core will pulsate in radial direction. Normally, it will not cause any operational problems, unless is coincide with system dynamics oscillations. If this happens, it can cause mass fluctuations that can propagate in the waterway.

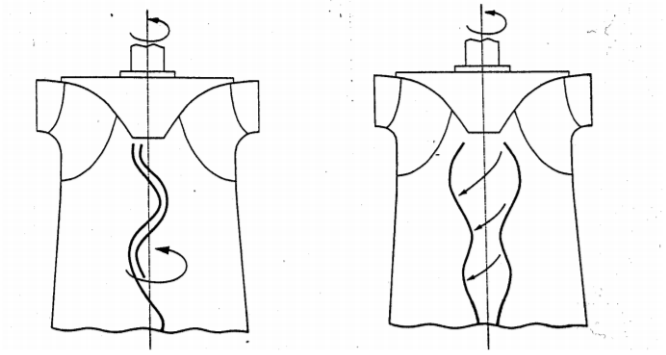

Figure 2.2: Left: part load vortex rope. Right: high load vortex core [10].

The draft tube pressure pulsations can be decomposed into an synchronous part and a non-synchronous part. They can be found if two pressure sensors are located 180 degrees apart and at the same height. The synchronous part is found by adding the pressure values and dividing by two, while the non-synchronous is found by subtracting the pressure values and dividing by two. The synchronous part is due to axial pulsations, which can cause mass fluctuations and damage to the turbine runner. The non-synchronous part is due to radial pulsations and can damage the draft tube walls.

2.1.3 Vortex shedding

Vortex shedding (or Von Karman vortices) is a flow phenomena that occurs for bodies in cross-flow at curtain Reynolds number. The separation point of the flow at the trailing edge will alternate between the two sides, causing a swirling component, called eddy swirls. This will cause a pressure that is fluctuating with the same frequencies as the formation of these swirls.

In a Francis turbine, vortex shedding will happen at the trailing edge of the stay vanes, guide vanes and runner blades. Vortex Shedding is a high-frequency phenomena, and can therefore be damaging over time due to high-cycle fatigue if the amplitudes are sufficient enough. It is also important that this frequency does not coincide with the natural frequency of the body producing it, to avoid lock-in effects and resonance. An empirical equation have been developed, based on the

work of G. Heskestad and D.R. Olberts [28], to estimate the frequencies due to vortex shedding in hydro turbines:

$$f_{vs} = 1.9 \cdot B \cdot \frac{v}{L + \delta_v} \tag{2.4}$$

$$\delta_v = 0.0297 \cdot \frac{x}{Re_x^{0.2}}$$

where B is an empirical value for a given geometry (can be found in [11]), L is the thickness of the trailing edge, δ_v is an empirical function based on a fraction of the boundary layer thickness at the trailing edge, Re_x is the Reynolds number and x is the blade length.

2.1.4 System dynamics oscillations

In rotating hydro machinery there will exists mass oscillation in the waterway, called water hammer oscillations or system dynamics oscillations. These oscillations is pressure waves that propagates in the water way with the speed of sound. It will always be present in the system, but a change in load will increase the amplitude [37]. The frequency of these pulsations can be calculated by equation 2.5, where L is the length of the waterway and *a* is the speed of sound. The speed of sound will vary with the system, and for a pipe it can be calculated by equation 2.6. These equations are taken from T. Nielsen [39].

$$f_{sd} = \frac{a}{4 \cdot L} \tag{2.5}$$

$$a = \sqrt{\frac{1}{\rho_w \cdot (\frac{1}{K_w} + \frac{D}{t \cdot E})}} \tag{2.6}$$

These pulsation will normally not affect the operational conditions of the turbine, unless it coincide with the other frequencies in the turbine. It is therefore important to know what frequencies to expect, to be able to avoid operations where they coincide.

2.2 Hill chart and hydraulic efficiency

Hill Chart is a diagram that shows the performance of a model-turbine. Figure 2.3 illustrate a typical chart, where the speed factor, N_{ED}, is plotted against the discharge factor, Q_{ED}. The horizontal lines are of constant guide vane opening, and the circular lines are lines of constant hydraulic efficiency. Additional information can be presented such as lines of constant power. The gray area in Figure 2.3 is where the producer is guaranteeing that the turbine safely can be operated.

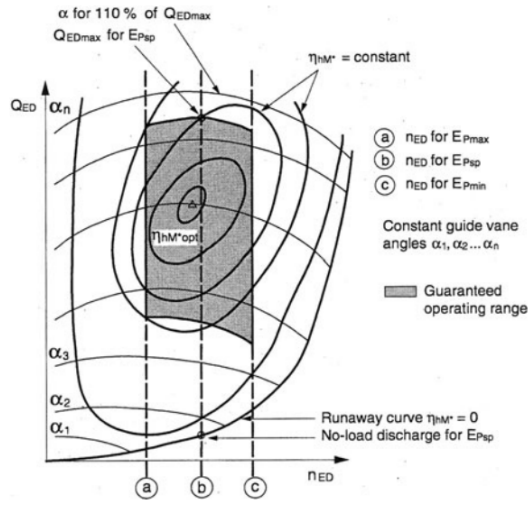

Figure 2.3: Illustration of a Hill Chart, taken from IEC60193 [1].

The way the hydraulic efficiency from a model test is calculated is standardized, and can be found in the IEC60193 [1]. The speed factor is defined in Equation 2.7 and the discharge factor in Equation 2.8.

$$N_{ED} = \frac{(n/60) \cdot D}{\sqrt{E_h}} \tag{2.7}$$

$$Q_{ED} = \frac{Q}{D^2 \cdot \sqrt{E_h}} \tag{2.8}$$

where n is the speed, D is the outlet diameter, Q is the flow rate and E_h is the specific hydraulic energy of the machine. The flow and speed is measured, while E_h has to be calculated. For heads below 40 meters (compressibility effects are negligible, i.e. density is constant), and with a differential pressure sensor between the inlet and the outlet of the turbine, E_h can be calculated by Equation 2.9 (page 255 in IEC60193). The density, ρ_w, is calculated with an empirical equation presented in IEC60193 at page 171, with an accuracy of $\pm 0.01\%$

$$E_h = g \cdot H = \frac{\Delta p}{\rho} + \frac{{Q_1/A_1}^2 - {Q_2/A_2}^2}{2} \tag{2.9}$$

The Hydraulic efficiency is then calculated with Equation 2.10

$$\eta_h = \frac{\omega \cdot (T_f + T_g)}{E_h \cdot \rho_w \cdot Q} \tag{2.10}$$

where ω is the angular velocity, T_f is the friction torque from the shaft bearing and T_g is the generator torque.

2.3 Variable speed operation

A Francis turbine is designed for fixed speed and one best efficiency point. The speed of the turbine is predetermined by the combination of pole pairs in the generator and the grid frequency, according to Equation 2.11

$$n = \frac{60 \cdot f_{grid}}{z_p} \tag{2.11}$$

where n is the speed, f_{grid} is the grid frequency and z_p is the number of pole pairs. The turbine power output is therefore controlled by changing the guide vane opening and thereby water discharge. By introducing a frequency converter, together with the synchronous generator, it is possible to operate with variable speed. The turbine and generator will be disconnected from the grid, and free to operate at different speeds [41]. The turbine will be more flexible, when it can regulate both speed and discharge. One of the drawback is additional converter losses and the need for more complex governing.

2.4 Mechanical properties and fatigue assessment

2.4.1 Stress and strain

If a load is applied to a body it will become in a state of stress. It is therefore important to know the material properties to be able to predict how the body reacts on a given load, and thereby design the component to avoid excessive deformation and fracture. Loads may be applied by simple tension (pulling), simple compression (pushing), pure shear (tearing) or hydrostatic pressure. Loads can be static or fluctuating periodic or stochastic, and introduce dynamical behavior. The intensity of the stress, σ, is measured by the instance force F, divided by the loaded area, A, according to Equation 2.12 [5].

$$\sigma = \frac{F}{A} \tag{2.12}$$

Materials respond to stress by straining [5]. For a given stress, deformation will occur. The relative deformation parallel to the load is called the nominal tensile strain, defined in Equation 2.13. This will also affect the lateral strain, and the ratio between lateral strain and tensile strain is called Poisson's ratio, defined in Equation 2.14.

$$\epsilon = \frac{\Delta L}{L} \tag{2.13}$$

$$\nu = \frac{\epsilon_l}{\epsilon_t} \tag{2.14}$$

A given material can deform both elastic an plastic, which means either non-permanent or permanent deformation. Steel, which is used in hydro turbines, is

an elastic material, and as all elastic materials it follows Hook's law. Hook's law is linear equation that connect stress and strain by a material property called Young's modules (Equation 2.15). It is important to notice that this law is only valid for very small strains, around 0.1% [5]. Figure 2.4 shows a typical stress-strain curve for a steel alloy. Elastic deformation occurs in the first part of the curve, and ends with the red dotted line, where the material starts to yield. The yield limit, σ_Y, is defined as where permanent plastic deformation starts, which often occurs at strain-offset of 0.2% from the linear elastic curve. Stress will continue to increase until it reaches ultimate tensile strength (UTS), which is the highest stress capacity of the material. If the stress is held at UTS, strain will continue to increase until fracture occurs.

$$\sigma = E \cdot \epsilon \tag{2.15}$$

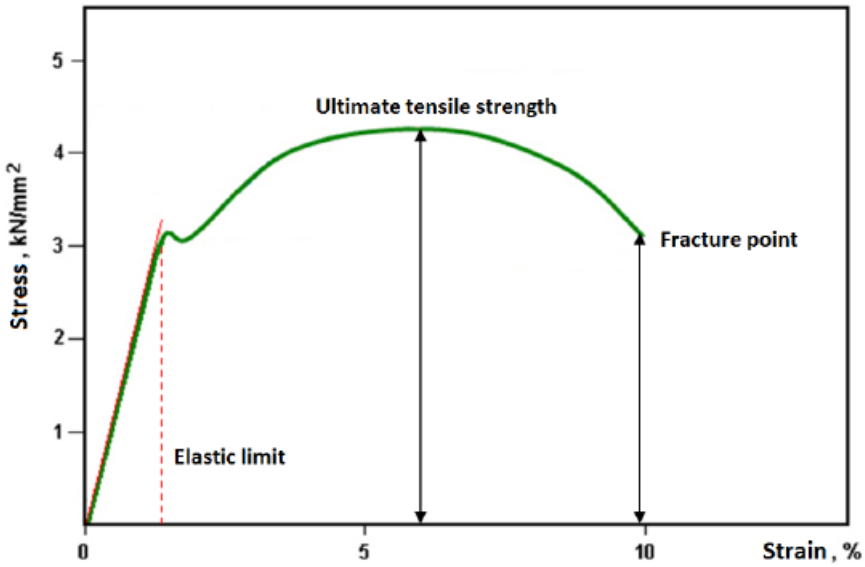

Figure 2.4: Stress-strain curve for a typical steel alloy [4].

2.4.2 Fatigue

Fracture can also occur at loads lower than the UTS and yield-strength of a material, either by fast fracture or by fatigue. Fast fracture occurs for a crack when the stress intensity factor suddenly reaches a critical value, while fatigue happens due to slow crack growth [5].

Many structures (or components) are exposed to alternating loading, such as vibration, rotation or pressure pulsation in a hydro turbine. There can be constant amplitude loading (CAL) or variable amplitude loading (VAL) [31]. To predict fatigue for a given material, test on several standardized specimen is conducted in order to estimate cycles-to-failure for a given stress amplitude. The result from these test are presented in S-N curves. Figure 2.5 illustrate a typical S-N curve, for both CAL and VAL. It is normal to differentiate between Low Cycle Fatigue (LCF), $N \leq 10^4$, High Cycle Fatigue (HCF), $10^4 \leq N \leq 10^7$, and Very High Cycle Fatigue (VHCF), $N \geq 10^7$, where N is the number of cycles.

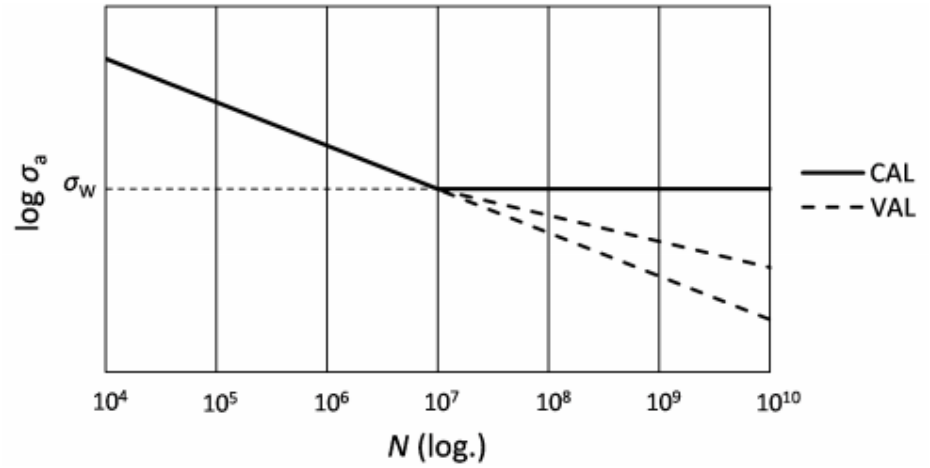

Figure 2.5: S-N curves, for both CAL and VAL, for a typical steel alloy [31].

If a structure is exposed to CAL, and the stress amplitude σ_A is below σ_w, which is the threshold limit for the stress, it is normal to assume infinite life. This is the same for VAL if all stress amplitudes are below σ_w. If one of them is higher, a crack can start to grow and cycles with lower amplitude can contribute to further crack growth [7]. The result of this is that the life of the structure will not be infinite, and for cycles above 10^7, the S-N curve will either be an extrapolation or a having a lower gradient as can be seen in Figure 2.5.

Mean stress effect

Most of the test results is conducted with a constant stress ratio of either 0 or -1, and with a constant amplitude loading. The amplitude of a periodic load is defined in Equation 2.16, while the stress ratio is defined in Equation 2.17. In reality this not the usual case, and the stress amplitude can vary around a higher mean. There have been developed several empirical models to account for the mean stress, and

estimate the effective stress for a curtain stress ratio. By doing this, the stress amplitude can be estimate for the same stress ratio as the S-N curve is based on and fatigue can be estimated.

$$\sigma_A = \frac{\sigma_{max} - \sigma_{min}}{2} \tag{2.16}$$

$$R = \frac{\sigma_{min}}{\sigma_{max}} \tag{2.17}$$

One of the methods to account the mean stress is called Goodman method. The method is illustrated in Figure 2.6, where the mean stress is along the x-axis and the alternating stress is along the y-axis. The mean and alternating stress is plotted in the diagram. It is assumed that the alternating stress amplitude follows a linear relationship with the mean stress. The effective alternating stress can be calculated for a stress ratio of R=-1 (altering around zero mean stress). The equation for this can be found to the right in Figure 2.6, where σ_u is the ultimate tensile stress.

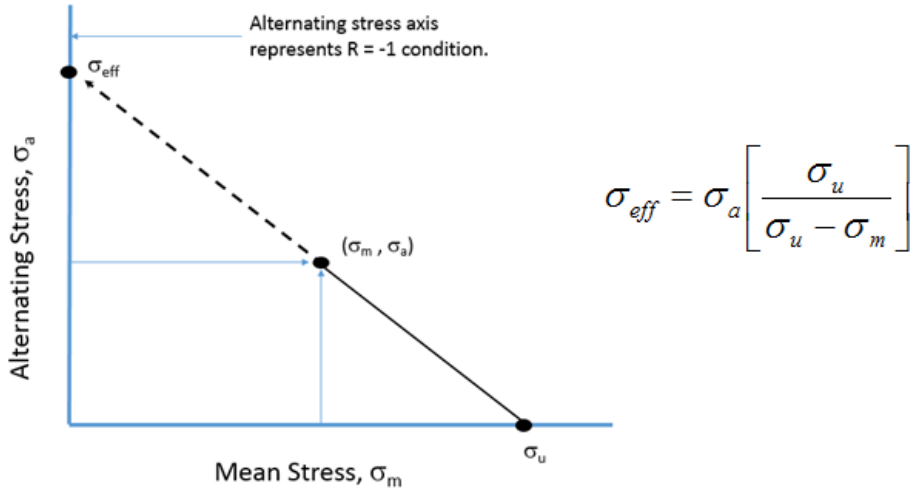

Figure 2.6: Goodman mean stress correction [6].

VAL and cumulative damage

When the amplitudes are varying during the lifetime of a structure, Minor's rule for cumulative damage can be used (Equation 2.18) [5].

$$D_A = \sum \frac{N_i}{N_{fi}} \tag{2.18}$$

where N_i is the number of cycles for a specific stress amplitude and N_{fi} is the number of cycles to failure for the same stress amplitude. Failure occurs when $D_A = 1$ [5].

Fatigue assessment of cracked structures
Fatigue approaches such as S-N curves assumes that there is no initial cracks in the structure or component. In reality, 90% of the fatigue life contributes to initiate a dominant crack before it starts to propagate until failure [23]. Large structures, and particularly welded structures, always contains cracks and pores [5]. Therefore, the life of the component is dependent on how many cycles until the crack grows to a critical size. To estimate the fatigue life properly, the stress intensity factor must be calculated and used further in a crack growth law such as Paris' law, or more advanced versions as the one El Haddad et al. presented in [18]. Crack growth models will not be used for further analysis, but the method is well described in [48], [47] and [23].

2.4.3 Fatigue analysis for a Francis runner

A Francis turbine will experience both (V)HCF and LCF. LCF is mainly due to starts and stops, and can contribute to large stress amplitudes. HCF and VHCF are mainly due to pressure pulsation and transient operations with smaller amplitudes. The most common way to perform a fatigue analysis of a turbine runner is by using the *local-stress approach*, combined with the Minor's rule [31]. A drawback for this approach is that it does not take the volume of the structure into consideration. A larger volume can have more defects that can cause an earlier failure. The *Weakest-link approach* is a probabilistic method that also takes the volume into account. It uses S-N data to calculate the probability for failure for the whole geometry to determine the fatigue life. This method requires Weibull parameters from test results which can be hard to come by without having raw data from the test available. Weakest-link can be used together with structural analysis results, and have proven ho give good results compared to experiments [48]. There are other approaches as well such as *single defect* and *random defects* which instead is using crack growth models to calculate the total lifetime of the runner. Only local-stress will be used further, but the other methods are well described in [47].

S-N tests are extremely sensitive to specimen material, size and roughness, type and frequency of loading, stress ratio as well as temperature and chemical properties of the environment [23]. It is therefore important to have test data from the same conditions that the turbine is operating in. Francis runners are typical made of a 13Cr-4Ni stainless steel [31], and suitable S-N data has to be found before performing fatigue analysis.

Local-stress
The local-stress approach assumes that the structure is smooth without no initial cracks. The most highly stressed area is compared with the S-N curve, to estimate the time until failure. Local-stress can be used for a Francis runner by using

Minor's rule for cumulative damage. All starts and stops, transients and pressure pulsations for an estimated operating pattern have to be summed up in order to calculate the total fatigue life. Pressure pulsation can be measured, and the number of cycles can be found by using a counting method, such as Rainflow counting, or by summing up known pulsation frequencies per operation hour.

Chapter 3

Analysis Methods

3.1 Histogram method - Amplitude of pressure pulsations

Literature has different definitions of pressure pulsation intensity such as peak-peak, rms and amplitude. It is therefore important to have a common understanding on which definition one is using when discussing pressure pulsation intensity. For instance; peak-peak = 2·amplitude = $2\sqrt{2}$·rms. Peak-peak values, which is the total variation in signal, will be used further in this thesis.

There are different methods for calculating peak-peak values, such as window method and statistical methods. IEC60193 [1] is suggesting that the peak-peak value should be the variation which contains a curtain percentage of the sampled signal, and 97% is a suggested interval. The histogram method is a statistical method that calculates an upper and lower bound, where a curtain percentage is in-between these bounds. This method is suggested by Dörfler et. al [16] and have been used by Gogstad [19] in his doctoral thesis. The histogram method has been chosen for analyzing pressure signals in this thesis.

The histogram method is illustrated in Figure 3.1, where all the sampled data is plotted in a histogram. Statistical analysis is used to calculate an upper and lower bound, where a chosen (97% in this case) percentage of the sampled data is between the two bounds. These bounds is calculated with a cumulative density function (CDF), where the lowest and highest 1.5% has been omitted. Figure 3.2 shows the time series with the upper and lower bound.

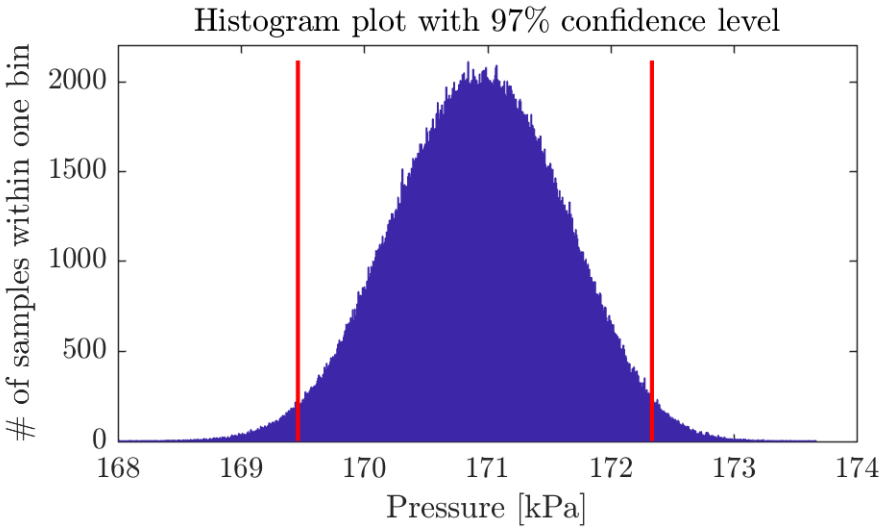

Figure 3.1: Illustration of the Histogram method, where the peak-peak values is the difference between the upper and lower bound. This results is from sensor PTGV4 at BEP.

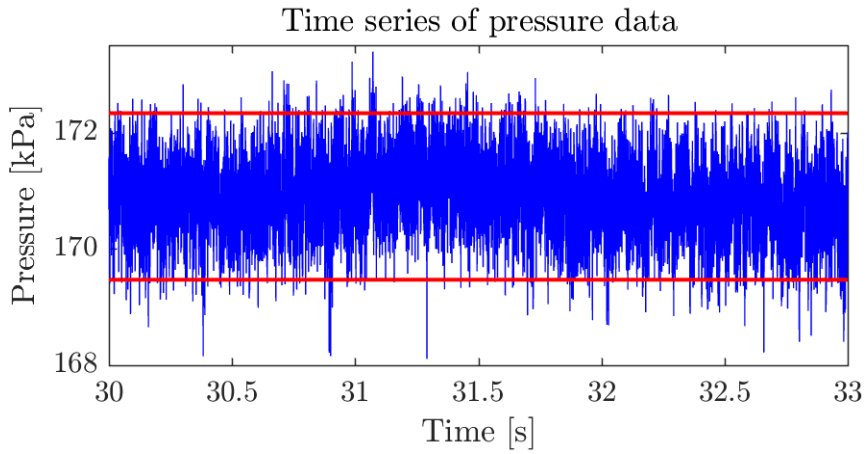

Figure 3.2: Pressure-time data with upper and lower bound. Between the two straight lines is 97% of all pressure data. From sensor PTGV4 at BEP.

3.2 Post processing of measured data

The theory presented is based on the authors project thesis during fall of 2017; Pressure Pulsation in a Francis Turbine [15].

3.2.1 Sampling rate

Measurements that are made of a time-varying signal, using a data-acquisition system, are only made at a discrete set of times. A sample can be taken, for example every 0.01 seconds, and all the information between the samples will be lost. The rate at which measurements are taken, is known as the sampling rate [46]. The Nyquist sampling theorem explains that the sampling frequency, f_{samp}, must be at least twice as big as the highest frequency of interest, f_m. The sampling rate-theorem is defined as:

$$f_{samp} > 2 \cdot f_m \tag{3.1}$$

If the sampling rate is too low compared to the highest frequency of interest aliasing can occur. Oversampling and filtering can therefore be used to reduce the effect of aliasing [19]. Oversampling means that the sample rate is higher than the sampling rate theorem criteria, often multiple times higher. In addition to reduce aliasing effects, oversampling increases frequency resolution and reduces noise in the measurements [19].

3.2.2 Spectral analysis

Spectral analysis is a method that can be applied to a time-varying signal to get information on the different frequency component in the signal [46]. This is done by Fourier transforming the measured signal. Because the signals are discrete, the Discrete Fourier transform (DFT) must be used. The DFT is computed by using Fast Fourier Transform algorithm (FFT). A requirement for using DFT is that there is no holes in the signal, and that the time step between each sample is constant.

The FFT is assuming the signal is periodic and that the sampled signal has an integer number of cycles (i.e starts and stops at the same values) [46]. This is rarely the case for experimental data, and you will end up with spectral leakage. That means that frequency component is smeared out, and the peak amplitude becomes smaller. In a Francis turbine the signals will be periodic and stochastic, and using Fourier transform directly will result in spectral leakage which will give a large uncertainty in the result.

Welch method is a method that can be used to reduce the effect of spectral leakage. The sampled data is divided into overlapping segments, and a window function is multiplied with each segment. Each segment is transformed by the FFT algorithm, and the overlapping segments are averaged. Figure 3.3 illustrate this

method. There is many different window functions, with different characteristics. For analyzing pressure pulsation, a Hann window is recommended by IEC60193 [1]. The optimal overlap for a Hann-window is 50% [20]. There will always be a trade-of between frequency resolution and variance in the result from Welch's method. Good accuracy and low variance will therefore require long data samples.

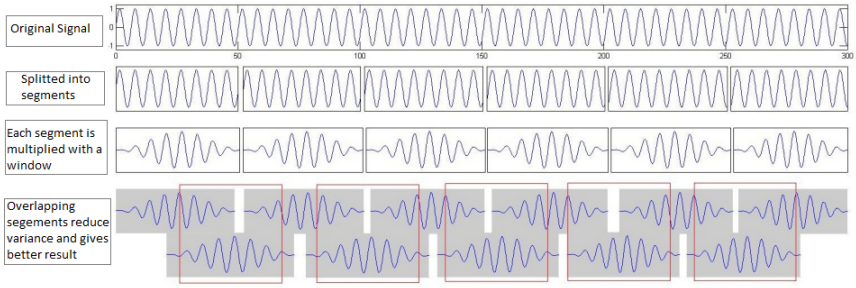

Figure 3.3: Illustration of Welch method with overlapping segments [12].

3.2.3 Filtering data

Filters are a way of removing noise and nonphysical component from a measured signal. Typical noise from a measurement is high frequency noise and different electrical component such as the grid frequency. Filters used for post processing, were design with MatLabs filterBuilder function. Infinite impulse response filter were used with a Chebyshev type II design method.

3.3 Structural analysis

Structural analysis is a computational tool that calculates deformation and stresses of structures/components exposed to loading. It can be used as an design method, or to evaluate existing systems such as an operating turbine. The most used numerical method for performing structural analysis is the Finite Element Method (FEM). This is a method where the structure is divided into an equivalent system of finite elements, which is sharing elements called nodes. Partial differential equation problems are translated into a set of algebraic equation for steady state problem, and ordinary differential equation for transient problems [42]. The solution for these equations are displacement, and stress and strain can easily be determined afterwards. As all numerical methods, FEM will introduce numerical errors. There will be round of errors due to computer floating point, and errors due to the numerical scheme that is used. These errors are normally small in commercialized FEM software. The error that is contributing the most is the discretization

error (mesh). A system that is discretized is only an approximation of the real one, and the will therefore introduce errors [43]. This error is normally minimized by performing a mesh independence test until the result is converging.

ANSYS Mechanical is a software for structural analysis which uses FEM. It can be used to analyze complex geometries, such as a Francis runner. It has different modules, and can be used to perform static, transient, modal and harmonic response analysis. Both linear and non-linear analysis can be conducted. It is also possible to use results from CFD directly as input to ANSYS Mechanical by using ANSYS Workbench.

Fluid-structure interactions
The description of FSI below is taken from Comsol's webpage [14].

Fluid-structure interactions is a multiphysics coupling between fluid dynamics and structural mechanics. When a fluid is interacting with a structure, stresses and strain will be exerted on the structure. The resulting structural deformation due to the fluid can be quite small or large, depending on the material properties and the pressure and velocity of the fluid. If the deformations are quite small and variations are relatively slow, the deformation of the structure will not greatly affect the fluid's behavior and the problem can be simplified by only looking at the stresses induced by the fluid. This is often called one-way FSI. If the variation in time is faster, then small deformation in the structure (vibrations) can cause pressure waves in the fluid, which can cause radiation of sound. These problems must be treated with an acoustic-structure interaction. This will of course depend on the interest of the analysis. If the deformation of the structure is large, the pressure and velocity will be affected, and the problem must be treated as a bidirectionally coupled multiphysics analysis, called a two-way FSI.

For a Francis turbine, it is normal to evaluate stresses and strain by performing a one-way FSI. Pressure distribution from CFD results is applied to a mechanical model, and the resulting stresses and strain is calculated based on FEM. This method as proven to give accurate results [33] [30], and is a lot faster than a two-way FSI. Another advantage is that the work can be split between people. ANSYS has the possibility of performing both one-way and two-way FSI simulations. By using ANSYS workbench, CFD result can be "dragged" into the structure project, and both transient and static simulations can be perform with the pressure distribution from CFD as pressure loads on the mechanical model. It is important that the geometry for the mechanical model is equal to the CFD model, and that they are placed in the same coordinate system with the same orientation.

Chapter 4

Experimental Setup, Instruments and Measurements

Measurements in the laboratory were used to investigate pressure pulsation in the Francis-99 turbine at NTNU. A description of the facility, setup, measurements and instrumentation will be presented, together with calibration methods and uncertainties for the instruments.

4.1 Francis model test rig

Measurements were conducted at the Francis model test rig located at the Waterpower laboratory at NTNU. The Francis rig has been designed to meet the criteria of IEC60193 - Model Acceptance Test [1], which gives us the opportunity to perform high quality measurements. The Francis rig has two different ways of operating; closed loop and open loop. Open loop system was chosen for these measurements, and its schematic can be seen in Figure 4.1. The Waterpower Laboratory consists of a lower reservoir in the basement with two centrifugal pumps, which can be run in both series and parallel.

For the open loop configuration, water is pumped up into an u-formed open channel on the top floor of the building. From the open channel, water is flowing down to an upstream pressure tank, before it enters the turbine. The Francis turbine is a model of the Tokke-turbine (scale: 1:5.1), and has a configuration of 28 guide vanes, 14 stay vanes and 30 runner blades (15 splitter blades and 15 full length blades). The outlet diameter is 0.349m, inlet diameter is 0.63m and the inlet height is 0.06m. The turbines is installed together with a 352kW DC-generator produced by Siemens.

Downstream the turbine is a pressure tank that has the function as an imaginary lower reservoir. It is the pressure difference between the inlet of the downstream pressure tank and the inlet of the turbine that forces the water through the turbine. There is a possibility to lower the pressure in the downstream tank, if this is of interests, but for these measurement the water level was open to atmospheric pressure. After the downstream pressure tank, the water is flowing back to the basement reservoir.

The generator is controlled by a PLS (programmable logic control) system delivered by Siemens, which gives us the possibility to set the speed and torque of the turbine, and to monitor pressure values in the pipe system. The PLS system is also used for start-up and shutdown of the turbine. The procedure for this, and the measurement, is given in Appendix C. The main valves can also be controlled by the PLS system. The guide vanes is operated by a switch in the control room, and the operating conditions is monitored by a LabView program.

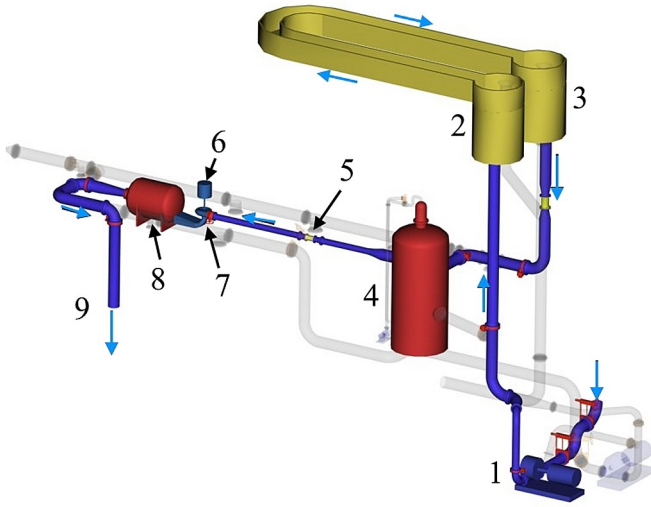

Figure 4.1: Illustration of the open loop system in the laboratory. (1) centrifugal pump, (2) open channel inlet, (3) open channel outlet, (4) upstream pressure tank, (5) flowmeter, (6) generator, (7) Francis turbine, (8) downstream pressure tank, (9) water outlet.

4.2 Instrumentation

The measurement system that is used is a complete setup with all the necessary equipment for calculating the efficiency (and to make a Hill Chart), according to IEC60193 [1]. There was also installed additional pressure sensors for logging pressure pulsations. The different instruments used is listed in Table 4.1.

Pressure Sensors

Pressure Sensors for measuring pressure pulsation were mounted along the guide vanes, on-board the runner and at the draft tube cone. Five pressure sensors was located along the guide vanes (PTGV1-PTGV6), and four was located on-board the runner (PTR1-PTR4), according to Figure 4.2. Two sensors was placed on the upper part of the draft tube cone, PTDT13 and PTDT17, according to Figure 4.3. The on-board sensors were transmitting signals via a slip ring on the turbine shaft.

Operation point sensors
Several sensors were installed around the Francis rig to measure the operation condition for calculating the hydraulic efficiency of the runner. The different sensors were located according to Figure 4.4. An induction flow meter, FTQ1, is placed on the pipe upstream the turbine. Pressure sensor, PTDP, is measuring the differential pressure between the inlet and the outlet of the turbine. WTT1 and WTT2 are load cells that is measuring the torque of the generator and the axial bearing. The ZT41 is measuring the rotational speed of the turbine shaft, and is recording a pulse for each rotation. The water temperate (TT41) is measured upstream the turbine.

Table 4.1: Instrumentation and sensors used during measurements

Sensor	Description	Sensor type
PT IN1	Upstream after pressure tank	Kulite HKM375
PT IN2	Inlet before spiral casing	Kulite HKM 375
PT R1	Onboard 1	TE XP5
PT R2	Onboard 2	TE XP5
PT R3	Onboard 3	TE XP5
PT R4	Onboard 4	TE XP5
PT GV1	Along GV	TE XP5
PT GV3	Along GV	TE XP5
PT GV4	Along GV	TE XP5
PT GV5	Along GV	TE XP5
PT GV6	Along GV	TE XP5
PT DT13	Upper draft tube cone	Kulite HKM 375
PT DT17	Upper draft tube cone	Kulite HKM 375
FT Q1	Inlet pipe flow	Krohne
PT PIN	Inlet pipe pressure	Fuji Electronics FHCW36
PT DP	Diff pressure inlet outlet	Fuji Electronics FHCW36
WT T1	Generator torque	Load Cell
WT T2	Friction torque	Load Cell
ZT 41	Generator shaft position (rpm)	P+F FSS58N
ZT 42	Guide vane position	ENA42HD-S***-Analog
TT 41	Inlet temp	Pt100
P ATM	Atmospheric pressure	Vaisala PTB330

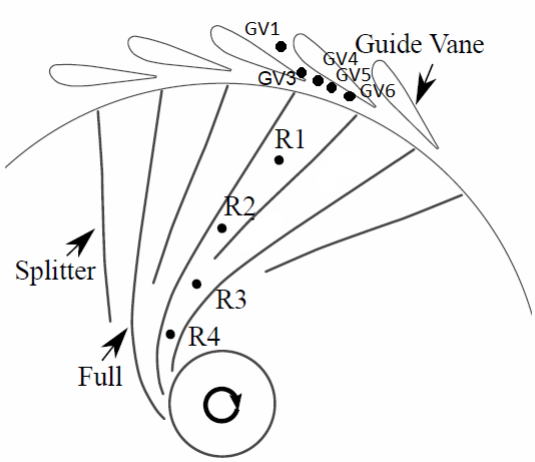

Figure 4.2: Pressure sensors used for measuring pressure pulsations. Sensors along guide vanes, GV1-GV6, and on-board sensors, R1-R4.

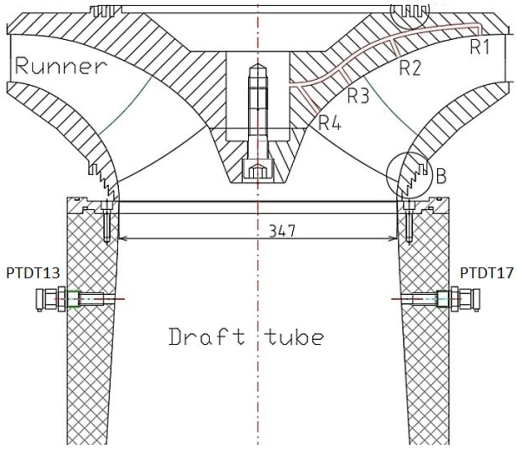

Figure 4.3: Pressure sensors used for measuring pressure pulsations. On-board sensors, R1-R4, and draft tube sensors DT13 and DT17.

4.3 Data logging and measurement procedure

All sensors were connected to a data acquisition (DAQ) system designed by PhD. Candidate Einar Agnalt at NTNU. Figure 4.5 shows the connection box were the sensors is connected. It consist of 14 individual modules that is connected via a

compact DAQ chassis, before it goes through a filter and are sent to the logging program. All sensors were directly wired to the DAQ system, except the on-board sensors which was wired through a slip-ring.

The logging software that is connected to the data acquisition system is a LabView program developed by PhD. Candidate Carl Bergan from NTNU. From the logging program it is possible to choose which channels you want to use together with the sampling frequency. Only raw data is logged, and the offset and scaling (from calibration) is input parameters in the program. The results is a TDMS file with all the raw data that can post-processed in another software, such as MatLab. Logging frequency was set to 10240 samples per second. Only the pressure sensors for measuring pressure pulsations had the possibility of logging with this sampling frequency, and the rest of the sensor used their max-sampling rate. For

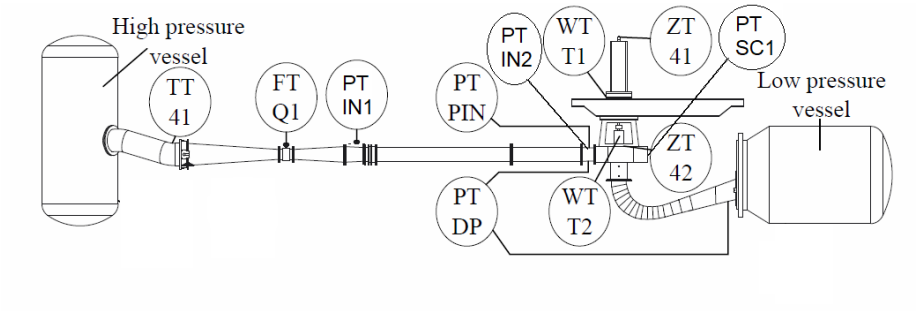

Figure 4.4: Operation point sensors for the Francis rig.

Figure 4.5: Picture showing the DAQ system.

these sensor, the logging program was coping the last value to store data with a frequency of 10240Hz.

Measurement was conducted with the open loop configuration. This was done to have an uniform water level which gives the same conditions for all operation points. This gave a pressure head of approximately 12meters for all measurements. Steady state measurements were done for the whole operation range of the turbine. From guide vane opening of 1 degree to 14 degrees (full opening) and from N_{ED}=0.08 to run-away speed. The increment between each measurement was $N_{ED} = 0.01$, and 1 degree between each guide vane opening. This gave a total of 269 individual steady state operation point. All sensors were logged for 60 seconds for each operation point. Measurement procedure and start- and stop procedure can be found in Appendix C.

4.4 Calibration

Pressure sensors and operation point sensor was calibrated previous to the measurements, by PhD. Candidate Einar Agnalt and PhD. Candidate Igor Iliev. The plan was that the author should calibrate the equipment one more time after the measurements was finished. This was unfortunately not possible, due to other waiting projects in the laboratory that required the same equipment.

All the sensors was calibrated in accordance to the guidelines in IEC60193 [1]. The pressure sensors were calibrated with the dead weight method, with the whole chain taken into account (through the slip-ring for the on-board senors). The flow meter (FT Q1) was calibrated with the weighing tank method. Both the friction torque and the generator torque (WTT1, WTT2) load cells were calibrated by putting weighing masses on a lever system. These methods are considered as primary calibration methods.

4.5 Uncertainty

The uncertainty results presented here is taken from a Measurement Report written by Einar Agnalt [3], based on the calibration that were done previous to the measurements.

Errors from measurement is the deviation from the actual value and the measured value. The error is not known but can be estimated by using statistical methods [36]. From the calibration results a confidence interval can be calculated, where with a curtain probability the real value will be within. This probability, or confidence level, can be chosen, but the industry uses 95% as a standard [36]. It is normal to differentiate between spurious errors, systematic errors and random errors.

Spurious errors are due to human errors or errors in the measuring equipment. Systematic errors is due to poorly calibrated instruments, hysteresis, non-linearity in the instruments or drifting [36]. Random errors are caused by fluctuations around a mean in the measurements, due to a combination of the instrument itself and small changes in pressure, temperature etc. of the system. It is important to minimize these errors. This is normally done by careful handling of equipment, proper calibration and long enough measurements to minimize the random errors. The total error is found by adding the systematic and random error by the root-mean-square method.

Pressure sensors
Calibration constants, offset and scale, were found for each sensor by using linear regression. The deviation between the regression-line and the sensor output was used to estimate the uncertainty with a 95% confidence level. The uncertainty presented here is the maximum found at the calibration interval and can be seen in the third column in Table 4.2. To evaluate the long time stability and temperature sensitivity, substitute calibration were done in the beginning and end of each day at zero-flow conditions. The substitute sensor was initially calibrated and mounted on the top of the draft tube cone. To evaluate the repeatability of the pressure sensors, BEP was recorded at the beginning and end of each day to find the deviation in measurements for the whole measurement period. The uncertainty for the long time stability and repeatability are calculated with a coverage factor of 2, which means 95% confidence level for normal distributed data. The total uncertainty is calculated by adding these three uncertainties with the root-mean-square method. The results can be seen in Table 4.2.

The amplitudes of pressure pulsation, which are of main interest, is a dynamical property and static calibration may not be valid to evaluate amplitudes [3]. Since it is stated by the producers that all the pressure sensors has resonance frequencies above 25kHz, and the largest system frequencies are below 1.2% of resonance, it is assumed that the uncertainty due to the dynamical behaviour can be neglected [3].

Operation point sensors
Linear regression was used to find the offset and scaling factor for the sensor output. Also for these sensors, the long time stability and repeatability uncertainty have been calculated in the same way as the pressure sensors. A coverage of 2 (95% confidence level) was used for all the uncertainty calculations. The rotational speed (ZT41) is not calibrated, as it only register pulses for each rotation. The repeatability is still introducing an uncertainty for the speed measurements.

Table 4.2: Expanded uncertainties for pressure sensors. Long time stability is estimated based on zero-flow measurements while repeatability is estimated based on BEP measurements.

Sensor	Mean Pressure [kPa]	Expanded Calibration Uncertainty [kPa]	Expanded Long time Stability [kPa]	Expanded Measurement Repeatability [kPa]	Total Expanded Uncertainty
PT IN1	218	0.2	0.5	1.6	0.8%
PT IN2	217	0.1	0.5	1.5	0.7%
PT GV4	174	0.07	1.1	1.1	0.9%
PT R1	128	0.8	2.1	2.6	2.7%
PT R2	101	1.2	3.0	2.2	3.9%
PT R3	88	0.6	1.1	0.7	1.6%
PT R4	80	0.2	0.9	1.0	1.4%
PT DT13	100	0.03	0.4	0.6	0.7%
PT DT17	100	0.05	0.4	0.4	0.6%

Table 4.3: Expanded uncertainties for the operation sensors. Long time stability is estimated based on zero-flow measurements while repeatability is estimated based on BEP measurements.

Sensor	Mean Value	Expanded Calibration Uncertainty	Expanded Long time Stability	Expanded Measurement Repeatability	Total Expanded Uncertainty
FT Q1	0.203	0.3e-3	0.01e-3	1.1e-3	0.56%
PTP IN	137	0.2	0.5	1.2	0.96%
PTDP	115	0.02	0.22	0.16	0.24%
WTT1	624	0.3	0.6	5.6	0.90%
WTT2	5	0.2	0.5	0.5	14.70%
ZT41	334	0	-	1.1	0.33%
ZT42	10	0.1	-	0.1	1.41%
TT41	15	0.1	-	0.3	2.00%

Chapter 5

Structural Analysis

Structural analysis of the Francis runner was performed in ANSYS Mechanical using static structural analysis. Unfortunately, it was not possible to use already calculated CFD results to perform an one-way FSI simulation, due to differences between CFD model and the mechanical model. Attempts were made to try to fit the mechanical model to the model used for CFD, but without results. Instead, the runner blades of the mechanical model was split into segments and pressure was manually applied to each segment. Pressure on suction side and pressure side were calculated based on a theoretical approach using flow analysis in a rotating channel. Pressure measurement from the experiment were used together with the equation for energy conservation in a rotating channel (rothalpi). The procedure for these calculations can be found in Appendix B.

It is important to say that the method that is used here is a simplification of the real problem, and that the simulations are purely static, i.e. no dynamical effects.

5.1 ANSYS Mechanical - Setup and model

The geometry consist of 1/15 part of the runner (1 full length and one splitter blade) and can be seen in Figure 5.2. By applying cyclic symmetry conditions, it is possible to simulate the whole runner by only using one symmetrical part (only for static simulation). Cyclic regions were applied on the hub, shroud and center of the geometry together with match control, which is used to match cyclic faces. The result of the simulation is strain and stress distribution for the whole runner. It is also possible to choose how man section that should be displayed, for more detailed view of the stress distribution.

To be able to apply the calculated pressure on the blade, it had to be split into several segments. This was done by using SpaceClaim, a 3D modelling software available in ANSYS. The full length blade was split into sixteen segments, while the splitter blade was split into eighth segments. Figure 5.2 shows the model were the blades is split into segments.

The material for the runner blades of the Francis model turbine is a copper-tin alloy called JM 3 [42]. The properties of this alloy is can be found in Table 5.1. In

ANSYS Mechanical, materials can be chosen or specified in the Engineering Data library. JM 3 alloy had to be specified since it was not available in the material library. The material for the hub and shroud is another copper-tin alloy called JM 7. The JM 7 properties are a bit different, and both yield strength and tensile strength is higher. Since only the blades are of interest, the JM 3 properties was used for the whole 3D model.

Table 5.1: Material Properties of JM3 Alloy

Material Properties	
Density [kg/m^3]	8800
Yield strength [MPa]	150
Tensile strength [MPa]	270
Young's modulus [MPa]	100000
Poisson's ratio [-]	0.34

Mesh
Because of the complexity of the model, tetrahedral mesh elements, with 10 nodes (TET10) were used for the whole body. Body sizing were used for the hub and shroud to specify the maximum allowed mesh size, which was set to 8mm. To get a higher mesh resolution on the blades, face sizing were used with a maximum value of 2mm. Pinch control was used to repair a bad mesh on narrow and sharp edges. Match control was applied to the hub, shroud and center to make sure that the mesh matches when the model is putted together to the whole runner. Figure 5.1 shows a histogram of the mesh quality, where the x-axis displays the element quality between 0 and 1. Most of the elements are to the right in the Figure, which tells that most of the mesh elements are of high quality.

A mesh independence test was conducted by changing the maximum allowed size for the mesh on the blades, while the body sizing was kept constant. Table 5.2 shows the results from the BEP simulation when the maximum size was changed from 8mm to 1.8mm. It can be seen that the stresses converged towards $\approx$ 7.6MPa quickly. In order to reduce computational time, a size of 2mm was chosen for the rest of the simulations.

Boundary conditions
Constrains and boundary conditions were applied to the 3D model, to ensure that the operating conditions are the same as for the real turbine. Standard earth gravity was applied in the negative z-direction. Rotational speed was applied to include the centrifugal forces. Displacement constrains was applied to the turbine shaft surfaces, to make sure that the runner would stay at the same location and only

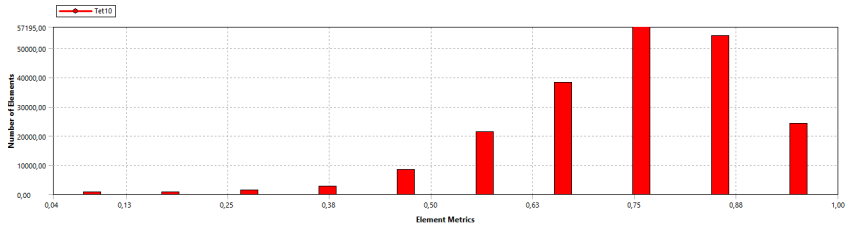

Figure 5.1: Mesh quality for the mesh used for all simulations.

Table 5.2: Mesh independence test, with TET10-elements. Stress value taken from the suction side of the trailing edge near the hub.

Elements	Nodes	Size of element on blades	Max stresses
38284	63542	8mm	8.557MPa
46227	78139	6mm	8.331MPa
68307	117969	4mm	8.100MPa
101043	175546	3mm	7.945MPa
110917	193361	2.5mm	7.813MPa
138239	239591	2mm	7.575MPa
155580	268742	1.8mm	7.61MPa

rotating with the applied speed. Pressure load were applied to each blade segment, according to the operation point. A total of 48 pressure values had to be manually entered for each simulation. Pressure values were based on measurements values, together with a flow analysis for calculating the corresponding pressure distribution on the suction-side and pressure-side of the blade. Figure 5.2 shows the 3D model with the pressure loading, speed and gravitational acceleration. The displacement constrains can not be seen from the view-direction.

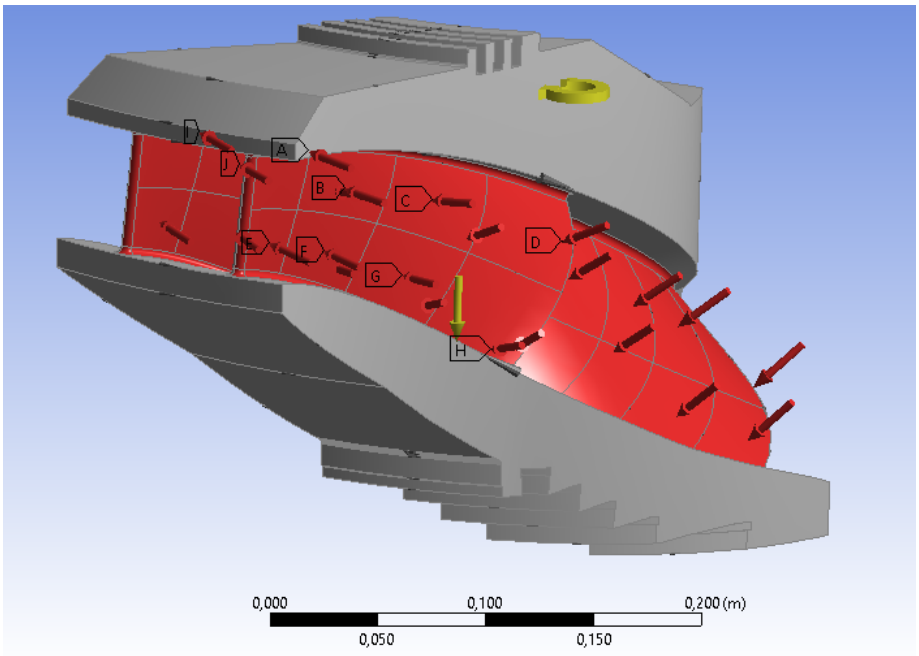

Figure 5.2: 1/15 part of the runner. The runner blades is split into segments. Pressure loading and boundary condition is applied at mechanical model.

Chapter 6

Results

6.1 Experimental results

All 269 individual operation point have used for creating a complete Hill Chart of the Francis-99 turbine. The result can be seen in Figure 6.1. The best efficiency point can be found at $N_{ED} \approx 0.1795$, with a speed of 335 rpm. The best efficiency is just above 92%.

Pressure pulsations were analyzed for sensor; PTGV4, PTR1, PTR2, PTR3, PTR4, PTDT13 and PTDT17. Peak-peak values were calculated for each sensor based on the Histogram method with 97% confidence level. MatLab code for the peak-peak calculation can be found in Appendix E. Pressure pulsation diagram was created for all sensors, and Figure 6.2, 6.3 and 6.4 shows the result for sensor PTDT17, PTR1 and PTGV4. The diagrams for the other pressure sensors can be found in Appendix D. The pressure diagrams are normalized based on the value at BEP, which can be found in the Figure description and in Table 6.2 - 6.6. MatLab code for creating pressure pulsation diagram, together with Hill Chart can be found in Appendix E. In addition to this, six points were chosen for further analysis; Speed-No-Load (SNL), Minimum Load (ML), Part Load (PL), Best Efficiency Point (BEP), High Load (HL) and Full Load (FL). Each point were compared with another operational point with the same guide vane opening, were the speed was reduced by 50rpm (≈15%) and 100rpm (≈30%). Table 6.1 shows more detailed information on these points. Table 6.2 - 6.6 shows the change in peak-peak value relative to the normal operation point with synchronous speed (335rpm).

Frequency analysis have been conducted using Welch method, with a Hann window with 50% overlap. This have been done for the six same operating points as above, for both synchronous and reduced speed, to find out which pressure pulsation phenomena that occurs and which is most dominating. Figure 6.5 shows the frequency plot for the different sensors at PL operation, while Figure 6.5 shows the same for HL operation. The plots for the other operation points, for synchronous speed, can be found in Appendix D. A MatLab script of the analysis is included in Appendix E.

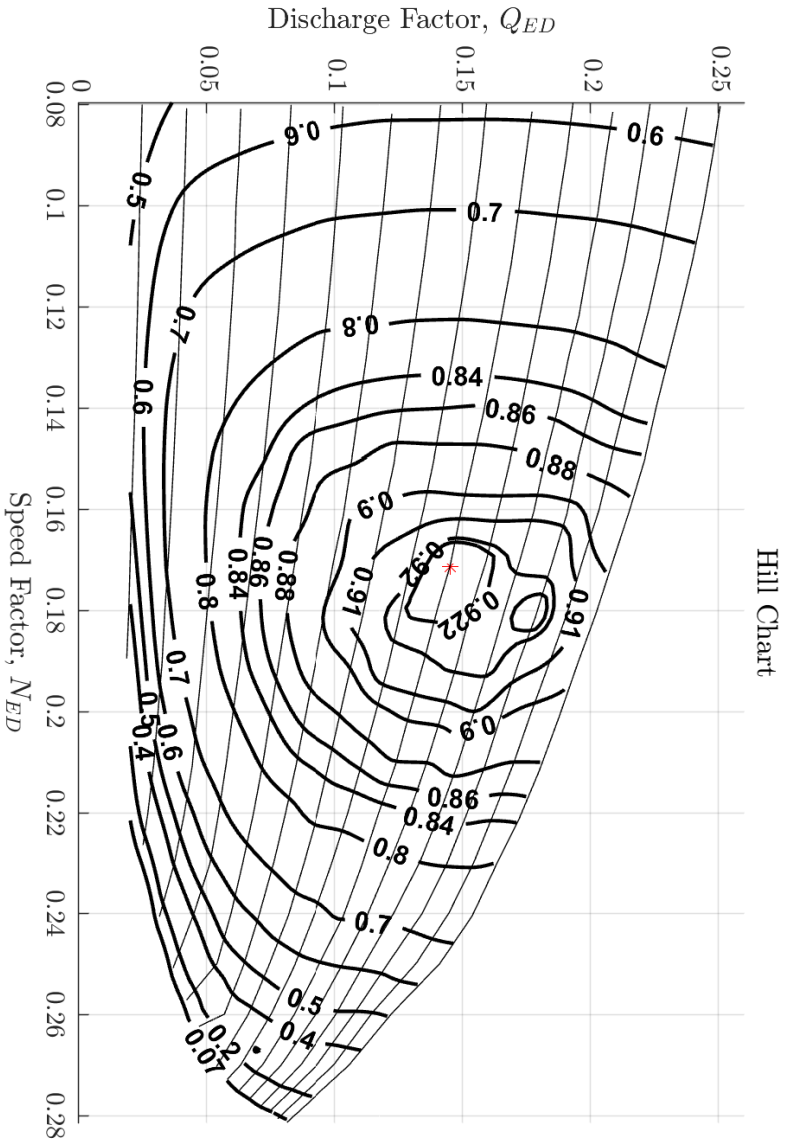

Figure 6.1: Hill Chart for the Francis-99 turbine for the whole operating range.

Table 6.1: Detailed information on operational points used in further analysis

	GV opening [degree]	Efficiency [%]	N_{ED} [-]	Q_{ED} [-]	Speed [rpm]	Power [kW]
ML	4	84.9	0.1798	0.067	338	9.04
PL	7	91.3	0.1795	0.111	336	15.9
BEP	10	92.2	0.1795	0.155	335	22.1
HL	12	92.2	0.1795	0.178	334	25.4
FL	14	90.7	0.1795	0.201	333	28.0
SNL	1	40	0.1795	0.02	340	1.3

Table 6.2: Peak-peak values for PTDT17, 97% confidence level. The last two columns show the change in value relative to the synchronous speed. All values are in kPa.

	Sync. speed [≈335rpm]	Reduced 1 [≈280rpm]	Reduced 2 [≈244rpm]	Relative change 1	2
ML	2.730	1.371	0.827	-49.8%	-69.7%
PL	2.116	1.650	1.680	-22.0%	-20.6%
BEP	2.288	2.503	2.252	+9.4%	-1.6%
HL	2.322	2.873	3.360	+23.7%	+44.7%
FL	3.032	3.685	4.868	+21.5%	+60.5%
SNL	5.270	3.488	2.705	-33.8%	-48.7%

Table 6.3: Peak-peak values for PTR1, 97% confidence level. The last two columns show the change in value relative to the synchronous speed. All values are in kPa.

	Sync. speed [≈335rpm]	Reduced 1 [≈280rpm]	Reduced 2 [≈244rpm]	Relative change 1	2
ML	4.329	5.821	6.931	+34.5%	+60.1%
PL	3.494	8.709	11.897	+149.2%	+240.5%
BEP	3.679	7.395	13.773	+101.0%	+274.4%
HL	3.739	6.564	12.815	+75.6%	+242.7%
FL	4.263	4.723	11.036	+10.8%	+158.9%
SNL	4.333	4.086	3.687	-5.7%	-14.9%

Table 6.4: Peak-peak values for PTR2, 97% confidence level. The last two columns show the change in value relative to the synchronous speed. All values are in kPa.

	Sync. speed [≈335rpm]	Reduced 1 [≈280rpm]	Reduced 2 [≈244rpm]	Relative change 1	2
ML	4.196	2.898	3.293	-30.9%	-21.5%
PL	2.860	3.059	3.951	+7.0%	+38.1%
BEP	3.042	3.167	4.627	+4.1%	+52.1%
HL	3.043	3.397	4.441	+11.6%	+45.9%
FL	3.425	3.604	4.944	+5.2%	+44.3%
SNL	4.79	3.173	2.471	-33.8%	-48.4%

Table 6.5: Peak-peak values for PTR4, 97% confidence level. The last two columns show the change in value relative to the synchronous speed. All values are in kPa.

	Sync. speed [≈335rpm]	Reduced 1 [≈280rpm]	Reduced 2 [≈244rpm]	Relative change 1	2
ML	5.769	1.618	1.586	-72%	-72.5%
PL	1.624	1.504	1.688	-7.4%	+3.9%
BEP	1.671	1.713	1.931	+2.5%	+15.6%
HL	1.657	1.838	2.573	+10.9%	+55.3%
FL	1.928	2.449	3.753	+20.7%	+94.7%
SNL	4.89	3.795	2.28	-22.4%	-53.4%

Table 6.6: Peak-peak values for PTGV4, 97% confidence level. The last two columns show the change in value relative to the synchronous speed. All values are in kPa.

	Sync. speed [≈335rpm]	Reduced 1 [≈280rpm]	Reduced 2 [≈244rpm]	Relative change 1	2
ML	2.957	2.618	2.944	-11.5%	-0.5%
PL	2.872	2.892	3.608	+0.7%	+25.6%
BEP	2.361	2.543	2.995	+7.7%	+26.8%
HL	2.563	2.497	3.195	-2.6%	+24.6%
FL	3.214	3.331	3.903	+3.6%	+21.4%
SNL	2.743	1.829	1.361	-33.3%	-50.4%

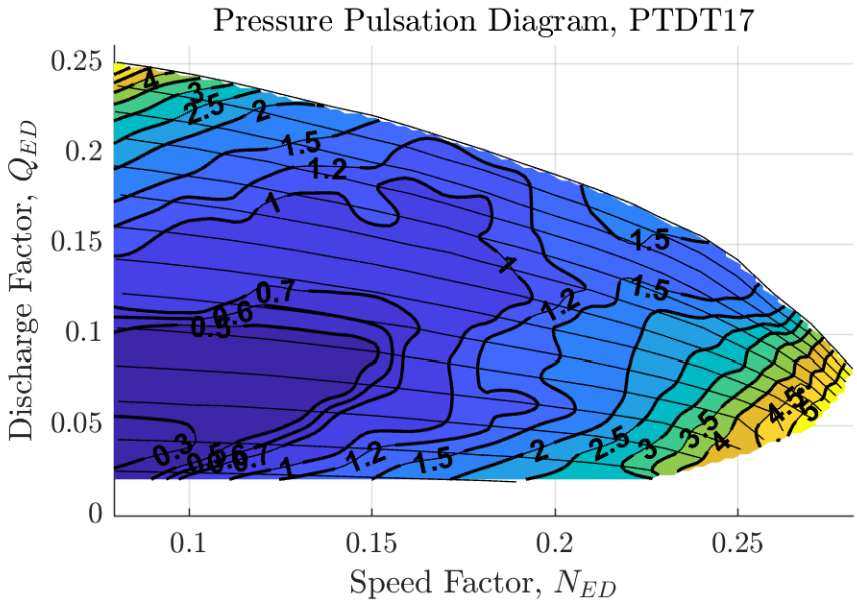

Figure 6.2: Peak-peak values are normalized based on BEP value (2.29kPa)

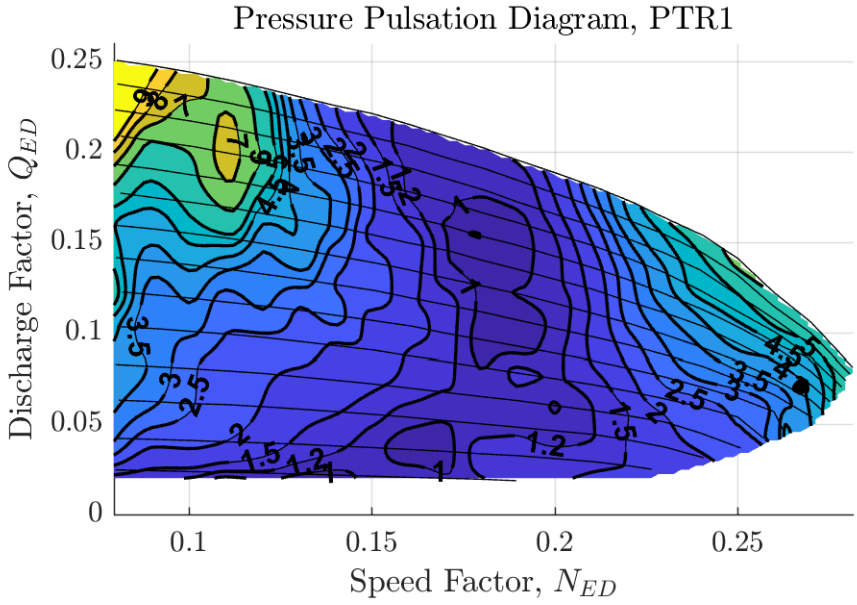

Figure 6.3: Peak-peak values are normalized based on BEP value (3.67kPa)

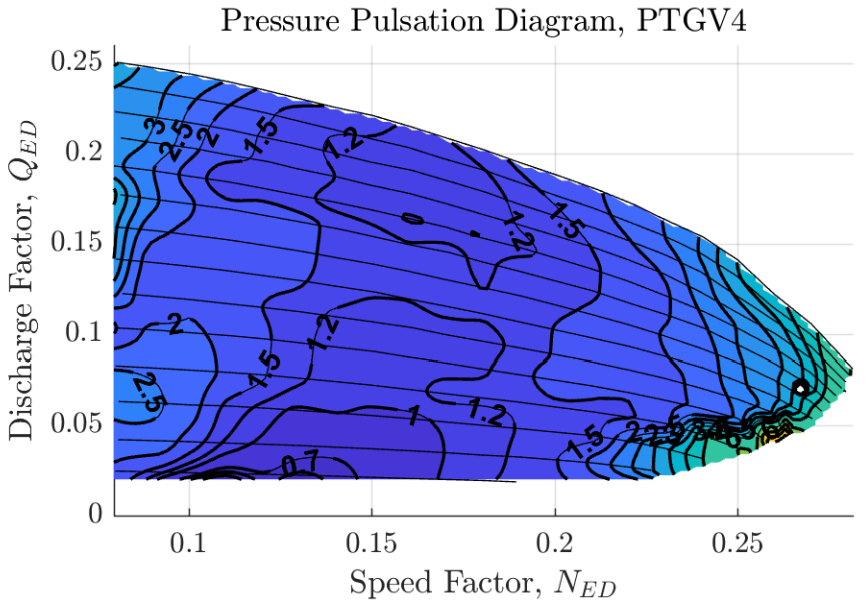

Figure 6.4: Peak-peak values are normalized based on BEP value (2.37kPa)

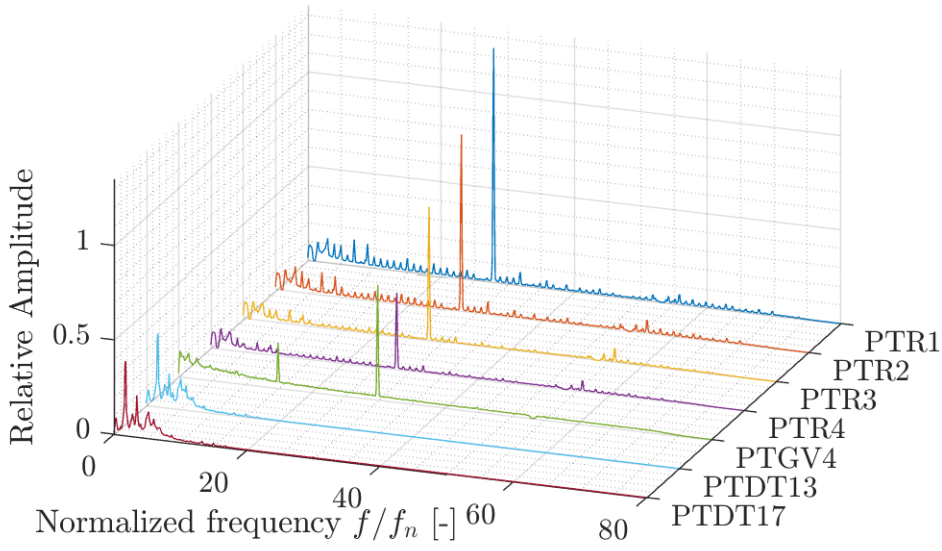

Figure 6.5: Frequency analysis for PL operation point. Frequency is normalized based on the runner frequency.

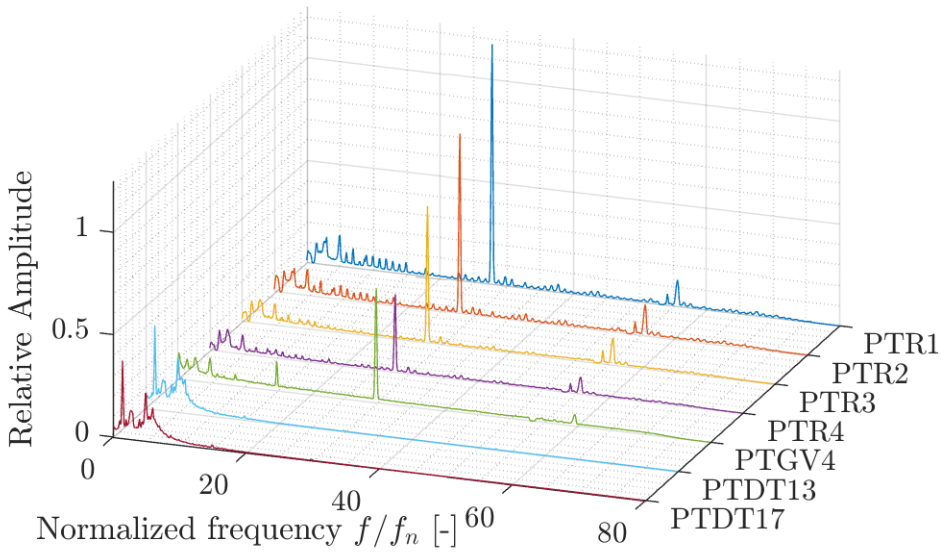

Figure 6.6: Frequency analysis for HL operation point. Frequency is normalized based on the runner frequency.

6.2 Structural results and validation

Structural analysis was conducted in ANSYS Mechanical with the static structural analysis system. A total of eighth operation points with two simulation per point were simulated. One with the mean pressure, and the other with additional pressure due to the pressure pulsations. The difference in pressure (for the same operation point) is assumed to be the stress amplitude. Detailed information about the different operation point can be seen in Table 6.7. Figure 6.7 shows the result for the whole runner at PL operation, while Figure 6.8 shows the result for the suction side for one section of the runner also at PL operation. The stresses presented here is calculated with von-Mises equivalent stress.

A section of the full length blade is not fastened to the shroud. This causes a sharp corner in the mechanical model, were Figure 6.8 shows the maximum stresses, which is not present in the real model turbine. The sharp corner causes a stress singularity in the model, and the stresses increases with the mesh resolution. It can also be seen by the high stress gradient near the corner. Therefore, the point with highest stresses is found at the suction side of the trailing edge near the hub. At the inlet, the highest stresses is found at the leading edge near the shroud, but this value is small compare to the trailing edge stresses. Table 6.8 shows the result from the simulations. Maximum stresses is taken from the suction side of the trailing

edge near the hub. The stress amplitude $\Delta\sigma_A$ is the difference between maximum stresses for the two simulations (mean pressure, and mean pressure with half the peak-peak value added).

Validation of results

Validation of stresses in a structural analysis is normally done by comparing results with experiments, and often by comparing strain-measurement from curtain positions on the runner blade [33]. Strain was not measured during the experiment, and it is therefore not possible to validate the results by strain. Instead, torque measurements can be used. Table 6.8 shows the simulated torque and the measured torque during the experiment. The deviation from the measured torque is varying from $\approx$1% (ML-50rpm) to $\approx$22% (ML). In addition, similar work have been done in a previous master thesis written at the Waterpower Laboratory at NTNU for the same turbine and same head at BEP [42]. The maximum stresses at BEP were found at the trailing edge, with a stress value of 7.07MPa, which is similar to the maximum stresses found in this result.

Table 6.7: Operation point used in structural analysis

	GV opening [degree]	N_{ED} [-]	Q_{ED} [-]	Speed [rpm]	Mech Power [kW]
BEP	10	0.1785	0.154	333	22.1
BEP-50rpm	10	0.1505	0.1685	280	23.2
PL	7	0.1806	0.1112	338	15.9
PL-50rpm	7	0.1509	0.1232	282	17.1
PL-100rpm	7	0.1309	0.1295	244	16.8
ML	4	0.1805	0.065	340	8.8
ML-50rpm	4	0.1499	0.0722	282	9.7
ML-100rpm	4	0.1299	0.0761	244	9.7

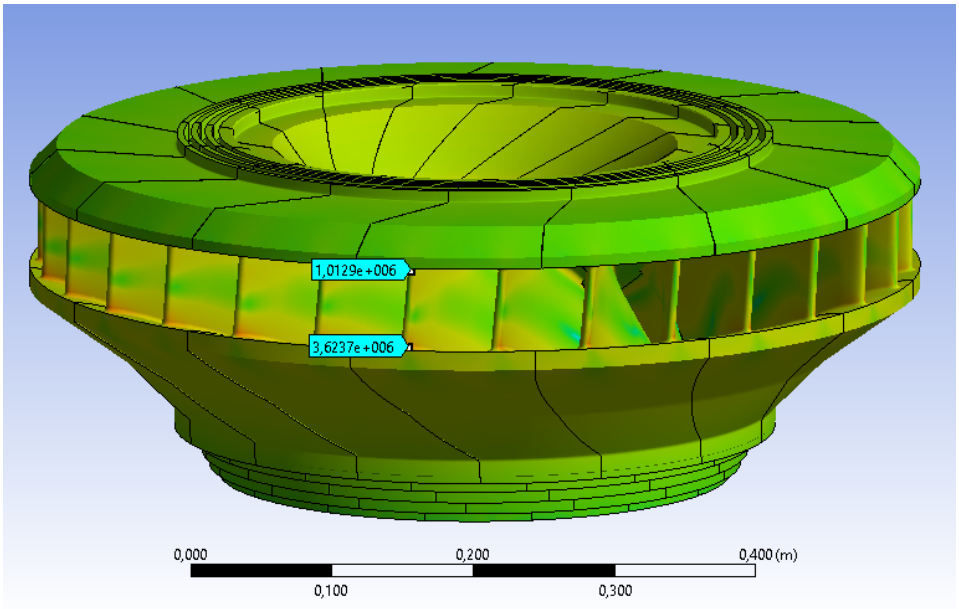

Figure 6.7: Stress distribution in the runner at PL operation. It shows that the highest stresses at the inlet is found at the pressure side of the leading edge near the shroud, with a stress value of 3.62MPa. The stress at the pressure side of leading edge near the hub is 1.01MPa.

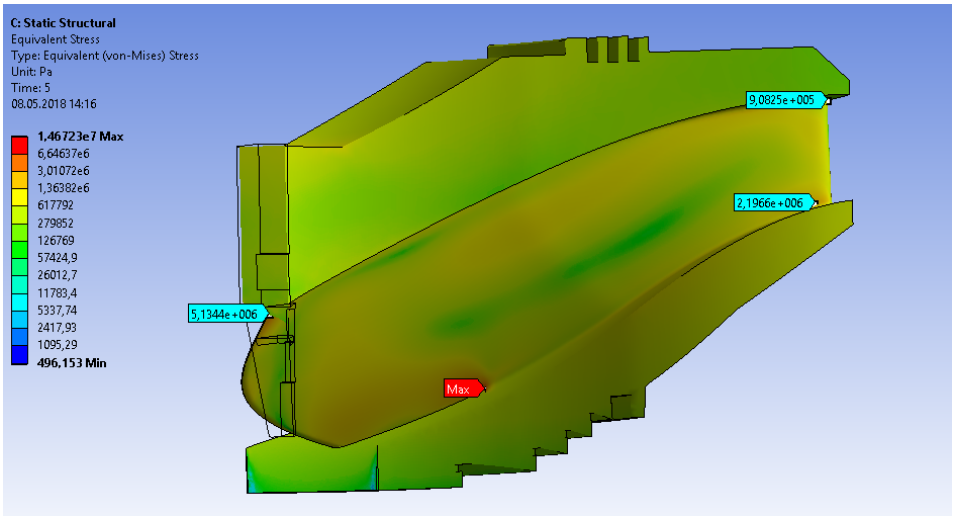

Figure 6.8: Stress distribution at the suction side of one full length blade at PL operation. Maximum stress is found in the sharp corner where the blade is not fastened towards the shroud anymore, with a value of 14.67MPa. Because of stress singularity, this value is strongly depended on mesh resolution. The other point with high stresses are at the trailing edge near the hub, with a stress value of 5.13MPa.

Table 6.8: Stress and torque results from structural simulations. Max stress value is from suction side of trailing edge near the hub. $\Delta\sigma_A$ shows the increase in stress when the pressure pulsation effect is added to the mean pressure. Comparing of torque is used for validation.

	N_{ED} [-]	Max stress [MPa]	$\Delta\sigma_A$ [Nm]	Torque [Nm]	Exp. torque [Nm]
BEP	0.1785	7.575	1.844	664	634
BEP -50rpm	0.1505	7.419	1.791	709	788
PL	0.1806	5.138	2.190	490	451
PL-50rpm	0.1509	4.888	1.467	514	580
PL-100rpm	0.1309	4.600	1.373	548	656
ML	0.1806	2.301	8.122	302	247
ML-50rpm	0.1499	2.302	1.675	324	327
ML-100rpm	0.1299	2.135	1.607	312	378

6.3 Fatigue assessment

In order to perform fatigue assessment, valid S-N data must be found for the correct material. The highest stresses in the runner is found in in the T-joint between the blade and the hub, which is normally welded and thereafter grinded to a smooth surface (for a prototype)[31]. S-N data from the International Institute of Welding (IIW) for a 13Cr-4Ni weld, with stress ratio of R=-1, have been used. Specimen with a smoothed butt weld was used for creating the S-N data, and not for a T-joint. A butt weld is assumed to have no residual stresses, while a T-joint have stress gradients. Because of this, a butt weld tends to fail before a T-joint [31]. Therefore, the S-N curves can be somewhat conservative. By using equation 6.1, together with the curve constants in Table 6.9, the S-N curves for both CAL and VAL can be created. S-N curves can be seen in Figure 6.9. The S-N data is limited to 10^9 cycles [21].

Goodman method was used to find the effective stresses for a the same stress ratio as the S-N data (R=-1). Table 6.10 shows the effective stresses. From the frequency analysis it can be seen that the guide vane passing frequency is the most dominating pressure pulsation on-board the runner for all operation point, except for ML, where draft tube pulsation also has high amplitudes. It is therefore assumed that the effective amplitudes in Table 6.10 can be used together with the guide vane passing frequency to estimate accumulated damage on the runner during steady state operation. Since the objective of this thesis is to find the operating range for the turbine with lowest material stresses, the different operation points will be compared to each other. Table 6.11 shows the accumulated damage per 1000 operation hour for the different points, and the relative change by reducing the speed of the turbine. The accumulated damage is calculated by using Minor's rule (Equation 2.18) together with the corresponding cycles to failure for the effective stress amplitude for the VAL curve. The number of cycles to failure is presented in Table 6.11.

Table 6.9: Curve constants for S-N curves for 13Cr-4Ni, taken from [21].

Cycles	C	m
$N \leq 1e7$	$2.82e12$	3
$N > 1e7$, CAL	$9.064e46$	22
$N > 1e7$, VAL	$1.207e16$	5

$$2\sigma_A = \left(\frac{C}{m}\right)^{\frac{1}{m}} \tag{6.1}$$

Table 6.10: Stress amplitudes form structural analysis converted to effective stress for stress ratio R=-1, using Goodman method. All values are in MPa.

BEP	BEP-50	PL	PL-50	PL-100	ML	ML-50	ML-100
1.897	1.842	2.233	1.494	1.397	8.192	1.689	1.620

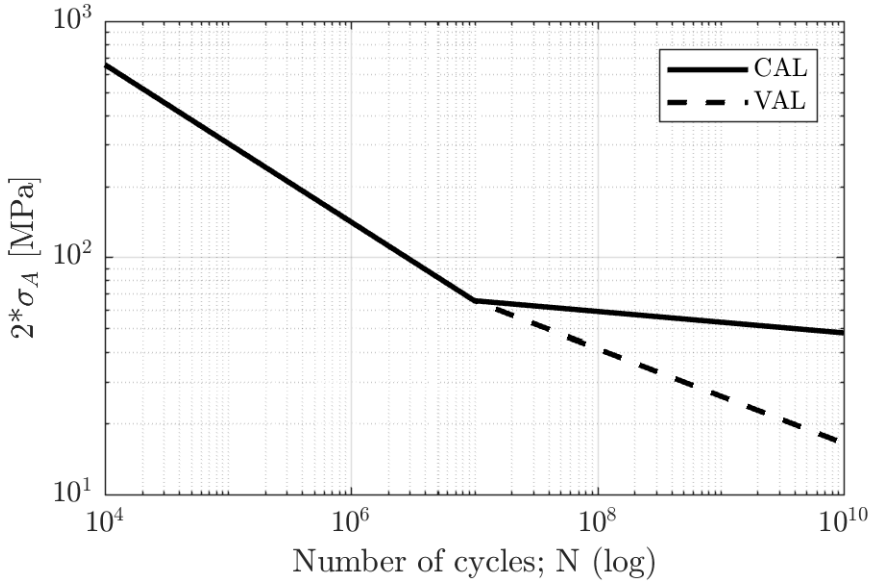

Figure 6.9: S-N curve created in MatLab from the constants in Table 6.9. S-N curve is for a smooth butt weld for 13Cr-4Ni steel. Curves are created with a failure probability of: $P_f \leq 5\%$

Table 6.11: Accumulated damage per 1000 operation hours. Stress amplitudes from Table 6.10 is used to find the number of cycles to failure. Number of cycles per 1000 operating hours is found based on the guide vane passing frequency.

	Cycles to failure	Accumulated damage	Relative Change from synchronous speed
BEP	1.5354e13	3.643e-5	-
BEP-50rpm	1.7787e13	2.6446e-5	-27.40%
PL	6.7938e12	8.358e-5	-
PL-50rpm	5.0676e13	9.3488e-6	-88.82%
PL-100rpm	7.0888e13	5.7826e-6	-93.08%
ML	1.0223e10	5.5870e-2	-
ML-50rpm	2.7442e13	1.7264e-5	-99.97%
ML-100rpm	3.3805e13	1.2126e-5	-99.98%

Chapter 7

Discussion

7.1 Experimental measurements

A Hill Chart is used to present the performance for the model turbine, for the whole operating range. It was therefore natural to use the Hill Chart as inspiration when creating pressure pulsations diagrams for the whole turbine. Since each pressure sensor is measuring different pressure, one diagram had to be made for each of the sensors. Pressure diagrams presented in this thesis are normalized based on the value at BEP, to show how the pulsations are varying. Figure 6.4 - 6.2 shows that the pulsations are behaving differently through the turbine. This makes sense, as there are different pulsation phenomena at different locations. The pressure diagram for the draft tube (PTDT17 sensor) shows a trend towards lower pulsation for lower speed and discharge. At the inlet of the runner (PTR1 sensor), it is clear that the pulsations are lowest in an area around BEP, and when the speed is slightly reduced. In Appendix D, the other diagrams for the on-board sensors can be found, which shows a similar shape as the one for PTR1. Specially PTR2 sensor is showing a similar shape, while PTR3 and PTR4 gives indications that peak-peak values can be decreased by reducing the speed of the runner at operation blow BEP. The PTGV4 pressure diagram is having a similar shape as the on-board sensors, but it seems as the pulsations are lowest around the synchronous speed and an area where the speed is slightly reduced.

7.1.1 Change in pressure pulsation amplitudes

Six operating points were chosen for further analysis; ML, PL, BEP, HL, FL and SNL. Pressure pulsations were compared for synchronous speed operation, and operation when the speed is reduced by $\approx$50rpm and $\approx$100rpm, with constant guide vane opening. In the paper that was written for CRHT-VIII'18 Conference [32], operation point with an increase of 50rpm were analyzed as well, but all results showed an increase in pressure pulsation intensity. Therefore the focus is only for speed reduction. Table 6.2 - 6.6 shows the results for most of the pressure sensors, and the relative change of peak-peak values. The results shows that for operation at BEP and higher loads, pressure pulsations intensity are lowest at synchronous speed for all pressure sensors. The same trend can also be seen directly from the pressure pulsation diagrams.

For operation below BEP, the trend is changing. For PL operation, the peak-peak values are reduced only for the draft tube. This makes sense, as reducing the speed reduces the swirling component in the draft tube. The results shows that the pressure pulsations for PTDT17 is reduced by approximately 21% for both speed reductions, while for ML and SNL, the pulsations are reduced even further. For the other sensors, the peak-peak values are increased for PL operation. Operation at ML shows that peak-peak values is reduced for all sensors except PTR1, and the highest reduction is for the PTR4 sensor, where peak-peak values is dropping with 72% when the speed is reduced. For PTDT17 (and PTDT13) it is clear that a further speed reduction will results in lower and lower values, while for the other sensors, peak-peak values are decreasing at first before it starts increasing again. This trend is more clear when looking at the pressure pulsation diagrams. For SNL operation, peak-peak values are decreasing for all sensors when the speed is reduced. At the PTR4 sensor with speed reduced by 100rpm, there is an 53.4% decrease compared to synchronous speed. This can also be seen in the pressure pulsation diagrams, where the pulsation are reduced for decreasing speed.

A speed reduction of 50rpm and 100rpm was chosen arbitrarily and other values can give even lower pressure pulsations. This should be checked in further work, and one alternative would be to optimize the operation pattern based on the lowest peak-peak values. This can be done by optimizing based on the lowest peak-peak value for each Q_{ED} value.

7.1.2 Frequency analysis

Frequency analysis was conducted for the six different operation points discussed above. The analysis reviled what pulsating phenomena that was most dominating for the different operation conditions. By using the theory in Chapter 2, it is possible to predict what frequencies that will occur and than locate them in the frequency analysis. The results from frequency analysis is presented in Figure 6.5 and 6.6, while the Figures for BEP, ML, FL and SNL is attached in Appendix D. Analysis have also been conducted for the same guide vane opening when the speed is reduced, but the plots are not included.

Speed-No-Load

At SNL the flow is irregular and consist of stochastic pulsation in the low frequency range. On-board the runner, the dominating frequency is the guide vane frequency ($28 \cdot f_n$) together with a low frequency at $0.32 \cdot f_n$. The same normalized frequencies is also dominating when the speed is reduced, but with lower amplitudes and with more stochastic pulsation in the low frequency range. Along the guide vanes, the blade passing frequency ($30 \cdot f_n$) is most dominating. Due to the

effect of splitter blades another frequency which is half of the blade passing is also contributing.

Minimum Load
At minimum load there are stochastic pulsation in the low frequency range, and the RSI is dominating both on-board the runner an along the guide vanes. In addition, the draft tube vortex rope is dominating in the draft tube with a frequency of $0.33 \cdot f_n$. When the speed is reduced, the draft tube pulsation due to the vortex rope is almost removed. Also the stochastic pulsation has been drastically lowered. The reason for this is most likely due to a reduction of the swirl component because the speed is reduced. This reduction is most likely the reason why the overall pulsation are being lowered when operating at reduced speed at ML.

Part Load
At Part Load, the blade passing frequency, and half the blade passing frequency due to splitter blades, is most dominating along the guide vanes, while the guide vane passing frequency is dominating on-board the runner. In the draft tube, the vortex rope is most dominating, but with relative small amplitudes compared to RSI. When the speed is reduced, the draft tube pulsation are lowered, while the RSI seems to increase.

Best Efficiency Point
At BEP, RSI is the most dominating frequency on-board the runner and along the guide vanes, together with half the blade passing frequencies due to the splitter blades. Also the second harmony of the RSI can be seen. In the draft tube there is a frequency of $1.69 \cdot f_n$, but it is unclear what it comes from. When the speed is changed, the same frequencies are dominating, but the amount of stochastic pulsation are increasing.

High Load and Full Load
High Load and Full Load has most of the same behaviour with regard to the frequencies. Along the guide vanes, the blade passing frequency is dominating. On-board the runner the guide vane passing frequency is dominating. Also the 2. harmonic of the RSI can be seen in the frequency analysis. There are also some stochastic pulsation in the low frequency range at all sensors. Also here the $\approx 1.69 \cdot f_n$ frequency is present, but only in the draft tube. It is not clear what it comes from, but vibration from the rig itself might be the solution. Normalized frequencies are the same when operating at lower speeds.

Transients, SNL and RSI are considered the main fatigue contributors for high head Francis turbines [34], when excluding LCF such as starts and stops. There-

fore it is of highest interest to lower the pressure pulsation intensity for SNL operation, and where RSI is dominating with large amplitudes. It is quite clear from the frequency analysis that RSI is most dominating from PL operating up to FL operation, which is normal for a High Head Francis turbine. From the analysis it seems as the most preferable operation is normal operation at synchronous speed when operating above PL, with regard to RSI. For ML and SNL operation, speed reduction can reduce the pulsation by varying degree. Therefore, to lower the fatigue contributing from deep part load and SNL operation, speed reduction can be used. RSI frequencies are speed dependent, and will change by changing the speed. It is therefore vital to know the natural frequencies of the structure to avoid operation that can cause resonance in the system.

7.2 Structural analysis

Structural analysis was performed to find the stresses in the runner due to pressure pulsation. Only the runner was investigated, since its the most vulnerable part of the turbine. The most used method for determine stresses is to use CFD results and map the pressure distribution to the mechanical model (one-way FSI), or to evaluate the dynamical behaviour and stresses by a harmonic response analysis [33]. Because the mechanical model was not exactly similar to the one used for CFD, it was not possible to perform a one-way FSI simulation with already calculated CFD results. Instead a static mechanical simulation had to be done, were pressure was manually applied to the model. By doing this, all dynamical effects are excluded and the simulations are purely static. Since the dynamical behaviour can induce large stresses, the result will only be an approximation, and can be used to compare the operation points relatively to each other. It is assumed that the frequencies of the simulated operation points is not closed to the natural frequency of the runner, and it will not be excited by the pressure pulsations.

7.2.1 Known errors

In all numerical simulation, there will be numerical errors due to the scheme that is used, computer floating point errors and discretization errors. In this case, since the applied pressure loading is calculated by an theoretical approach, with several assumption, this will be the main contribution for errors in the results. In Appendix B, the assumptions was explained briefly. One assumptions was the change of relative velocity through the turbine is the same for all operation point. This was necessary in order to calculate the pressure, but in reality this is not the case. Flow- and speed-changes will change the inlet and outlet angle of the flow. This will cause a change of relative velocity through the runner. The pressure distribution that is calculated will therefore only be an approximation of the real one.

To be able to calculate the pressure not only at the hub-streamline, it was assumed that the pressure was the same at the center- and shroud lines as at the hub line, which will introduce more uncertainties in the results.

To calculate the pressure at the suction side and pressure side the Rothalpi equation was used. Rothalpi is an expression for the energy conservation in a rotating channel and its value is constant along a streamline if friction is neglected. In a Francis runner it is assumed that Rothalpi is constant in the whole runner channel. During the calculation of Rothalpi, it was clear that its value was not even closed to constant, and varied from 50 m^2/s^2 to 100 m^2/s^2. Since the pressure is measured, and the angular velocity is known is this an indication that the geometry, and therefore also the curvature, is not properly calculated. This will result in a incorrect pressure distribution in the runner channel.
It was chosen to split the full length blade into 16 segment (each side), and more segments would have given better results due to more accurate pressure values. It was not made any attempt to increase the number of segments due to the time it took to manually apply the pressure on the model.

7.2.2 Stress results

The results are showing the the most stressed area in the runner is on the suction side of the trailing edge on the blade near the hub. Also the point were the blade is no longer fastened towards the shroud had high stress concentration, but because of a non-real sharp corner on the model the stresses did not converge. It is assumed that the real stress at this location is lower than at the hub, because the stresses is dropping with an order of magnitude close to the corner. For a high head Francis turbine, it is normal that the highest stresses ate at the trailing edge near the hub and near the shroud [33].

From the simulation when only the mean pressure was used, the maximum stress is reduced from BEP to PL to ML. This makes sense as the load is lowered, which gives lower power output and therefore less stresses. The stress amplitude, $\Delta\sigma_A$, is found based on the difference in the maximum stresses between the simulation with the mean pressure and when the pressure pulsation effect is added. Half the peak-peak value of the pulsation is added on the pressure side, while its subtracted on the suction side. This results in a worst-case situation that gives the maximum static stresses from the pressure. Therefore, it is assumed that the results can be used to investigate trends and the relative change in stresses between the different operation points.

For ML operation, the max stress is relatively low (only 2.3MPa). This is expected since the turbine is only operating at 12 meters head, and therefore low pressures.

What is interesting is that the stress amplitude is a almost 4 time higher (8.1MPa). From the pressure pulsation diagrams, we can see that the pulsations are increasing a lot a ML compared to PL and BEP, especially for PTR3 and PTR4 sensor. When the speed is reduced, the maximum stress (without the pressure pulsation effect) is quite similar, but the stress amplitude drops from 8.1MPa to 1.7MPa. This shows good consistence with the pressure pulsation diagram for PTR4 sensor. For comparison, a reduction of 50rpm resulted in a 72% reduction in pressure pulsation, and a 79% reduction in stress amplitude. The same occurs for a reduction of 100rpm as well. This gives some indications that the stresses is showing the same trend as the pressure diagram of PTR4 sensor.

Also for part load the same trend is seen, where the stress amplitude is lowered when the speed is reduced. The only difference here is that the peak-peak values are increasing for all the on-board senors at PL, except PTR4 when the speed is reduced by 50 rpm. When looking are the pressure diagrams, there is almost no difference for when the speed is changed for PTR3 and PTR4 sensor. The drop in stress amplitude for reduced speed can be due to a change in pressure distribution on the blade when the speed is reduced, or due to errors in the calculation of the pressure distribution. What it seems is that the max stress, and the stress amplitude is mostly effected by the pressure at the PTR4 and PTR3 location, which makes sense in a static analysis since they are closest to the point of maximum stress. Also at BEP the stress amplitude is lowered from BEP to BEP-50rpm, even though the pressure pulsations are increased. But the change in stress amplitude is only 2%. From the pressure diagram, PTR4 and PTR3, it seems as there is no difference between these points, and it therefore makes sense that the stresses are similar.

From the eight points simulated, it seems as the stress amplitude is correlated with the pressure pulsations, and especially the pressure pulsations measured at PTR4, since this is closest to the point of highest stresses. It makes sense, at least in a static structural analysis that the stresses are directly correlated with the pressure, since their both are defined as load per area. The point with highest stresses is found based on the static analysis, but other areas can have large stresses as well due to excitation of the runner. This is not included in this work, but it is important to know that there is other areas with stress concentrations as well.

7.3 Fatigue

The stresses found in the structural analysis was used further for a fatigue assessment. Because the stresses in a model turbine is very low, and the corresponding cycles to failure is higher most S-N data are valid for, it was chosen to use a relative approach. This is done by comparing the accumulated damage between the different operation point. The material for the model turbine is a combination of

two copper alloys (JM3 and JM7), but it is chosen to use S-N data for 13Cr-4Ni stainless steel. This is because 13Cr-4Ni is mostly used for prototype turbines and thereby can this method, with the same S-N data, be used for fatigue assessment for prototypes later.

The Goodman method was used to calculate an effective stress amplitude, to accommodate for the mean stress. The result can be seen in Table 6.10. The local-stress approach was used together with Minor's rule in order to calculate the accumulated damage per 1000 operation hours. Since the guide vane passing frequency is most dominating on-board the runner, its frequency was used to calculate the number of cycles per 1000 hours operation. S-N data for 13Cr-4Ni from IIW was used to estimate the number of cycles to failure for variable amplitude loading, for the corresponding effective stress amplitude. The accumulated damage, cycles to failure and the relative change in accumulated damage can be seen in Table 6.11.

Since the results are based on the stresses from the structural analysis, the results will be directly linked to these results. All the cycles to failure are in the range of 10^{13} while operation at ML are in the range of 10^{10}. The accumulated damage for the different operation point shows the damage rate at the runner per 1000 operating hours. It can be seen ta the largest benefits comes from reducing the speed at ML. The accumulated damage is reduced by 99.97% when reducing the speed by 50rpm, and 99.98% when reducing by 100rpm, which is quite a drastic change. Also for PL operation, the accumulated damage is reduced by 88.8% (-50rpm) and 93% (-100rpm). For BEP, the accumulated damage is reduced by 27%, even though the effective stresses are quite similar. This shows that even a small change in the effective stress can have a large influence on the fatigue life.

Even though the guide vane passing frequency is used here to calculate the number of cycles to failure, other pressure pulsations will off course contribute to shorten the operating life. Stresses at SNL was not calculated, but at this operating point stochastic pressure pulsation will influence the runner. If the runner is excited by the RSI, large bending movement can occur, which will influence the fatigue life as well. When estimating the total fatigue life, and not only the effect for curtain loads, the number of starts and stops should also be taken into account. Because the focus for this work was to find the operating range were the stresses are lowest, and not estimating the total fatigue life, these topics has not been investigated further.

The S-N data used for calculations are only valid for cycles up to 10^9 [21], even though cycles up to $7 \cdot 10^{13}$ have been used. This is due to the small stresses that occurs in a model turbine that is operating at 12 meters head. Most test that aim

to create S-N data is only running up to 10^9 cycles, and the one that do not fracture before that is assumed run-outs [8]. Cycles that fracture before 10^7 cycles is mostly because of surface cracks, while fracture after is mostly because of subsurface cracks [8]. The cycles to failure that have been calculated here, is done by extrapolating the VAL line in the S-N data. This is not valid, but for this case it is assumed that it can be used to calculate the relative change. For a prototype, the stresses will be a lot higher, and this method can be used to perform a correct fatigue assessment.

Chapter 8

Conclusion

Pressure and efficiency measurement was conducted for the whole operating range of the Francis turbine at the Waterpower Laboratory at NTNU. Pressure pulsation diagrams were made for all pressure sensor in order to find the operating conditions with lowest pressure pulsation. The result are showing that for operation at PL and higher loads, pressure pulsation are lowest at synchronous speed. For operation below PL, pressure pulsation can be reduced by reducing the runner speed. The highest overall reduction is found for SNL, where a speed reduction resulted in a 53.4% reduction in peak-peak values for the PTR4 sensor. Frequency analysis reviled that the RSI is the most influencing flow phenomena with respect to pressure pulsation, but stochastic pulsation is also contributing at low loads, especially ML and SNL. Since the frequency of RSI is speed dependent, it is important to avoid operation where the frequencies can coincide with the natural frequency of the runner and/or other system frequencies.

Structural analysis was conducted to find the stresses in the turbine, and to correlate the stresses with the pressure pulsations. A total of eight operation point, with both synchronous speed and reduced speed, was chosen for analysis. Static simulation was done, where the stress distribution was calculated for each operation point. Dynamical effects are therefore excluded in the simulations. The effect of pressure pulsation was included by adding half the peak-peak values on the pressure and perform a second static simulation for the same point. The highest stresses was found on the suction side of the trailing edge near the hub. The results showed that the stress amplitude was reduced for BEP, PL and ML when the speed was reduced. The highest reduction was for ML. The results seems to correlate with the pressure pulsation diagram for PTR4 and PTR3. It can therefore by assumed that the stresses for the rest of the operation range also follows the same trend as these pressure pulsation diagram, but this has to be investigated further.

The stress amplitudes from the structure analysis was used in a fatigue assessment. The Goodman method was use to accommodate for the mean pressure and calculate an effective stress for a stress ratio of -1, so it could be used together with the S-N data. The S-N data was taken from 13Cr-4Ni stainless steel from IIW, for a butt weld specimen. The Local-stress approach was used, were the highest

stresses in the runner was used to estimate the accumulated damage. Since the effective stress is so low in the model turbine (since it operates at 12 meter head), the cycles to failure was out of validity of the S-N curve. Therefore only the accumulated damage per 1000 operation hours were used to compare the different operation point. The results showed that a reduction in effective stress amplitude had a large impact on the accumulated damage. The damage was reduced for all operation point when the speed was reduced, and the largest impact was for ML, where the damage was reduced by 99.97% and 99.98% for speed reduction of 50rpm and 100rpm.

Chapter 9

Further Work

In this thesis, only 8 operation points were investigated with respect to structural analysis. The results showed a trend that correlates with the pressure diagram of the PTR3 and PTR4 sensor. It would therefore be interesting to investigate other operation point above BEP, to check if the stresses also correlates with the same pressure diagram. It would also be beneficial to develop a mechanical model that is equal to the one used for CFD calculations at the Waterpower Laboratory. This way, CFD results can be used directly to perform a one-way FSI, which will give more accurate results. It is also of great importance to know the natural frequencies that can be excited in the turbine, especially when operation a variable speed. These can be found by conducting a modal analysis of the rotating runner.

The focus of this work was to find the operating range which give the lowest stresses, which was done by using the pressure pulsation diagrams. Another interesting approach would be to optimize the operation pattern with respect to variable speed, either by efficiency optimizing of pressure pulsation minimizing. If one should minimize pressure pulsation, it is the authors thought that the RSI should be minimize, since this is the main fatigue contributor to high head Francis turbines.

In the case of fatigue loading, a prototype should be investigate, since the stresses in a model turbine is too low to contribute to fatigue. It would therefore be interesting to perform measurements on a prototype runner that could operate with variable speed, and thereafter conduct a structural analysis and fatigue assessment. This measurements could be used to compare pressure pulsation diagram for a prototype and a model turbine.

For the fatigue assessment, the local-stress approach has used in this work due to its simplicity. This method has been used for several years by the industry, but is known to give conservative results due to high safety factors (S-N curves are made for low probability for failure). Since no S-N data was found for the same T-joint and environment that a turbine is operating in, it would be of importance to find/create more accurate data. Correct S-N data would give us the opportunity to perform more accurate fatigue calculations.

Another interesting possibility of variable speed would be to investigate if it can be used to reduce stresses at starts and stops and transient operation (load acceptance and load rejection). Starts and stops, together with transients give rise to high stresses in the runner. Today, the number of starts and stops and transient operation has increased and will most likely continue to increase when more intermittent power system is connected to the electrical grid. It would therefore be interesting to investigate the effect of introducing variable speed for these types of operation.

Even though a high head Francis turbine have been investigated in this thesis, both medium head and low head Francis turbines could benefit from using variable speed with respect to pressure pulsations. For medium and low head units it is the draft tube pressure pulsation at part load operation that normally causes highest damage to the turbine [33]. It is clear form the pressure diagram presented here that the pressure pulsation is drastically reduced in the draft tube when the speed is reduced. It can be assumed that the lower head units shows the same trend. It would therefore be interesting to investigate this, to see how much lower head units could benefit from variable speed.

Bibliography

[1] (1999). IEC 60193:1999, Hydrauic turbines, storage pumps and pump-turbines - Model acceptance tests, (1999-11-16). Technical report.

[2] (2001). HYDROPOWER IN NORWAY Mechanical Equipment.

[3] Agnalt, E. (2018). Measurement report 2017. HiFrancis WP 1.3. Technical report, NTNU.

[4] Alves, H., Otani, L., Segundinho, P., and Morales, E. (2015). Elastic moduli characterization of wood and wood products using the impulse excitation technique.

[5] Ashby, M. Jones, D. (2005). *'Engineering Materials 1*. Elsevier.

[6] Bak, M. (2016, accessed May 14, 2018). Mean stress corrections in fatigue. "https://caeai.com/blog/mean-stress-corrections-fatigue.

[7] Bathias, C. and Pineau, A., editors (2013). *Fatigue of Materials and Structures*. John Wiley & Sons, Inc., Hoboken, NJ, USA.

[8] Bathias, C. Paris, P. (2005). *'Gigacycle Fatigue in Mechanical Practice*.

[9] Bergan, C. and Dahlhaug, O. G. (2016). Experimental Investigation of a High Head Model Francis Turbine During Steady-State Operation at Off-Design Conditions.

[10] Brekke, H. (2001). HYDRAULIC TURBINES Design, Erection and Operation.

[11] Brekke, H. and Emeritus, P. A Review on Oscillatory Problems in Francis Turbines.

[12] Carl Bergan (2013). Trykkpulsasjoner i Francisturbiner - Prosjektoppgave.

[13] Centre, N. H. (2016, accessed May 11, 2018). High head francis - hifrancis. https://www.ntnu.edu/nvks/hifrancis.

[14] COMSOL (accessed May 30, 2018). Defining fluid-structure interactions. "https://www.comsol.com/multiphysics/fluid-structure-interaction.

[15] Daniel B. Sannes (2017). Pressure pulsations in a Francis turbine. Technical report.

[16] Dörfler, P., Sick, M., and Coutu, A. (2013). *Flow-Induced Pulsation and Vibration in Hydroelectric Machinery*. Springer London, London.

[17] Einar Kobro (2006). Trykkpulsasjoner i Francisturbiner - Masteroppgave.

[18] El Haddad, M. H., Smith, K. N., and Topper, T. H. (1979). Fatigue Crack Propagation of Short Cracks. *Journal of Engineering Materials and Technology*, page 42.

[19] Gogstad, P. J. (2017). Experimental investigation and mitigation of pressure pulsations in Francis turbines.

[20] Heinzel, G., Rüdiger, A., and Schilling, R. (2002). Spectrum and spectral density estimation by the Discrete Fourier transform (DFT), including a comprehensive list of window functions and some new flat-top windows.

[21] Hobbacher, A. F. (2016). *'Recommendations for Fatigue Design of Welded Joints and Components (IIW-2259-15)*.

[22] Huang, X., Chamberland-Lauzon, J., Oram, C., Klopfer, A., and Ruchonnet, N. (2014). Fatigue analyses of the prototype Francis runners based on site measurements and simulations. *IOP Conference Series: Earth and Environmental Science*, 22(1):012014.

[23] Huth, H.-J. Fatigue Design of Hydraulic Turbine Runners.

[24] HydroCen (2017, accessed May 11, 2018a). Turbiner som sprekker. "https://www.ntnutechzone.no/2017/06/turbiner-som-sprekker/.

[25] HydroCen (accessed May 29, 2018b). Variable speed operation. "https://www.ntnu.edu/hydrocen/2.1-variable-speed-operation.

[26] Kobro, E. (2010). Measurement of Pressure Pulsations in Francis Turbines.

[27] NVE (2016, accessed May 11, 2018). Energi i norge (energifolderen). https://www.nve.no/energiforsyning-og-konsesjon/energiforsyningsdata/energi-i-norge-energifolderen/.

[28] Olberts, D. R. and Mem ASME, A. Influence of Trailing-Edge Geometry on Hydraulic-Turbine-Blade Vibration Resulting From Vortex Excitation.

[29] Ole Gunnar Daglhaug lecture notes in Turbo Machinery, TEP 4195, N. (2017). Pressure oscillations in Francis turbines.

[30] Paquette, Y. and Pellone, C. Modelling of a Francis Turbine Runner Fatigue Failure Process Caused by Fluid-Structure Interaction.

[31] Qvale, P. (2016). Utmattingsanalyse av løpehjul til vannturbiner utsatt for spektrumsbelastning.

[32] Sannes, D., Iliev, I., Agnalt, E., and Dahlhaug, O. G. (2018). Pressure Pulsations in a High Head Francis Turbine Operating at Variable Speed.

[33] Seidel, U., Hübner, B., Löfflad, J., and Faigle, P. (2018). Evaluation of RSI-induced stresses in Francis runners.

[34] Seidel, U., Mende, C., Hübner, B., Weber, W., and Otto, A. Dynamic loads in Francis runners and their impact on fatigue life.

[35] Sintef and Forskning.no (2013, accessed May 11, 2018). Vannkraft åpner for vindkraft. https://forskning.no/alternativ-energi/2013/11/vannkraft-apner-vindkraft.

[36] Solemslie, B. W. Compendium in Instrumentation, Calibration Uncertainty Analysis. Technical report, NTNU.

[37] Solvik, S., Selmurzaev, M., and Dahlhaug, O. G. (2016). Pressure Pulsations and Vibration Measurements in Francis Turbines with and without Freely Rotating Runner Cone Extension.

[38] Storli, P.-T. and Nielsen, T. K. Dynamic load on a Francis turbine runner from simulations based on measurements.

[39] TORBJØRN NIELSEN ii, P. K. DYNAMIC DIMENSIONING OF HYDRO POWER PLANTS.

[40] Ukeblad, T. (2012, accessed May 11, 2018). Tynnere francisturbiner øker havarifaren. "https://www.tu.no/artikler/tynnere-francisturbiner-oker-havarifaren/244182.

[41] Valavi, M. and Nysveen, A. (2016). Variable-speed operation of hydropower plants: Past, present, and future. In *2016 XXII International Conference on Electrical Machines (ICEM)*, pages 640–646. IEEE.

[42] Valkvæ, I. (2016). Dynamic loads on Francis turbines. *163*.

[43] W., Y. and R., B. (2002). *'Roark's Formulas for Stress and Strain*.

[44] W. J. Rheingans (1940). Power Svings in Hydroelectric Power Plants.

[45] Wang, X. F., Li, H. L., and Zhu, F. W. The calculation of fluid-structure interaction and fatigue analysis for Francis turbine runner.

[46] Wheeler, A. J. and Ganji, A. R. A. R. *Introduction to engineering experimentation*.

[47] Wormsen, A. A Fatigue Assessment Methodology for Notched Components Containing Defects.

[48] Wormsen, A., Fjeldstad, A., and Härkegård, G. (2008). A post-processor for fatigue crack growth analysis based on a finite element stress field. *Computer Methods in Applied Mechanics and Engineering*, 197(6-8):834–845.

Appendix A

Paper for CRHT-VIII'18

April 20, the International Symposium on current Research in Hydraulic Turbine - VIII'18 was arranged at Kathmandu University in Nepal. The paper attached here was written by the author, and presented at the conference. The paper is written based on the results from the measurement presented in this thesis.

Pressure Pulsation in a High Head Francis Turbine Operating at Variable Speed

D. B. Sannes[1*], I. Iliev[1], E. Agnalt[1], O. G. Dahlhaug[1]
[1]Department of Energy and Process Engineering, NTNU, Norway
*Corresponding author (danielbsannes@gmail.no)

Abstract. This paper presents the preliminary work of the master thesis of the author, written at the Norwegian University of Science and Technology. Today, many Francis turbines experience formations of cracks in the runner due to pressure pulsations. This can eventually cause failure. One way to reduce this effect is to change the operation point of the turbine, by utilizing variable speed technology. This work presents the results from measurements of the Francis turbine at the Waterpower Laboratory at NTNU. Measurements of pressure pulsations and efficiency were done for the whole operating range of a high head Francis model turbine. The results will be presented in a similar diagram as the Hill Chart, but instead of constant efficiency curves there will be curves of constant peak-peak values. This way, it is possible to find an optimal operation point for the same power production, were the pressure pulsations are at its lowest. Six points were chosen for further analysis to instigate the effect of changing the speed by ±50 rpm. The analysis shows best results for operation below BEP when the speed was reduced. The change in speed also introduced the possibility to have other frequencies in the system. It is therefore important avoid runner speeds that can cause resonance in the system.

Keyword: Francis Turbine, Variable Speed, Pressure Pulsation, Hill Chart, Hydro Power

1. Introduction

The electrical grid is a complex system, which is coupled with different types of energy sources as hydro, wind and solar. Because of the flexibility that the Hydropower turbines offers, it is used to stabilize the grid by changing operating point, and therefore the power output [3]. The result of this is that the turbine more often is running off-design. Off-design phenomena such as power swings, rotating vortex rope and part load pressure pulsations can drastically reduce a runners operating life [5]. One of the problems with Francis turbines today is the formation cracks in the runner due to pressure fluctuations, and the industry if facing problems with both new and old Francis turbines [2]. It is therefore of interest to find methods for reducing the effects of pressure fluctuations, and prolong the lifetime of the runner. One potential method of doing this, is by introducing variable speed technology. This enables us to change operation point by changing the speed of the runner to where pressure pulsations are at its lowest.

The present work aims to investigate the pressure pulsations for the whole operating range, and to understand how pressure pulsation varies with different operational conditions. A total of 269 different operational points have been measured, from guide vane opening of 1 degree to 14 degree (full opening). By analysing these different operational conditions, it is possible to find out where to operate the turbine were the pressure pulsations are at its lowest. Six operational points, Full Load

(FL), High Load (HL), Best Efficiency Point (BEP), Part Load (PL), Minimum Load (ML) and Speed-No-Load (SNL) has been chosen for further analysis to check how the peak-peak values and frequency spectrum of pressure pulsation varies when the speed is changed by ±50 rpm.

1.1. Variable Speed Operation

A Francis turbine is designed for fixed speed and for one best efficiency point. The speed of the turbine is predetermined by the combination of pole pairs in the generator and the grid frequency. Therefore, turbine power output is controlled by changing the guide vane opening and thereby water discharge. By utilizing a frequency converter, together with the synchronous generator, it is possible to operate with variable speed. The generator is then decoupled from the grid, and free to operate at different speeds [5]. The turbine will be more flexible, when it can regulate both speed and water discharge, and can avoid operational conditions with cavitation problems and high pressure pulsation. The drawback is additional converter losses that must be considered.

2. Laboratory Setup and Methods

2.1. Francis Model Test Rig

Measurement were conducted at the Francis model test rig located at the Waterpower laboratory at NTNU. The test rig was operated by using an open loop configuration, as seen in Figure 1. The water is pumped from the basement reservoir to a channel located at the top of the laboratory. The water is then going through an upstream pressure tank before entering the turbine. Downstream the draft tube, there is a pressure tank which is used to regulate the pressure at the outlet from the runner. For this measurement the water level in the draft tube pressure tank was open to air. Water is then going back to the reservoir. The open loop configuration gives a uniform water level (≈12m) and provides same conditions for all operation points. The Francis turbine is a scaled down model (1:5.1) of the Tokke turbine. It has 14 stay vanes, 28 guide vanes and 30 runner blades (15 full length and 15 splitter blades).

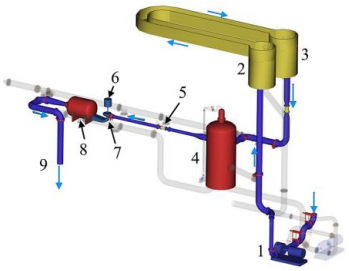

Figure 1. Open loop configuration. (1) centrifugal pump, (2) and (3) open water channel, (4) upstream pressure tank (5) flowmeter, (6) generator, (7) Francis turbine, (8) downstream pressure tank, (9) water outlet.

2.2. Logging Program and Equipment

The measurement system is a complete setup with all the necessary equipment for calculating the efficiency (and to draw a Hill Chart), according to the IEC60193. There is also additional pressure sensors along the guide vanes, on the draft tube cone and on-board the runner, according to Figure 2 and Figure 3. The draft tube pressure sensors (PTDT5, PTDT7, PTDT13, PTDT17) are mounted on the draft tube cone. Pressure sensors along guide vanes (PTGV1-PTGV6) is mounted on the top of the casing, and the on-board pressure sensors (PTR1-PTR6) is mounted between the blades on the crown. The on-board system is transmitting measurement signals via slip rings to the logging system. The logging frequency was 10240Hz for all sensors. A LabVIEW program, developed in the laboratory, was used as logging software.

2.3. Measurement Procedure

Measurements were done for guide vane opening from 1 degree to 14 degree opening (1, 2, …, 14). The starting point for each guide vane opening was N_{ED}=0.08, and the end point was run-away speed (≈0.28). The increment between each measurement was N_{ED}=0.01. This gave a total number of 269 measurement points, from deep part load to full load. All operational points were logged for 60 seconds.

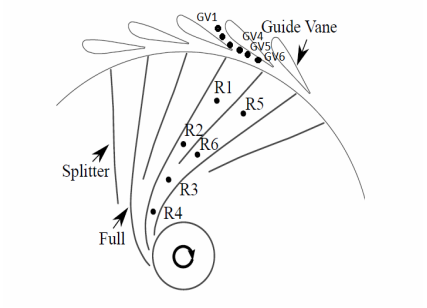

Figure 2. Pressure sensors. GV1-GV6 along guide vanes and R1-R6 on-board the runner.

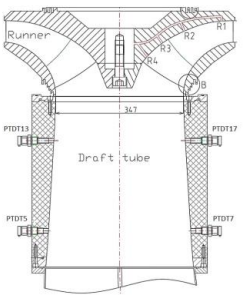

Figure 3. On-board sensors, R1-R4, and draft tube pressure sensors; DT5, DT7, DT13, DT17.

2.4. Data Analysis

MatLab were used for analysing all the measured data. Efficiency calculations for the Hill Chart was done according to IEC60193 [6]. For analysing peak-peak values of pressure data, the Histogram method was used, with a confidence level of 97% as suggested in IEC60193 [6]. The Histogram method has proven to give good results, and have been used by Gogstad in his PhD [8] and been suggested by Dörfler et.al. [7]. For the spectral analysis, Welch method was used together with a Hanning window with 50% overlap. A set of filters were applied to the pressure data to remove noise, before the data was used for analysis.

3. Results

Figure 4 shows the complete Hill Chart for the Francis turbine, from guide vane opening of 1 degree to 14 degree. The turbine would normally operate at N_{ED}≈0.18 (333rpm), and BEP is located at Q_{ED}≈0.154 with and maximum efficiency just above 92%. For the pressure pulsation analysis three different pressure sensors were used to obtain peak-peak values, PTDT13, PTR2 and PTGV4 (Figure 2 and Figure 3). These three sensors were chosen to investigate pressure pulsation effects in the whole turbine based on their location. Peak-peak values was calculated for all operation points, for each sensor, and are presented in a similar way as the Hill Chart. Instead of lines of constant efficiency, there is lines of constant peak-peak values. By doing this, it is easier to identify were pressure pulsation have high values, and which operational areas that should be avoided. In these diagrams, the 97% confidence level is used, as suggested in [6]. Other values may be more correct, and 99% was used by Gogstad [8], but this was not investigated further in this work. Figure 5 shows the results from the draft tube sensor, PTDT13. Diagrams for the other sensors can be found in the Appendix. Peak-peak values are normalised, based on the BEP value. The absolute values are given in Table 2.

Six points were chosen for further analysis; SNL, ML, PL, BEP, HL and FL. Table 1 shows more detailed information on the different operational point. Each point was compared with another

operational point, with the same power output, were the speed is reduced and increased by 50 rpm, to investigate how the pressure pulsation varies with a change in speed. The different points can be seen as dots in Figure 5 (along N_{ED}=0.155, N_{ED}=0.1795 and N_{ED}=0.208). The lines that goes through the different points are lines of constant power. Table 2-4 shows how peak-peak values varies when the speed was changed.

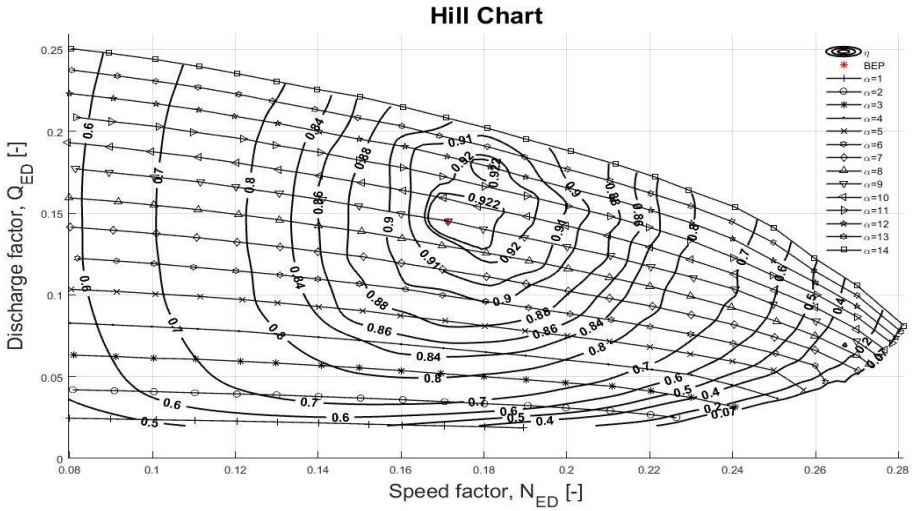

Figure 4. Hill Chart for the whole operation range. Guide vane opening from 1 degree to 14 degrees. N_{ED} varies from 0.08 to run away speed.

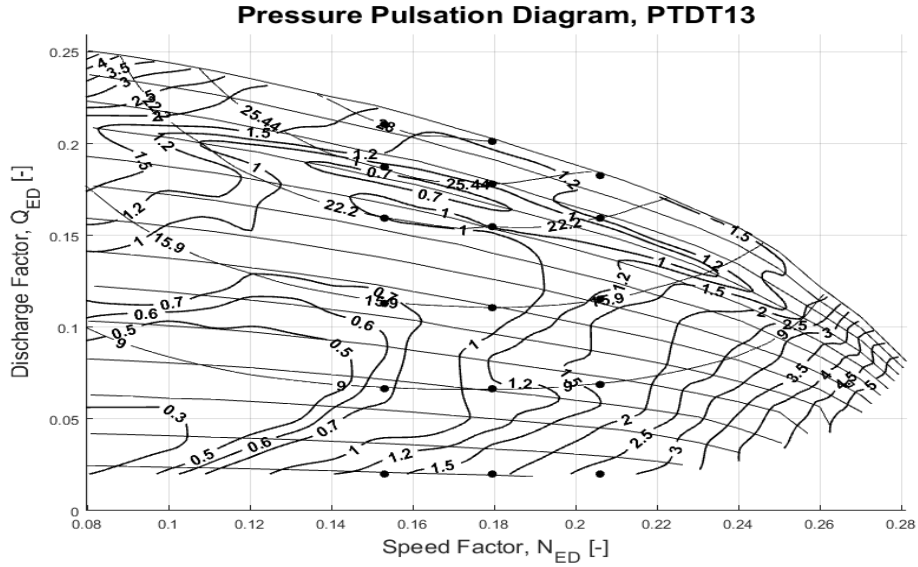

Figure 5. Pressure Pulsations diagram for PTDT13, draft tube sensor. Peak-peak values are normalised based on BEP value and are calculated based on 97% confidence level. The BEP value is calculated to be 2.39kPa. The marked points is used for further analysis, and the lines that goes through them is lines of constant power.

Table 1. Detailed information for operational points used in further analysis

	GV opening. [degree]	Efficiency [%]	N_{ED} [-]	Q_{ED} [-]	Speed [rpm]	Mech Power [kW]
ML	4	84.9	0.1798	0.067	338	9.04
PL	7	91.3	0.1795	0.111	336	15.9
BEP	10	92.2	0.1795	0.155	335	22.2
HL	12	92.2	0.1795	0.178	334	25.4
FL	14	90.7	0.1795	0.201	333	28.0
SNL	1	40	0.1795	0.02	340	1.3

Table 2. Peak-peak values for sensor PTDT13, 97% confidence level. The last two columns show the relative change in peak-peak between normal speed and changed speed. All values are in kPa.

	Normal speed (≈333rpm)	Reduced speed (≈286rpm)	Increased speed (≈386rpm)	Relative change when reducing speed	Relative change when increasing speed
ML	2.82	1.62	3.86	0.57	1.37
PL	2.16	1.62	3.04	0.75	1.41
BEP	2.39	2.39	2.95	1.0	1.23
HL	2.52	2.13	3.29	0.85	1.31
FL	3.12	3.1	-	0.99	-
SNL	1.88	1.31	2.74	0.70	1.46

Table 3. Peak-peak values for sensor PTGV4, 97% confidence level. The last two columns show the relative change in peak-peak between normal speed and changed speed. All values are in kPa.

	Normal speed (≈333rpm)	Reduced speed (≈286rpm)	Increased speed (≈386rpm)	Relative change when reducing speed	Relative change when increasing speed
ML	2.96	2.56	3.73	0.86	1.26
PL	2.87	2.7	3.51	0.94	1.22
BEP	2.37	2.76	2.59	1.16	1.09
HL	2.5	2.54	4.22	1.02	1.69
FL	3.1	2.82	-	0.91	-
SNL	1.15	0.78	1.59	0.68	1.38

Table 4. Peak-peak values for sensor PTR2, 97% confidence level. The last two columns show the relative change in peak-peak between normal speed and changed speed. All values are in kPa.

	Normal speed (≈333rpm)	Reduced speed (≈286rpm)	Increased speed (≈386rpm)	Relative change when reducing speed	Relative change when increasing speed
ML	4.1	2.86	4.84	0.70	1.18
PL	2.86	2.95	4.05	1.03	1.42
BEP	3.04	3.02	3.91	0.99	1.29
HL	3.05	3.32	4.44	1.09	1.46
FL	3.35	3.29	-	0.98	-
SNL	4.82	3.19	5.91	0.66	1.22

Frequency spectrum analysis was conducted for the six different points and the ones with changed speed. This provides information on which flow phenomena that causes pressure fluctuation in the turbine, and which is contributing the most. By using reduced frequencies, it is possible to compare the results when the speed is changed, and see if there are changes in the occurring frequencies. Pressure data was analysed with Welch method in MatLab. Figure 6 shows the result from spectrum analysis for sensor PTGV4 at High Load operation. Figure 7 shows the results for PTR2 at High Load operation.

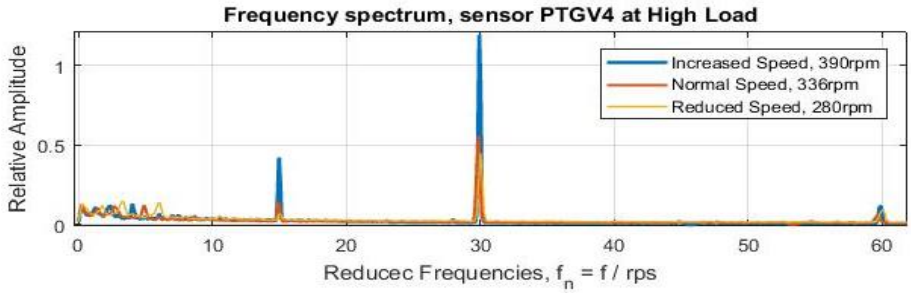

Figure 6. Frequency analysis of pressure data from PTGV4 at HL, for normal speed and changed speed. The blade passing frequency is most dominant with a frequency of 30 times the rotational frequency (f). There is also an effect due to the splitter blade that causes frequencies at 15*f. Stochastic pulsations occur in the low frequency region.

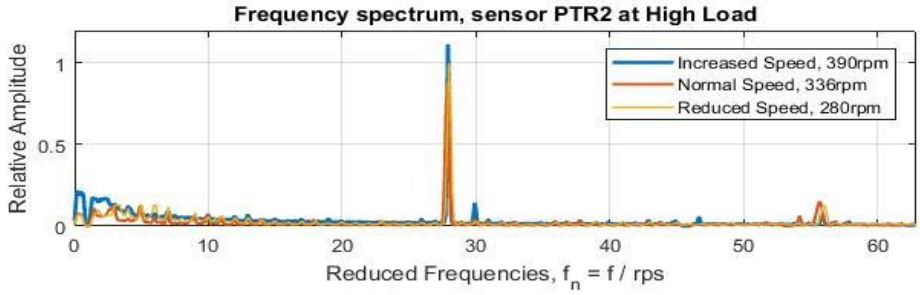

Figure 7. Frequency analysis of pressure data from PTR2 at HL, for normal speed and changed speed. The guide-vane-passing frequency is most dominating (28*f). There is also stochastic pulsations in the low frequency region.

4. Discussion

The three different pressure pulsation diagrams show different behaviour for the pressure pulsations. The draft tube pressure pulsation clearly shows a trend towards lower peak-peak values for lower speed and discharge, while the pulsation around the guide vanes and on-board the runner shows lowest values at BEP and around an area where the speed is reduced. There are also indications that it is possible to find optimum operation points for minimal pulsations, especially when reducing the speed, but there will be a give-and-take between lowest peak-peak values in the different part of the turbine.

The diagrams from PTGV4 and PTR2 show more similarities than the one for PTDT13. This make sense because Rotor-Stator Interaction (RSI) is the most dominating phenomena for both sensors (Figure 6 and Figure 7). It is therefore important to figure out what is most damaging for the turbine, and find optimal operation based on this.

From Table 2-4 we can see the result from changing the speed (±50 rpm) from six operation points. There was no effect at BEP for the three sensors. This is as expected since this is the design point. Also, when the speed is increased, the pressure pulsations are increasing for all operation points. On the other hand, if the speed was reduced, pressure pulsations dropped for almost all the sensor at all operation points, and the reduction is highest for operation below BEP. In the draft tube, the pressure pulsations are reduced with 25 %, 30% and 30% for PL, ML and SNL. While on-board the runner (PTR2), the same reduction is 0%, 29% and 34%, and 6%, 14% and 32% for PTGV4. Pressure pulsations for operation above BEP was not strongly affected by the reduction in speed, and peak-peak values on-board the runner increased with 9% at HL. It should be said that speed change is not limited to ±50 rpm, (15% change in speed), and different speed may give even lower pressure pulsations.

Frequency analysis was performed for all operation points, to investigate which pulsation phenomena that occurred for the different points, and to find out how the change in speed affected the frequencies. Figure 6 and Figure 7 shows the results from HL for PTGV4 and PTR2. For these two sensors, the RSI was found to be most dominant for all the operation point, except at part load operation, where the draft tube vortex rope was dominating. Also the effect of the splitter blades was found in the analysis, which was half the blade-passing frequency, along the guide vanes. For PTDT13, the pressure pulsations was dominated of a frequency between 1.45-1.8 times the runner frequency, combined with stochastic fluctuations. At part-load operation, the vortex rope was dominating the pressure pulsation. This proves some of the challenges that follows variable speed operation. Many of the frequencies are speed depended, such as RSI and the draft tube vortex rope. A change in speed will therefore introduce many more frequencies that potentially can cause resonance in the system.

5. Conclusion

An experimental investigation of a high head Francis turbine was conducted to investigate pressure pulsation for the whole operation range. The purpose of this was to see it is possible to reduce the effect of pressure pulsation by utilizing variable speed, and thereby avoid operational problems and crack formation in the runner. A Hill Chart was constructed, and pressure pulsation were analysed for three different sensors. Three pressure pulsation diagrams were created, similar to a Hill Chart but with lines of constant pressure pulsations (peak-peak values). Six points were chosen for further analysis to see how the pressure pulsation varied with a speed change of ±50 rpm, but with the same power output.

Increasing the speed resulted in higher peak-peak values for off-design operation, while reducing the speed resulted in reduced pressure pulsation in most of the cases. The highest reduction in pressure pulsation was found for operation below BEP, for all three sensors. The maximum reduction was found for Speed-No-Load, were the peak-peak values was reduced by more than 30%. The investigated points were chosen arbitrarily, and the pressure pulsation diagrams gives indication that other operational points would give even lower peak-peak values. RSI was found to be most dominating in the upper part of the turbine, together with the vortex rope at curtain part load operation points. These pressure fluctuations are speed dependent and will change according to the speed. It is there important avoid runner speed that can cause resonance in the system.

Appendices

A.1 PTGV4 Pressure Pulsation Diagram

Peak-peak values are calculated with 97% confidence level. All the values are normalise with respect to the BEP value. The BEP value is calculated to be 2.37kPa. Normal operating is along N_{ED}=0.18.

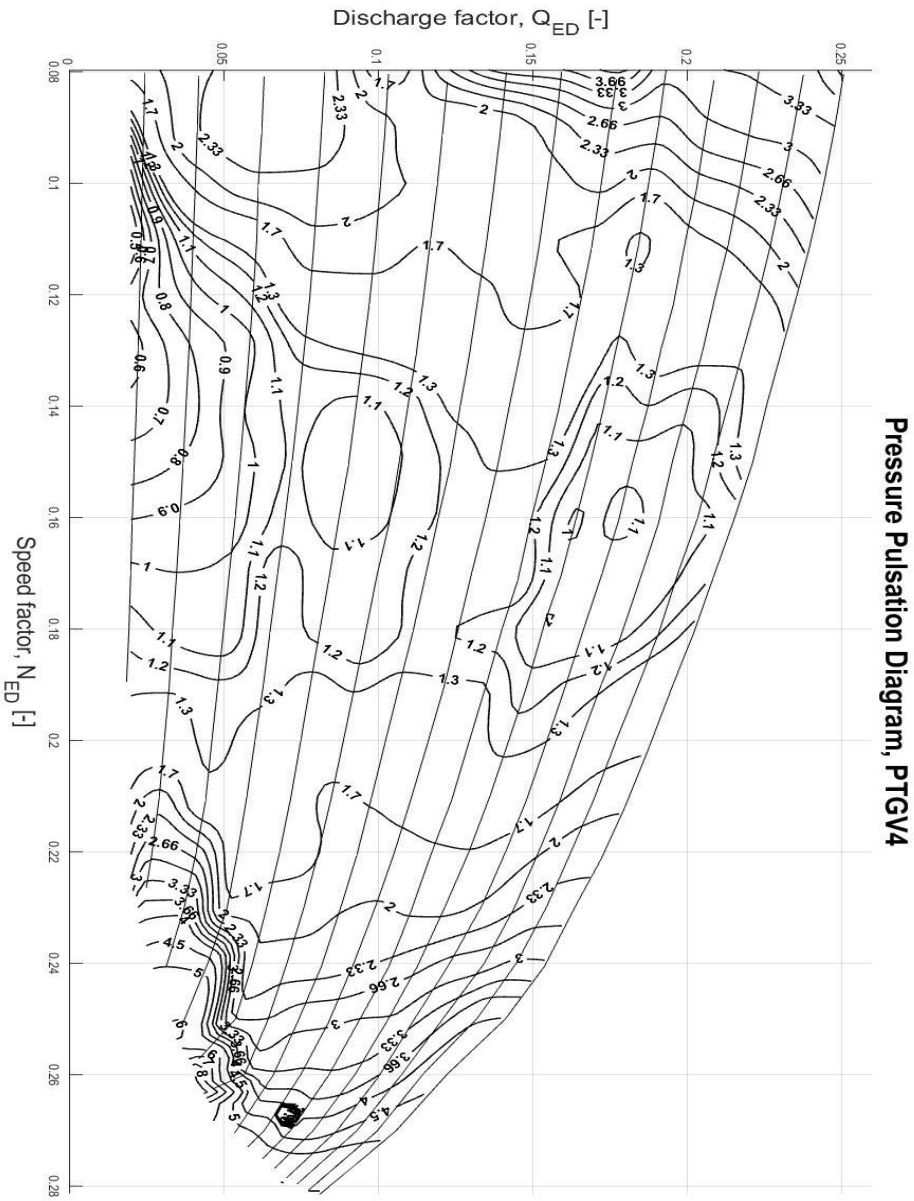

A.2 PTR2 Pressure Pulsation Diagram

Peak-peak values are calculated with 97% confidence level. All the values are normalise with respect to the BEP value. The BEP value is calculated to be 3.04kPa. Normal operating is along N_{ED}=0.18.

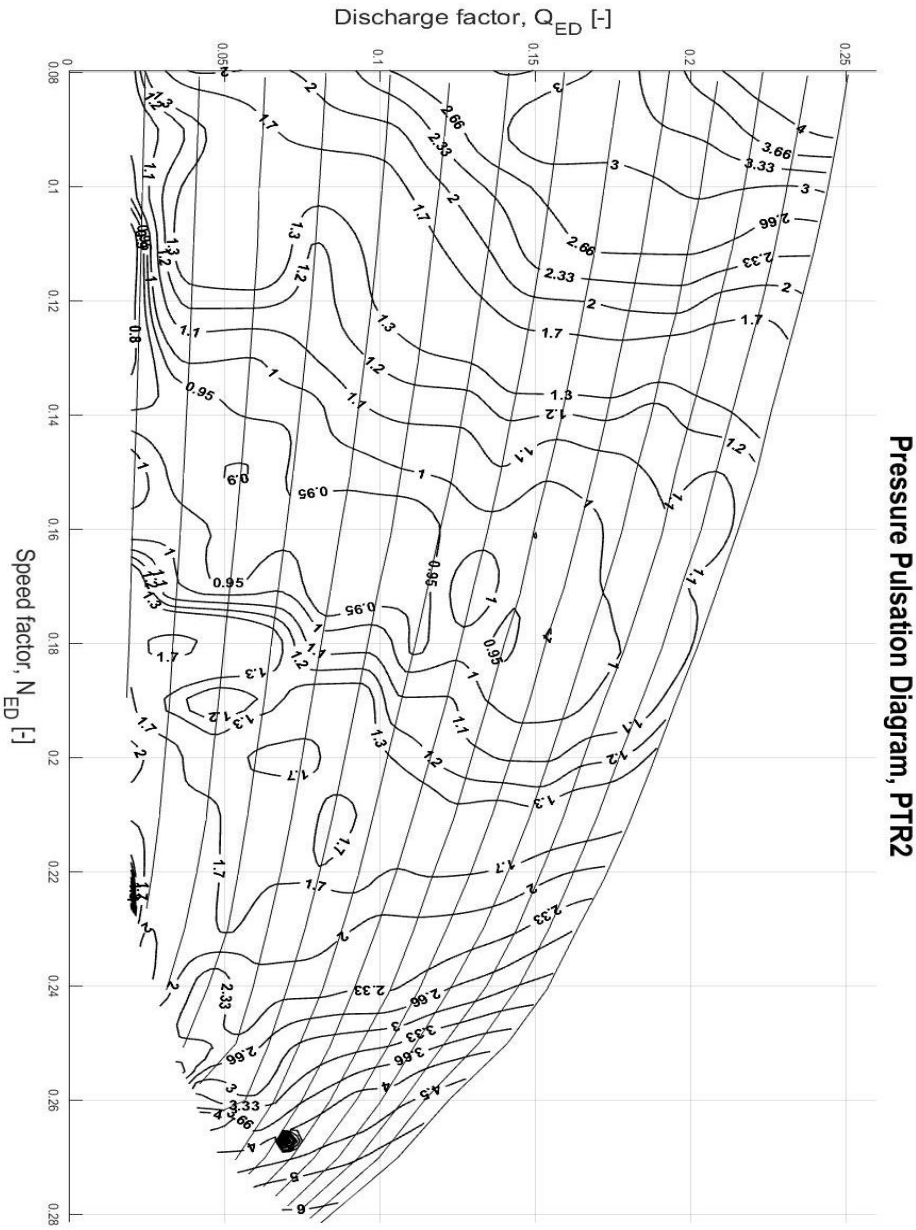

References

[1] Trivedi C, Agnalt E, Dahlhaug O G, 2017, *Investigations of unsteady pressure loading in Francis turbine during variable-speed operation*, Elsevier, Renewable Energy 113 (2017) 397-410.

[2] Norwegian Hydropower centre, *High Head Francis – HiFrancis*, https://www.ntnu.edu/nvks/hifrancis, read; 25.02.2018

[3] Trivedi C, Cervantes M J, Gandhi B K, Dahlhaug O G, 2013, *Experimental and Numerical Studies for a High Head Francis Turbine at several Operating Points*, ASME, Vol. 135.

[4] Bergan C, Dahlhaug O G, 2016, *Experimental Investigation of a High Head Model Francis Turbine During Steady-State operation at Off-Design Conditions*, CRHT2016-18, KU.

[5] Valavi M, Nysveen A, 2016, *Variable-Speed Operation of Hydropower Plants: Past, Present, and Future*, XXII International Conference on Electrical Machines (ICEM), 2016, pp 640-646.

[6] IEC 60193:1999, *Hydraulic turbines, storage pumps and pump-turbines – Model acceptance tests*, (1999-11-16).

[7] Dörfler P, Sick M, Coutu A, 2013, *Flow-Induced Pulsation and Vibration in Hydroelectric Machinery*. Springer London

[8] Gogstad P J, 2017, *Experimental investigation and mitigation of pressure pulsations in Francis turbines*, Doctoral Thesis at NTNU, 2017:202.

Appendix B

Procedure for calculating pressure distribution on runner blades

This part describe how pressure measurements from the experiment was used to calculate pressure distribution on both pressure and suction side of the blades for use in structural analysis. Only the calculation for the BEP will be presented, but the method is the same for the other operation points. In a rotating runner, the pressure and velocity field will be highly non-uniform, and the pressure will vary from the suction side to the pressure side. Values from the on-board pressure sensors from the measurements can be used, together with energy conservation, in order to calculated the pressure values at the surface of the blades at the same radius as the sensors. When these values are found the values in-between can be found by interpolating, and thereby getting the full pressure distribution on the blades. The primary method is described in [10], but is adjusted for this problem.

Four pressure sensors were logged on-board the runner during the measurement. Sensors were located at the top of the hub and between two runner blades, according to Figure B.1. The guide vane pressure sensor PTGV4, also according to Figure B.1, is used to get the inlet pressure of the runner. The radial distance for each sensors is given in Table B.1. It is assumed that the splitter blade has the same geometry as the half the full length blade, and the the change of relative velocity through the runner is equal for all the operation point. It is also assumed that the pressure in axial direction was constant, so that the pressure from the measurement could be used to calculate pressure at the different streamlines.

Table B.1: Radial distance for each pressure sensor

PTR1	PTR2	PTR3	PTR4	PTGV4
240.42mm	157.34mm	121.64mm	86.95mm	326.5mm

Three streamlines have been used to calculate the pressure on the blades; hub-streamline, center-streamline and shroud-streamline. This is done to get more accurate results, since the blade geometry is changing a lot in axial direction. The sensors from the experiments are placed in the middle of the blades, and the

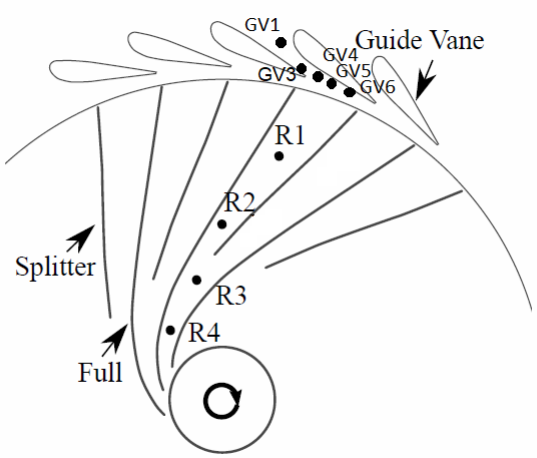

Figure B.1: Location of pressure sensors on-board the runner

pressure-change from the sensor location to the suction- and pressure side of the blades have to be calculated. The pressure difference at the inlet is calculated in the same way, but the pressure value is taken from the PTGV4 sensor. Mean pressure from the sensors is used for all calculations. At the trailing edge of the blades, it is assumed that the pressure difference is close to zero.

To calculate the pressure change from a streamline between to blades to the surface of the blades, a flow analysis had to be conducted. This is done by combining the Rothalpi equation (B.1);

$$I = \frac{p}{\rho} + \frac{w^2}{2} - \frac{u^2}{2} \tag{B.1}$$

where p is the pressure, ρ is the density, w is the relative velocity and u is the tangential velocity of the runner, together with the equation for relative velocity variation normal to a streamline (B.2);

$$\frac{dw}{dn} = -\frac{w}{r} - 2\omega \tag{B.2}$$

where dn is the distance between the middle streamline and the blade surface, r is the radius of the curvature at the streamline and ω is the angular velocity.
To use these equations the runner geometry has be known, since the relative velocity is dependent on the curvature of the streamline and the distance to the blade surfaces. The runner blades were reconstructed in a MatLab program called Khoj, which is developed at the Waterpower Laboratory at NTNU. The runner blades can be seen in Figure B.2a and B.2b. The coordinates for the three streamlines

was taken from the runner blade in Khoj, and used to plot the curvature and to calculate dn in MatLab. By choosing the correct energy distribution for the runner, Khoj will plot the relative velocity, w, along all three streamlines for BEP. The values from the hub-streamline can be seen in Figure B.3, where the x-axis is the normalized streamline length and the y-axis shows the w value relative to the inlet. By calculating the inlet relative velocity, it is possible to use these plots to calculate the relative velocity for any point where the sensors are located.

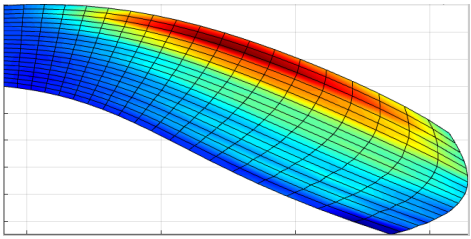

(a) Runner blade, radial view. Colors shows curvature

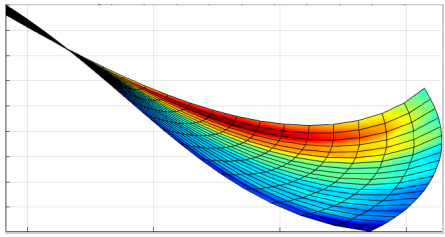

(b) Runner blade, axial view. Colors shows curvature

Figure B.2: Reconstruction of runner blades from Khoj

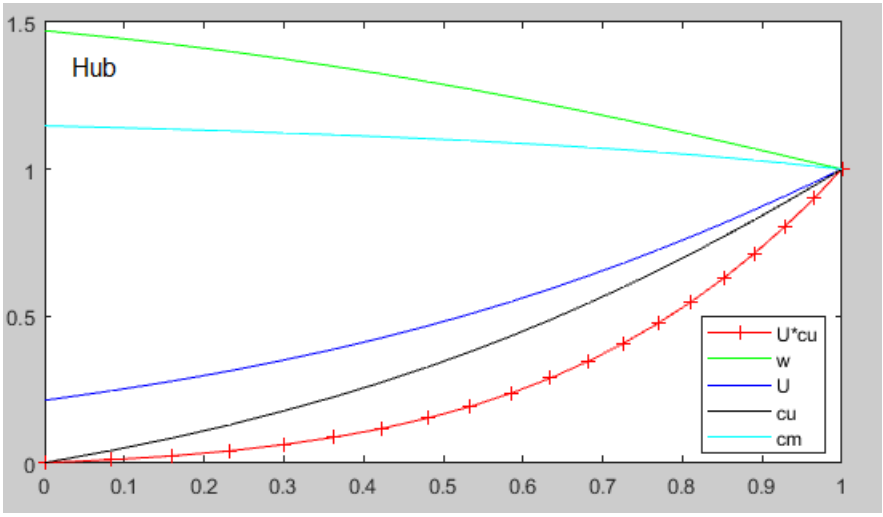

Figure B.3: A plot for Khoj. Shows how the velocities is changing relative to the inlet values through the runner, for the hub streamline.

The value of Rothalpi is constant for the whole runner channel, if friction is neglected [10]. Therefore, Rothalpi can be calculated for each of the sensor location

for each streamline. Thereafter the relative velocity at the blade surfaces can be calculated by using Equation B.2. Then, the Rothalpi equation can be rearranged in order to solve it for the surface pressure, since everything else is known. When all the surface pressures is calculated the values in between can be found be simply interpolating. Figure B.4 shows the results for BEP. The x-axis is the normalized streamline length, and the y-axis is the pressure in kPa. The upper line is the pressure side, while the lowest line is the suction side. The data has been interpolated with a third grade polynomial.

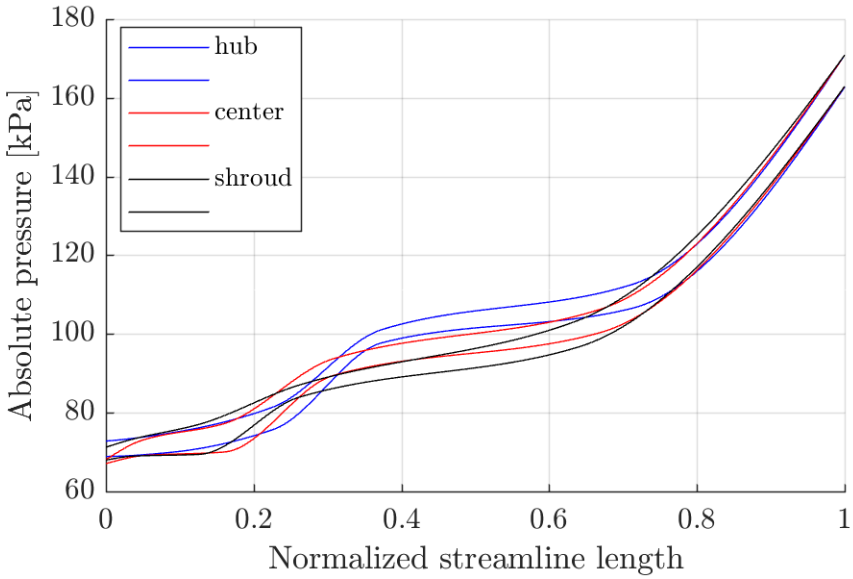

Figure B.4: Pressure for the suction side and pressure side for the three streamlines is plotted against the normalized streamline length. The upper line (of each color) is for the pressure side, while the lowest are for the suction side.

Until now, only the static pressure, using the mean pressure values, have been used. Since the simulations are only static, no dynamical effects will be accounted for. In order to get the dynamical effect of the pressure pulsation, additional pressure due to the peak-peak values has to be added to the pressure distribution. This have been done by assuming that the pressure pulsation measured at the sensor locations, is similar at the blade surfaces. Peak-peak values have been interpolated between PTR1 and PTR4 sensor. To get the peak-peak values from PTR1 and to the runner inlet, and from PTR4 and to the runner outlet, it have been assumed that extrapolation will give reliable results. Then half the peak-peak values were added to the pressure side of the blades, while half the peak-peak values were subtracted

from the suction side of the blade. That the pressure is increased at the pressure side, and decreased at the suction side is a "worst-case scenario" that most likely will not happen. But this will give information on how the pressure pulsations is effecting the stresses on the blades, and can be used for relative comparison between the different operation points.

By conduction two different simulation, one with only the mean pressure and one where the peak-peak value is added, it is possible to obtain a mean stress value and a stress amplitude. The stress amplitude is found by the difference in maximum stress in the two simulations. As said before, this will not give the correct stress amplitude, but it will give information on how the pressure pulsations is effecting the stresses on the blades, and can be used for relative comparison between the different operation points.

The mechanical model is split into 16 segments on each side, and the correct pressure load has to be applied for each segment. To find the correct pressure value, the radius for the different streamlines at the different segments was found in ANSYS SpaceClaim. The corresponding pressure values was then found from the pressure plot in Figure B.4. The pressure value at the upper segments was found be taken the mean of the hub and center streamlines for the different segments, while the mean of the center and shroud streamline was used to find the pressure values for the lower segments. The result of the MatLab code is two Tables with all the pressure values for one operation point. The first is for the mean pressure, while the second is with the effect of pressure pulsations. The Table for mean pressure at BEP can be seen in Figure B.5. Values correspond to the segments on the 3D model, were the first value is for the inlet. The MatLab code for these calculations is included below.

	pressureside_up	pressureside_down	suctionside_up	suctionside_down
1	140.5099	144.9389	133.1639	137.3080
2	113.7198	117.3862	107.4668	110.2246
3	104.9132	105.4114	99.8844	98.9973
4	99.9176	99.9734	95.8411	94.4802
5	89.0392	96.9887	83.9379	92.1365
6	85.6611	95.2072	80.8104	90.6582
7	83.3566	93.6916	78.6920	89.1582
8	80.8151	91.6592	76.0012	86.7171

Figure B.5: Result table from the MatLab code, with all the pressure values the for different segments in the 3D mode. These values are the results for the mean pressure values for BEP. Row 1 values are for the segments closest to the leading edge, while Row 8 is for the trailing edge. For the splitter blade, only the first 4 rows is used.

```
%Choose which operation point you want.
opPoint = 175; %175=BEP, %172=BEP-50. 113=PL, etc...

%oP is a vector with the pressure values for the sensor, the runner
 speed,
%Q_ED and Head.
oP(1)=mean(hillChart.PTR1(opPoint,:)); oP(2)=hillChart.RPM(opPoint);
oP(3)=hillChart.Qed(opPoint); oP(4)=hillChart.Head(opPoint);
%trykkblad function takes in which sensor, which streamline and the oP
%vector, and returns the pressure values for the suction and pressure
 side
%of the blade.
[p_trykk(1,2), p_sug(1,2), I(1,2)]=trykkblad(1,1,oP);
[p_trykk(2,2), p_sug(2,2), I(2,2)]=trykkblad(1,2,oP);
[p_trykk(3,2), p_sug(3,2), I(3,2)]=trykkblad(1,3,oP);

%Updating the first value of the oP vector when the values are
 calculated
%for a new sensor location.
oP(1)=mean(hillChart.PTR2(opPoint,:));
[p_trykk(1,3), p_sug(1,3), I(1,3)]=trykkblad(2,1,oP);
[p_trykk(2,3), p_sug(2,3), I(2,3)]=trykkblad(2,2,oP);
[p_trykk(3,3), p_sug(3,3), I(3,3)]=trykkblad(2,3,oP);

oP(1)=mean(hillChart.PTR3(opPoint,:));
[p_trykk(1,4), p_sug(1,4), I(1,4)]=trykkblad(3,1,oP);
[p_trykk(2,4), p_sug(2,4), I(2,4)]=trykkblad(3,2,oP);
[p_trykk(3,4), p_sug(3,4), I(3,4)]=trykkblad(3,3,oP);

oP(1)=mean(hillChart.PTR4(opPoint,:));
[p_trykk(1,5), p_sug(1,5), I(1,5)]=trykkblad(4,1,oP);
[p_trykk(2,5), p_sug(2,5), I(2,5)]=trykkblad(4,2,oP);
[p_trykk(3,5), p_sug(3,5), I(3,5)]=trykkblad(4,3,oP);

%The pressure value at the inlet is assumed to be the same as measured
 at
%PTGV4, but with a small pressure drop at 2kPa due to increase in
 kinetic energy.
oP(1)=mean(hillChart.PTGV4(opPoint,:))-2;
[p_trykk(1,1), p_sug(1,1), I(1,1)]=trykkblad(5,1,oP);
[p_trykk(2,1), p_sug(2,1), I(2,1)]=trykkblad(5,2,oP);
[p_trykk(3,1), p_sug(3,1), I(3,1)]=trykkblad(5,3,oP);

%Assuming that the outlet pressure values for the pressure and suction
 side
%is only experience a small pressure drop from the PTR4 sensor. These
%values are not influencing the result much, since the last segment at
 the 3D
%model is closed to the PTR4 sensor location.
p_trykk(1,6)=p_trykk(1,5)-2; p_sug(1,6)=p_sug(1,5)-1;
p_trykk(2,6)=p_trykk(2,5)-(p_trykk(2,5)-p_sug(2,5))/2-3;
p_sug(2,6)=p_sug(2,5)+(p_trykk(2,5)-p_sug(2,5))/2-4;
```

```
p_trykk(3,6)=p_trykk(3,5)-2; p_sug(3,6)=p_sug(3,5)-1;

%Normalize streamline values for the hub-streamline
xvalh = [1 0.7076 0.3734 0.221 0.0826 0];
%Absolute values for the hub-streamline.
xvalha=[rad_hub(1) r1 r2 r3 r4 rad_hub(end)];
%Normalize streamline values for the shroud-streamline
xvals = [1 0.6395 0.2615 0.1263 0.0353 0];
%Absolute values for the shroud-streamline.
xvalsa=[rad_shroud(1) rad_shroud(6) rad_shroud(12) rad_shroud(15)...
    rad_shroud(18) rad_shroud(end)];
%Normalize streamline values for the center-streamline
xvalc = [1 0.6689 0.3074 0.1604 0.0498 0];
%Absolute values for the center-streamline.
xvalca = [rad_center(1) rad_center(6) rad_center(12) rad_center(15)...
    rad_center(18) rad_center(end)];

%Creating a new x-vector, and interpolating the pressure values, so
 the
%values for each segment can found.
Xh = linspace(xvalha(1),xvalha(end),500);
Yh_p = interp1(xvalha,p_trykk(1,:),Xh,'pchip');
Yh_s = interp1(xvalha,p_sug(1,:),Xh,'pchip');
Xc = linspace(xvalca(1),xvalca(end),500);
Yc_p = interp1(xvalca,p_trykk(2,:),Xc,'pchip');
Yc_s = interp1(xvalca,p_sug(2,:),Xc,'pchip');
Xs = linspace(xvalsa(1),xvalsa(end),500);
Ys_p = interp1(xvalsa,p_trykk(3,:),Xs,'pchip');
Ys_s = interp1(xvalsa,p_sug(3,:),Xs,'pchip');

%Option to plot how the pressure values are varying along the
 streamlines
% figure()
% hold on; plot(Xh,Yh_p,'b',Xh,Yh_s,'b');
 plot(Xc,Yc_p,'r',Xc,Yc_s,'r');
%plot(Xs,Ys_p,'k',Xs,Ys_s,'k');
% legend('hub','','center','','shroud','','location','northwest')

%Locating the correct pressure value for each segment for the 3D
 model. The
%value av Xh, (Xh-0.xxx) is the radius value in the middle of the
 segment.
temp = find(abs(Xh-0.281) < 0.0002); P_p(1)=Yh_p(temp(1));
temp = find(abs(Xh-0.24) < 0.00025); P_p(2)=Yh_p(temp(1));
temp = find(abs(Xh-0.197) < 0.0002); P_p(3)=Yh_p(temp(1));
temp = find(abs(Xh-0.155) < 0.0002); P_p(4)=Yh_p(temp(1));
temp = find(abs(Xh-0.121) < 0.0002); P_p(5)=Yh_p(temp(1));
temp = find(abs(Xh-0.101) < 0.0002); P_p(6)=Yh_p(temp(1));
temp = find(abs(Xh-0.086) < 0.0002); P_p(7)=Yh_p(temp(1));
temp = find(abs(Xh-0.071) < 0.0002); P_p(8)=Yh_p(temp(1));
temp = find(abs(Xh-0.284) < 0.0002); P_p(9)=Yc_p(temp(1));
temp = find(abs(Xh-0.250) < 0.0002); P_p(10)=Yc_p(temp(1));
temp = find(abs(Xh-0.214) < 0.00025); P_p(11)=Yc_p(temp(1));
temp = find(abs(Xh-0.182) < 0.0002); P_p(12)=Yc_p(temp(1));
```

```
temp = find(abs(Xh-0.158) < 0.00025); P_p(13)=Yc_p(temp(1));
temp = find(abs(Xh-0.145) < 0.0002); P_p(14)=Yc_p(temp(1));
temp = find(abs(Xh-0.136) < 0.00025); P_p(15)=Yc_p(temp(1));
temp = find(abs(Xh-0.129) < 0.0002); P_p(16)=Yc_p(temp(1));
temp = find(abs(Xh-0.288) < 0.0002); P_p(17)=Ys_p(temp(1));
temp = find(abs(Xh-0.255) < 0.0002); P_p(18)=Ys_p(temp(1));
temp = find(abs(Xh-0.234) < 0.0002); P_p(19)=Ys_p(temp(1));
temp = find(abs(Xh-0.211) < 0.00025); P_p(20)=Ys_p(temp(1));
temp = find(abs(Xh-0.194) < 0.0002); P_p(21)=Ys_p(temp(1));
temp = find(abs(Xh-0.186) < 0.00025); P_p(22)=Ys_p(temp(1));
temp = find(abs(Xh-0.182) < 0.0002); P_p(23)=Ys_p(temp(1));
temp = find(abs(Xh-0.178) < 0.0002); P_p(24)=Ys_p(temp(1));

%Doing the same for the suction side og the blades.
temp = find(abs(Xh-0.281) < 0.0002); P_s(1)=Yh_s(temp(1));
temp = find(abs(Xh-0.24) < 0.00025); P_s(2)=Yh_s(temp(1));
temp = find(abs(Xh-0.197) < 0.0002); P_s(3)=Yh_s(temp(1));
temp = find(abs(Xh-0.155) < 0.0002); P_s(4)=Yh_s(temp(1));
temp = find(abs(Xh-0.121) < 0.0002); P_s(5)=Yh_s(temp(1));
temp = find(abs(Xh-0.101) < 0.0002); P_s(6)=Yh_s(temp(1));
temp = find(abs(Xh-0.086) < 0.0002); P_s(7)=Yh_s(temp(1));
temp = find(abs(Xh-0.071) < 0.0002); P_s(8)=Yh_s(temp(1));
temp = find(abs(Xh-0.284) < 0.0002); P_s(9)=Yc_s(temp(1));
temp = find(abs(Xh-0.250) < 0.0002); P_s(10)=Yc_s(temp(1));
temp = find(abs(Xh-0.214) < 0.00025); P_s(11)=Yc_s(temp(1));
temp = find(abs(Xh-0.182) < 0.0002); P_s(12)=Yc_s(temp(1));
temp = find(abs(Xh-0.158) < 0.00025); P_s(13)=Yc_s(temp(1));
temp = find(abs(Xh-0.145) < 0.0002); P_s(14)=Yc_s(temp(1));
temp = find(abs(Xh-0.136) < 0.00025); P_s(15)=Yc_s(temp(1));
temp = find(abs(Xh-0.129) < 0.0002); P_s(16)=Yc_s(temp(1));
temp = find(abs(Xh-0.288) < 0.0002); P_s(17)=Ys_s(temp(1));
temp = find(abs(Xh-0.255) < 0.0002); P_s(18)=Ys_s(temp(1));
temp = find(abs(Xh-0.234) < 0.0002); P_s(19)=Ys_s(temp(1));
temp = find(abs(Xh-0.211) < 0.00025); P_s(20)=Ys_s(temp(1));
temp = find(abs(Xh-0.194) < 0.0002); P_s(21)=Ys_s(temp(1));
temp = find(abs(Xh-0.186) < 0.00025); P_s(22)=Ys_s(temp(1));
temp = find(abs(Xh-0.182) < 0.0002); P_s(23)=Ys_s(temp(1));
temp = find(abs(Xh-0.178) < 0.0002); P_s(24)=Ys_s(temp(1));

%New values with adding pressurePulsation: +pp/2 on pressure side and
 -pp/2
%on suction side.
peak(2)=peakData.fPTR1(opPoint); peak(3)=peakData.fPTR2(opPoint);
peak(4)=peakData.fPTR3(opPoint); peak(5)=peakData.fPTR4(opPoint);
peak(1)=peak(2)+(peak(2)-peak(3))*1.6; peak(6)=peak(5)-0.5;

%Interpolating between the peak-peak values, and then using the same
 method
%as above to locate the correct value for each segment in the 3D
 model.
Y_pp = interp1(xvalha,peak,Xh,'pchip');
temp = find(abs(Xh-0.281) < 0.0002); Peak(1)=Y_pp(temp(1));
temp = find(abs(Xh-0.24) < 0.00025); Peak(2)=Y_pp(temp(1));
temp = find(abs(Xh-0.197) < 0.0002); Peak(3)=Y_pp(temp(1));
```

```
temp = find(abs(Xh-0.155) < 0.0002); Peak(4)=Y_pp(temp(1));
temp = find(abs(Xh-0.121) < 0.0002); Peak(5)=Y_pp(temp(1));
temp = find(abs(Xh-0.101) < 0.0002); Peak(6)=Y_pp(temp(1));
temp = find(abs(Xh-0.086) < 0.0002); Peak(7)=Y_pp(temp(1));
temp = find(abs(Xh-0.071) < 0.0002); Peak(8)=Y_pp(temp(1));

%tables
for k=1:8
%Taking the mean of the values for the hub and center line to
 calculate the
%upper segment values, and doing the same for the center and shroud to
%calculate the values for the lower segments.
upper_p(k) = (P_p(k)+P_p(k+8))/2;
lower_p(k) = (P_p(k+8)+P_p(k+16))/2;
upper_s(k) = (P_s(k)+P_s(k+8))/2;
lower_s(k) = (P_s(k+8)+P_s(k+16))/2;

%Creating new vectors were the peak-peak effects are added.
peak_overst_p(k) = upper_p(k)+0.5*Peak(k);
peak_nederst_p(k) = lower_p(k)+0.5*Peak(k);
peak_overst_s(k) = upper_s(k)-0.5*Peak(k);
peak_nederst_s(k) = lower_s(k)-0.5*Peak(k);
end

%Option to create 2 tables with the values for the segments in the 3D
%model. The first table is only with the mean pressure values, while
 the
%second one is with the effect of pressure pulsations.

% figure()
% title('Mean Pressure Values for use in ANSYS, BEP')
% T1=table(overst_p', nederst_p', overst_s',
 nederst_s','VariableNames',...
%{'pressureside_up';'pressureside_down';'suctionside_up';'suctionside_down'});
%
 uitable('Data',T1{:,:},'ColumnName',T1.Properties.VariableNames,'Units'...
%,'Normalized','Position',[0, 0, 1, 1]);
%
% figure()
% title('peak Pressure Values for use in ANSYS, BEP')
% T2=table(peak_overst_p', peak_nederst_p', peak_overst_s',
 peak_nederst_s'...
%,'VariableNames',
{'pressureside_up';'pressureside_down';'suctionside_up';...
%'suctionside_down'});
%
 uitable('Data',T2{:,:},'ColumnName',T2.Properties.VariableNames,'Units'...
%,'Normalized','Position',[0, 0, 1, 1]);

%trykkblad function
function [P_pside, P_sside, I]=trykkblad(sensor,loc,oP)
%Sensor: 1 2 3 4 5(inlet). Loc: 1(hub) 2(center) 3(shroud) %Operation
 point from the
%experiment list.
```

```
%Runner dimensions
D1=0.63; D2=0.349; B1=0.06; beta_1=59.85; rho=998;

%operation point values from oP. Then the flow, angular velocity, and
 the
%inlet velocity triangle values are calculated.
P=oP(1)*10^3; rpm=oP(2); Qed=oP(3); H=oP(4);
 Q=Qed*(D2^2)*sqrt(H*9.82146516);
omega=pi*rpm/30; u1=omega*(D1/2); cm1=Q/(pi*D1*B1); cm2=cm1*1.1;
 cu1=u1-cm1/(tand(beta_1));
w1=sqrt((u1-cu1)^2+cm1^2);

%Coordinates for the three streamlines, extracted from the blade
%reconstruction in Khoj.
X_hub = [1.585 1.51 1.434 1.356 1.277 1.195 1.113 1.028 0.9425 0.8537
 0.7634 0.6715 ...
    0.5778 0.4823 0.3852 0.2894 0.1907 0.09639 0.008712
 -0.07069]./5.1;
Y_hub = [0.03907 0.08165 0.124 0.1659 0.2071 0.2474 0.2857 0.3225
 0.3567 0.3885 0.4167 ...
    0.4405 0.4592 0.4717 0.4766 0.4725 0.4572 0.4292 0.3874
 0.3293]./5.1;
X_shroud = [1.585,1.535,1.484,1.433,1.381,1.328,1.273,
 1.217,1.159,1.099,1.036,0.9684 ...
    ,0.897,0.8195,0.735,0.6411,0.533,0.4172,0.284,0.145]./5.1;
Y_shroud =
 [0,0.033,0.067,0.104,0.143,0.185,0.229,0.276,0.326,0.377,0.431,0.4889,0.548 ...
    ,0.607,0.668,0.727,0.785,0.833,0.873,0.896]./5.1;
X_center =
 [1.585,1.522,1.458,1.393,1.326,1.257,1.187,1.114,1.038,0.959,0.875, ...
    0.789,0.696,0.597,0.492,0.382,0.264,0.139,0.012,-0.118]./5.1;
Y_center =
 [0.021,0.06,0.1,0.142,0.186,0.231,0.277,0.324,0.373,0.421,0.4697, ...
    0.516,0.561,0.603,0.639,0.667,0.685,0.69,0.679,0.647]./5.1;

%Relative velocity for the three stremlines at the sensor locations.
 The
%last value in the vector is only the inlet value.
%The curvature is calculated based on the streamline coordinate and
 the
%LineCurvature2D function. To calculate its radius, use the invers of
 the
%curvature.
w_hub = [1.27 1.237 1.3589 1.5479 1];
Vert_hub(:,1)=X_hub; Vert_hub(:,2)=Y_hub;
temp=LineCurvature2D(Vert_hub); k_hub=1./temp;
w_center = [1.384 1.978 2.196 2.35 1];
Vert_center(:,1)=X_center; Vert_center(:,2)=Y_center;
temp=LineCurvature2D(Vert_center); k_center=1./temp;
w_shroud = [1.55 2.4 2.52 3 1];
Vert_shroud(:,1)=X_shroud; Vert_shroud(:,2)=Y_shroud;
temp=LineCurvature2D(Vert_shroud); k_shroud=1./temp;
```

```
%Setting the above vectors into 2 matrices.
w(:,1)=w_hub; w(:,2)=w_center; w(:,3)=w_shroud;
k=[];
k(:,1)=k_hub([6 12 15 18 1]); k(:,2)=k_center([6 12 15 18 1]);
k(:,3)=k_shroud([6 12 15 18 1]);

%Radius of sensors location
r = [0.24042 0.15734 0.12164 0.08695 0.3109; 0.2506 0.1849 0.1581 ...
    0.1380 0.3108; 0.2629 0.2127 0.1947 0.1827 0.3108];
r=r';

%delta_n is the nearest distance from the sensor to blade surfaces.
 Also
%the blade thicknes is subtracted, as can be seen below.
delta_n=[0.04-0.0068, 0.02336-0.00565, 0.03-0.00436,0.02-0.00314
 0.0581;...
    0.038-0.0068, 0.0191-0.00525, 0.0232-0.00382,0.0117-0.0026
 0.0581;...
    0.039-0.0068, 0.0136-0.00485,0.0214-0.00337,0.0101-0.00235
 0.0581]./2;
delta_n=delta_n';

%Calculating the dw/dn value. And then calculating the relative
 valocity on
%the suction side surface and pressure side surface.
dwdn = -2*omega - (w1*w(sensor,loc))/k(sensor,loc);
w_pressure = w1*w(sensor,loc)+delta_n(sensor,loc)*dwdn;
w_suction = w1*w(sensor,loc)-delta_n(sensor,loc)*dwdn;

%Calculating the Rothalpi value at the sensor location. I is constant
 along
%and perpendicular to a streamline, and by rearanging the eqution, the
%pressure at the suciton and pressure side can be calculated.
I = P/rho+((w1*w(sensor,loc))^2)/2-((omega*r(sensor,loc))^2)/2;
P_pside=((I-(w_pressure^2)/2+((omega*r(sensor,loc))^2)/2)*rho)/1000;
P_sside=((I-(w_suction^2)/2+((omega*r(sensor,loc))^2)/2)*rho)/1000;
end
```

Published with MATLAB® R2017a

Appendix C

Start up, shut down and measurements procedure

This section describes the procedure for start up, measurements and shut down for the Francis rig at NTNU. Details are excluded, and only the main part is described.

Start Up

1. Turn on the computer connected to the measurement system, and check that all sensors are working.
2. Turn on the hydraulic and its cooling water. Check that the pressure gauges is set at the correct value. (Oil temperature should be constant when measuring).
3. Turn on the frequency converter in the pump room.
4. Check the open channel and the top of the building to see that the channel in clean.
5. Turn on the fans in the laboratory.
6. Control the valves in the PLS system, and check additional valves in the laboratory, so that the correct valves are closed, and that water can flow through the turbine and back into the basement reservoir.
7. Check that the valve in top of the upstream pressure tank is open, and start to fill the rig with water by starting the pump and increasing the pump speed.
8. When the water level have reach the upper level in the upstream pressure tank, close the valve in top of it.
9. Continue to increase the pump speed until the water flows through the open channel. There should be overflow as well to ensure steady water level.
10. Open the guide vanes slowly, and when the runner have accelerated to 333 rpm, start the generator. Make sure that setpoint torque is minimum set to 1000, and the the setpoint speed is set to 333 rpm. When the generator is

started, the guide vane can be opened to 10 degrees, so that the downstream pressure tank fills up faster.

11. When the rig is filled with water, bleed the system from air.

12. Reduce the guide vane opening to below 1 degree, and shut down the generator and close the inlet valve. Bleed the draft tube pressure sensors.

13. Turn the turbine on again, and bleed the system one more time before starting measurement.

Measurement

Measurement were done for 269 different points, for guide vane opening of 1 degree to 14 degrees with an increment of 1 degree. This procedure describes how it was done for one guide vane opening. The same procedure was applied for all other opening as well. Torque control were used to increase stability at each operation condition.

1. Set guide vane opening to correct position, and change speed to a value below $N_{ED} = 0.08$.

2. Reduce the setpoint torque until N_{ED} reaches 0.08.

3. Wait until the system has become stable and record the operation point for 60 seconds.

4. Reduce setpoint torque until reaching $N_{ED} = 0.09$ and wait until the system i stable before recording.

5. Repeat with an increment of $N_{ED} = 0.01$ until the mechanical torque is approaching zero.

6. When the torque is all most zero, turn of the generator and the runner goes to run-away speed. Wait for it to stable, and record the last point for this guide vane opening.

7. Increase the setpoint torque to 1000, and adjust the setpoint speed to 333rpm. Change the guide vane opening to reduce the runner speed until reaching 333rpm, and turn on the generator again. Repeat for another guide-vane opening.

Shut Down

1. Turn of the generator and close guide vanes. Close the inlet valve.
2. Open the valve between the upstream pressure tank and the pump outlet. And reduce the pump speed.
3. Keep reducing the pump speed until the water level have reach the upper level in the upstream tank and open the valve in top of the pressure tank.
4. Reduce the pump speed further before turning off the pump.
5. Open the two valves in the downstream pressure tank to empty the water into the basement reservoir.
6. When the system is emptied, turn of the hydraulic and cooling water, turn of the frequency converter in the pump room and turn of the fans in the laboratory.
7. Take a last check in the laboratory to see that everything looks as it should.

Appendix D

Pressure Pulsation Diagram and Frequency analysis

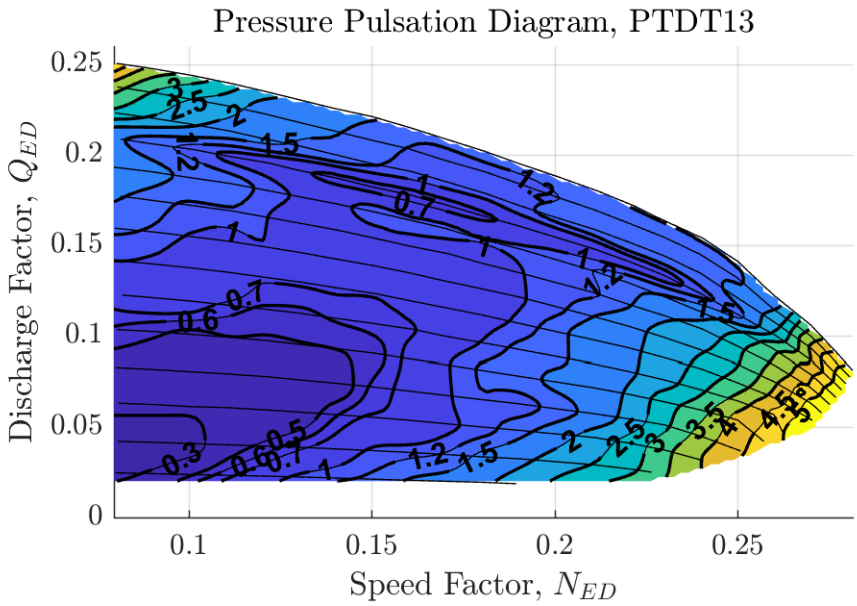

Figure D.1: Peak-peak values are normalized based on BEP value (2.39kPa)

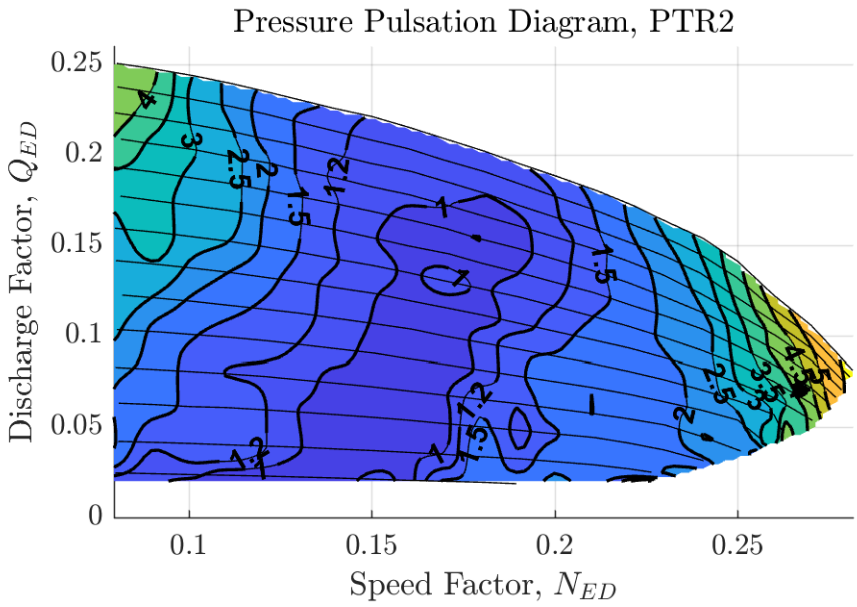

Figure D.2: Peak-peak values are normalized based on BEP value (3.04kPa)

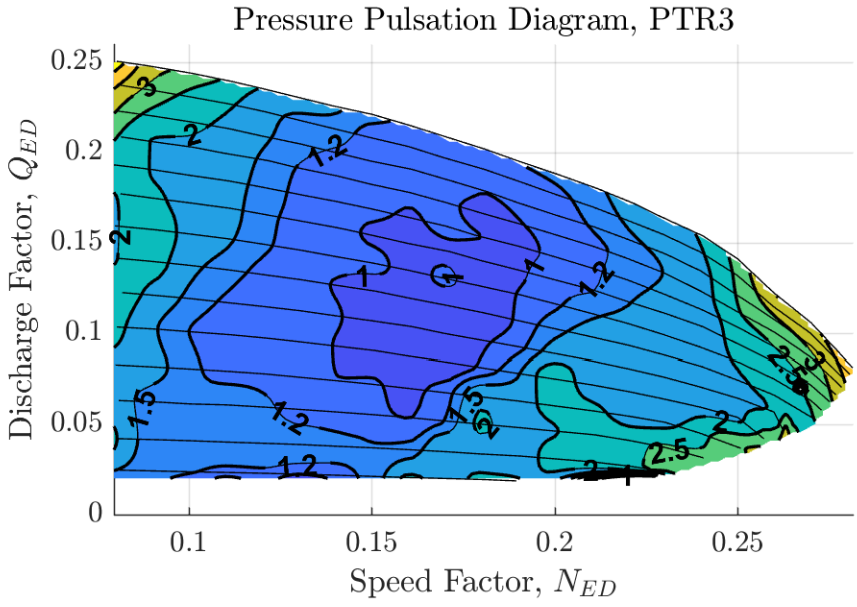

Figure D.3: Peak-peak values are normalized based on BEP value (2.39kPa)

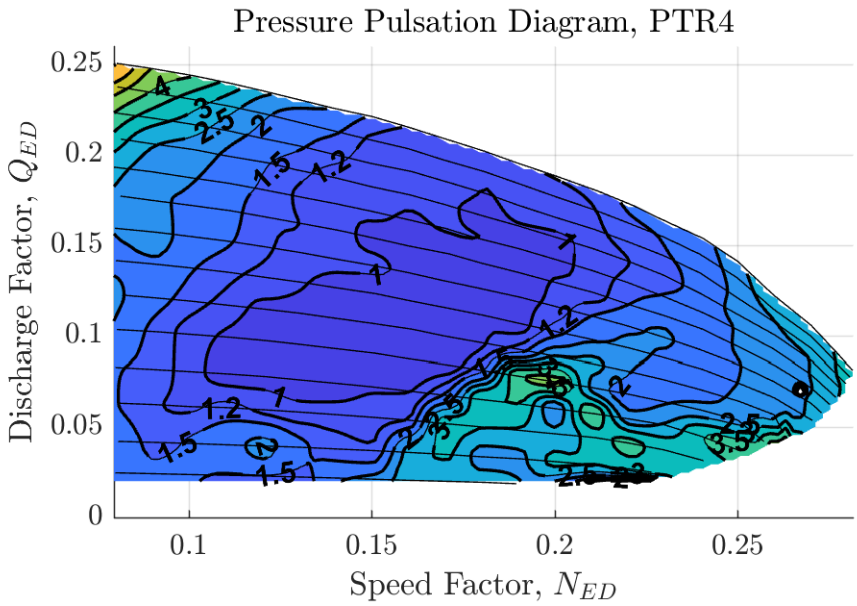

Figure D.4: Peak-peak values are normalized based on BEP value (1.67kPa)

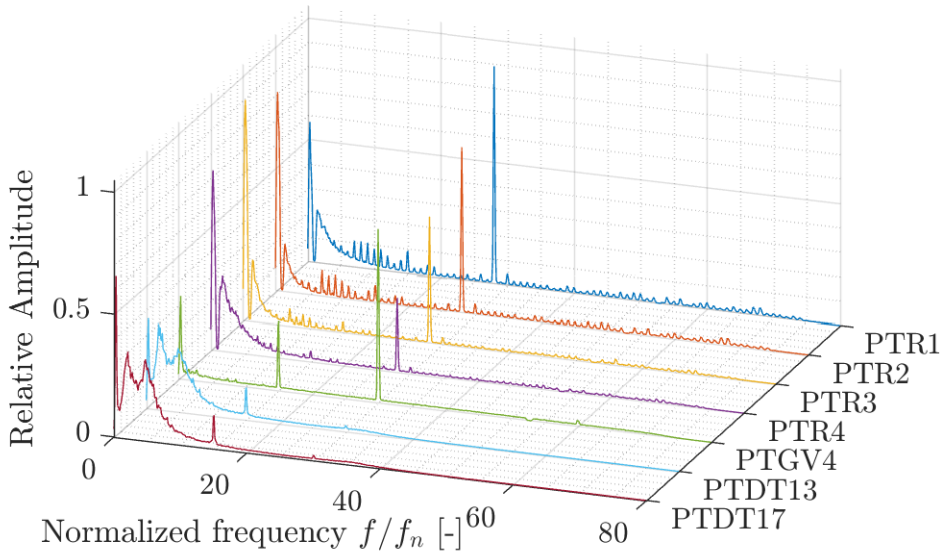

Figure D.5: Frequency analysis for SNL operation point. Frequency is normalized based on the runner frequency.

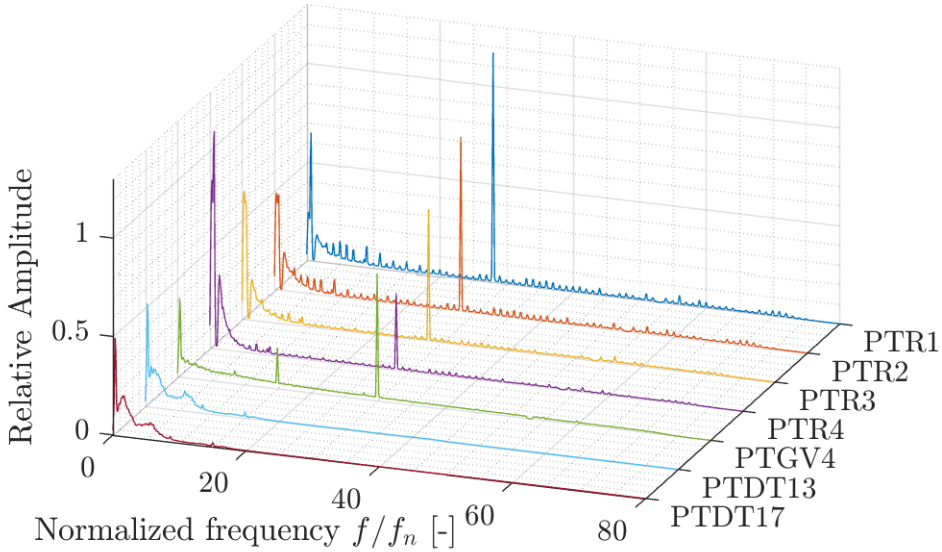

Figure D.6: Frequency analysis for ML operation point. Frequency is normalized based on the runner frequency.

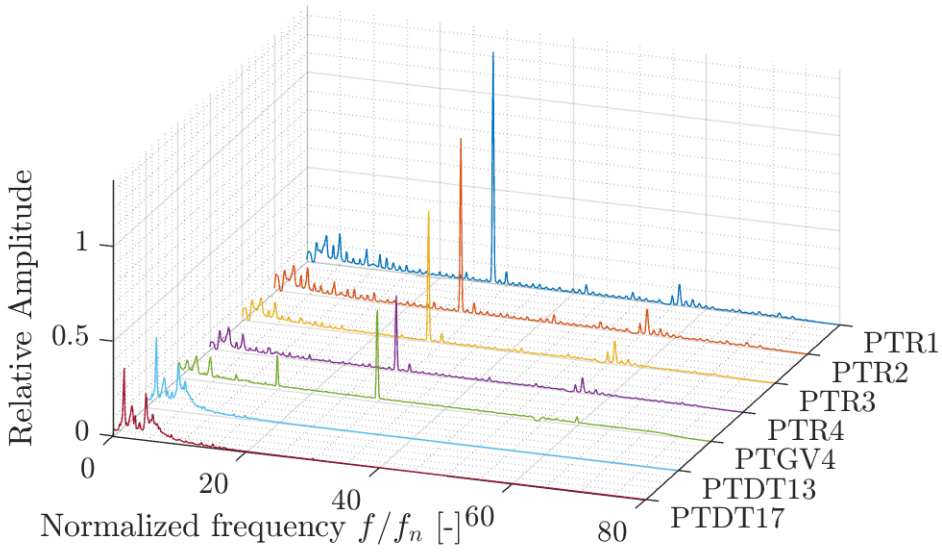

Figure D.7: Frequency analysis for BEP operation point. Frequency is normalized based on the runner frequency.

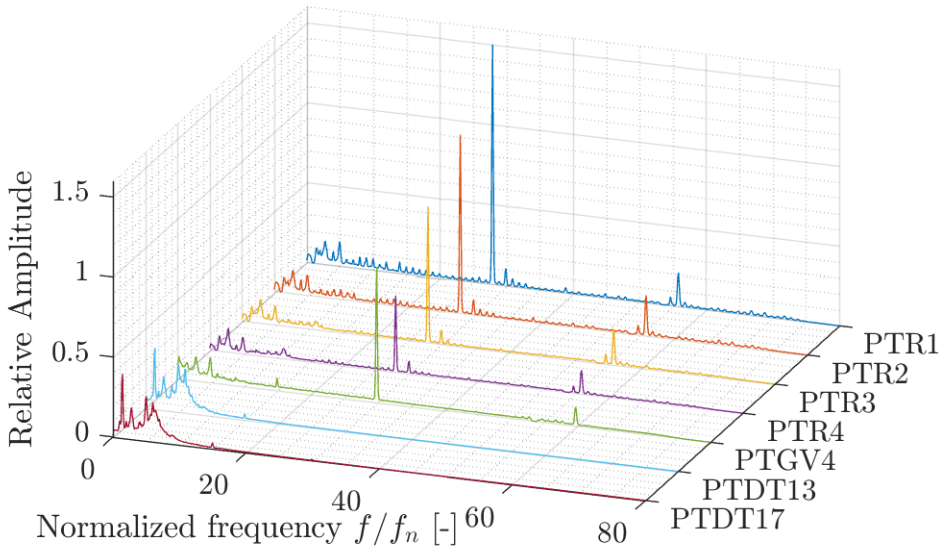

Figure D.8: Frequency analysis for FL operation point. Frequency is normalized based on the runner frequency.

Appendix E

MatLab scripts for calculation

The MatLab code for creating the the Hill Chart and the Pressure Pulsations diagram is attached first. Second is the code for frequency analysis of the pressure signal. Third is the code for calculating the peak-peak values with the histogram method.

```
%HillChart and Pressure Pulsation Diagram
%Can choose which you want to display

%load('hillChart.mat')  %Loading a structure with operation point
 values
Ned = hillChart.Ned;
Qed = hillChart.Qed;
eta = hillChart.eta;
Head = hillChart.Head;
Pm = hillChart.P_mech./1000;
rpm = hillChart.RPM;

%load('peakData.mat')  %Loading a structure with peak-peak values
%calculated with the Histogram method
fPTR2 = peakData.fPTR2;
fPTGV4 = peakData.fPTGV4;
fPTDT13 = peakData.fPTDT13;
fPTDT17 = peakData.fPTDT17;
fPTR1 = peakData.fPTR1;
fPTR3 = peakData.fPTR3;
fPTR4 = peakData.fPTR4;
fPTSC1 = peakData.fPTSC1;

peak = fPTR4;  %choose which pressure diagram you want to display

%Alpha values, guide vane opening
LINESPEC=cellstr(['-k+'; '-ko'; '-k*'; '-k.'; '-kx'; '-kh'; '-kd';...
 '-k^'; '-kv'; '-k<'; '-k>'; '-kp'; '-kh'; '-ks';]);
fontSizeLabel=11; fontSizeAxes=11; fontweight='bold';

%BEP
[eta_bep,I]=max(eta(:));
Ned_bep = Ned(I);
Qed_bep = Qed(I);

%figure(1)
%hold on
%grid on;
%textPosition=[0.232 91.7];
%text(textPosition(1),textPosition(2)-0.04,
 ['Qed*=',num2str(Qed_bep)],...
% 'fontSize',fontSizeLabel, 'fontWeight', fontweight);
%text(textPosition(1),textPosition(2)-0.05,['Ned*=',
 num2str(Ned_bep)],...
%  'fontSize' , fontSizeLabel, 'fontWeight', fontweight);
% xlabel('Ned', 'fontSize' , fontSizeLabel ) ; ylabel(' Qed', ...
%  'fontSize' , fontSizeLabel);
% legend('\alpha=1', '\alpha=2' , '\alpha=3', '\alpha=4',
 '\alpha=5',...
%  '\alpha=6' , '\alpha=7', '\alpha=8' ,'\alpha=9', '\alpha=10',
 '\alpha=11',...
%  'alpha=12', 'alpha=13', 'alpha=14', 'Location', 'NorthEast');
```

```
% legend('boxoff');
% axis([0.0796 0.2814 0 0.26 ])

numb=100; % Number of point that should be interpolated
x=linspace(0.0796,0.2814,numb); %creating a x-vector for interpolation

%Interpolates new Q_ed
q(:,1)=interp1(Ned(1:12),Qed(1:12),x,'PCHIP','extrap');
q(:,2)=interp1(Ned(13:28),Qed(13:28),x,'PCHIP','extrap');
q(:,3)=interp1(Ned(29:45),Qed(29:45),x,'PCHIP','extrap');
q(:,4)=interp1(Ned(46:63),Qed(46:63),x,'PCHIP','extrap');
q(:,5)=interp1(Ned(64:82),Qed(64:82),x,'PCHIP','extrap');
q(:,6)=interp1(Ned(83:102),Qed(83:102),x,'PCHIP','extrap');
q(:,7)=interp1(Ned(103:122),Qed(103:122),x,'PCHIP','extrap');
q(:,8)=interp1(Ned(123:143),Qed(123:143),x,'PCHIP','extrap');
q(:,9)=interp1(Ned(144:164),Qed(144:164),x,'PCHIP','extrap');
q(:,10)=interp1(Ned(165:185),Qed(165:185),x,'PCHIP','extrap');
q(:,11)=interp1(Ned(186:206),Qed(186:206),x,'PCHIP','extrap');
q(:,12)=interp1(Ned(207:227),Qed(207:227),x,'PCHIP','extrap');
q(:,13)=interp1(Ned(228:248),Qed(228:248),x,'PCHIP','extrap');
q(:,14)=interp1(Ned(249:269),Qed(249:269),x,'PCHIP','extrap');

%Interpolates new Efficiency
e(:,1)=interp1(Ned(1:12),eta(1:12),x,'PCHIP','extrap');
e(:,2)=interp1(Ned(13:28),eta(13:28),x,'PCHIP','extrap');
e(:,3)=interp1(Ned(29:45),eta(29:45),x,'PCHIP','extrap');
e(:,4)=interp1(Ned(46:63),eta(46:63),x,'PCHIP','extrap');
e(:,5)=interp1(Ned(64:82),eta(64:82),x,'PCHIP','extrap');
e(:,6)=interp1(Ned(83:102),eta(83:102),x,'PCHIP','extrap');
e(:,7)=interp1(Ned(103:122),eta(103:122),x,'PCHIP','extrap');
e(:,8)=interp1(Ned(123:143),eta(123:143),x,'PCHIP','extrap');
e(:,9)=interp1(Ned(144:164),eta(144:164),x,'PCHIP','extrap');
e(:,10)=interp1(Ned(165:185),eta(165:185),x,'PCHIP','extrap');
e(:,11)=interp1(Ned(186:206),eta(186:206),x,'PCHIP','extrap');
e(:,12)=interp1(Ned(207:227),eta(207:227),x,'PCHIP','extrap');
e(:,13)=interp1(Ned(228:248),eta(228:248),x,'PCHIP','extrap');
e(:,14)=interp1(Ned(249:269),eta(249:269),x,'PCHIP','extrap');

%Interpolates between power-output
p(:,1)=interp1(Ned(1:12),Pm(1:12),x,'PCHIP','extrap');
p(:,2)=interp1(Ned(13:28),Pm(13:28),x,'PCHIP','extrap');
p(:,3)=interp1(Ned(29:45),Pm(29:45),x,'PCHIP','extrap');
p(:,4)=interp1(Ned(46:63),Pm(46:63),x,'PCHIP','extrap');
p(:,5)=interp1(Ned(64:82),Pm(64:82),x,'PCHIP','extrap');
p(:,6)=interp1(Ned(83:102),Pm(83:102),x,'PCHIP','extrap');
p(:,7)=interp1(Ned(103:122),Pm(103:122),x,'PCHIP','extrap');
p(:,8)=interp1(Ned(123:143),Pm(123:143),x,'PCHIP','extrap');
p(:,9)=interp1(Ned(144:164),Pm(144:164),x,'PCHIP','extrap');
p(:,10)=interp1(Ned(165:185),Pm(165:185),x,'PCHIP','extrap');
p(:,11)=interp1(Ned(186:206),Pm(186:206),x,'PCHIP','extrap');
p(:,12)=interp1(Ned(207:227),Pm(207:227),x,'PCHIP','extrap');
p(:,13)=interp1(Ned(228:248),Pm(228:248),x,'PCHIP','extrap');
p(:,14)=interp1(Ned(249:269),Pm(249:269),x,'PCHIP','extrap');
```

```
%Interpolate between peak-peak values
Peak(:,1)=interp1(Ned(1:12),peak(1:12),x,'PCHIP','extrap');
Peak(:,2)=interp1(Ned(13:28),peak(13:28),x,'PCHIP','extrap');
Peak(:,3)=interp1(Ned(29:45),peak(29:45),x,'PCHIP','extrap');
Peak(:,4)=interp1(Ned(46:63),peak(46:63),x,'PCHIP','extrap');
Peak(:,5)=interp1(Ned(64:82),peak(64:82),x,'PCHIP','extrap');
Peak(:,6)=interp1(Ned(83:102),peak(83:102),x,'PCHIP','extrap');
Peak(:,7)=interp1(Ned(103:122),peak(103:122),x,'PCHIP','extrap');
Peak(:,8)=interp1(Ned(123:143),peak(123:143),x,'PCHIP','extrap');
Peak(:,9)=interp1(Ned(144:164),peak(144:164),x,'PCHIP','extrap');
Peak(:,10)=interp1(Ned(165:185),peak(165:185),x,'PCHIP','extrap');
Peak(:,11)=interp1(Ned(186:206),peak(186:206),x,'PCHIP','extrap');
Peak(:,12)=interp1(Ned(207:227),peak(207:227),x,'PCHIP','extrap');
Peak(:,13)=interp1(Ned(228:248),peak(228:248),x,'PCHIP','extrap');
Peak(:,14)=interp1(Ned(249:269),peak(249:269),x,'PCHIP','extrap');

%Interpolate between speed
Rpm(:,1)=interp1(Ned(1:12),rpm(1:12),x,'PCHIP','extrap');
Rpm(:,2)=interp1(Ned(13:28),rpm(13:28),x,'PCHIP','extrap');
Rpm(:,3)=interp1(Ned(29:45),rpm(29:45),x,'PCHIP','extrap');
Rpm(:,4)=interp1(Ned(46:63),rpm(46:63),x,'PCHIP','extrap');
Rpm(:,5)=interp1(Ned(64:82),rpm(64:82),x,'PCHIP','extrap');
Rpm(:,6)=interp1(Ned(83:102),rpm(83:102),x,'PCHIP','extrap');
Rpm(:,7)=interp1(Ned(103:122),rpm(103:122),x,'PCHIP','extrap');
Rpm(:,8)=interp1(Ned(123:143),rpm(123:143),x,'PCHIP','extrap');
Rpm(:,9)=interp1(Ned(144:164),rpm(144:164),x,'PCHIP','extrap');
Rpm(:,10)=interp1(Ned(165:185),rpm(165:185),x,'PCHIP','extrap');
Rpm(:,11)=interp1(Ned(186:206),rpm(186:206),x,'PCHIP','extrap');
Rpm(:,12)=interp1(Ned(207:227),rpm(207:227),x,'PCHIP','extrap');
Rpm(:,13)=interp1(Ned(228:248),rpm(228:248),x,'PCHIP','extrap');
Rpm(:,14)=interp1(Ned(249:269),rpm(249:269),x,'PCHIP','extrap');

%Creating a new matrix with interpolated N_ed, Q_ed, Efficiency, Power
%output, Peak-peak values and speed values that can be used to create
 the
%hill chart with counter-plot
N=zeros(numb,numb); Q=N; E=N;
for t=1:numb
    N(:,t)=x;
    Q(t,:)=linspace(0.25,0.02,numb);
    E(t,:)=interp1(q(t,:),e(t,:),Q(t,:),'PCHIP','extrap');
    P(t,:)=interp1(q(t,:),p(t,:),Q(t,:),'PCHIP','extrap');
    PEAK(t,:)=interp1(q(t,:),Peak(t,:),Q(t,:),'PCHIP','extrap');
    RPM(t,:)=interp1(q(t,:),Rpm(t,:),Q(t,:),'PCHIP','extrap');
end

%Remove invalid extrapolated data.
vec(1:12)=Ned(1:12); vec(13)=Ned(28); vec(14)=Ned(45);
 vec(15)=Ned(63); vec(16)=Ned(82);
vec(17)=Ned(102); vec(18)=Ned(122); vec(19)=Ned(143);
 vec(20)=Ned(164); vec(21)=Ned(185);
vec(22)=Ned(206); vec(23)=Ned(227); vec(24)=Ned(248);
 vec(25)=Ned(269);
```

```
vec2(1:12)=Qed(1:12); vec2(13)=Qed(28); vec2(14)=Qed(45);
 vec2(15)=Qed(63); vec2(16)=Qed(82);
vec2(17)=Qed(102); vec2(18)=Qed(122); vec2(19)=Qed(143);
 vec2(20)=Qed(164); vec2(21)=Qed(185);
vec2(22)=Qed(206); vec2(23)=Qed(227); vec2(24)=Qed(248);
 vec2(25)=Qed(269);
underline = interp1(vec,vec2,x,'PCHIP','extrap');
for o=1:numb
    for k=1:numb
        if Q(k,o) > q(k,14)
        E(k,o) = NaN;
        P(k,o) = NaN;
        PEAK(k,o) = NaN;
        RPM(k,o) = NaN;
        elseif Q(k,o) < underline(k)-0.005
            E(k,o) = NaN;
            P(k,o) = NaN;
            PEAK(k,o) = NaN;
            RPM(k,o) = NaN;
        end
        end
end
PEAK = PEAK./PEAK(50,42); %Normalize peak-peak values based on BEP
 value

%Choose witch constant-value-lines to display.
%Change for each diagram to get a best fit.
powerLines=[9 15.9 22.2 25.44 28]; %kPa
efficiencies=[92.2 92 91 90 88 86 84 80 70 60 50 40 20 7]/100;
peakpeakVal=[0.1 0.3 0.5 0.6 0.7 1  1.2  1.5  2 2.5 3 3.5 3 4 4.5 5 6
 7 8 9];

%Creating a contourf plot for pressure pulsation diagram
%contourf(N, Q, PEAK, peakpeakVal);

%Creating contour lines of constant power-values
%[CC,hh]=contour(N, Q, P ,powerLines);
%set(hh,'LineStyle','-','LineColor','k')
%clabel(CC, hh,'fontSize' , fontSizeLabel,'fontWeight', fontweight)

%Creating contour lines of constant peak-peak values);
% set(jj,'LineStyle','-','LineColor','k','LineWidth',1.2)
% clabel(PP, jj,'fontSize' , fontSizeLabel,'fontWeight', fontweight)

%Creating contour lines for the Hill Chart
%  [C,h]=contour(N, Q, E ,efficiencies);
%  set(h,'LineStyle','-','LineColor','k','LineWidth',1.5)
%  clabel(C, h,'fontSize' , fontSizeLabel,'fontWeight', fontweight)
%  plot(Ned_bep,Qed_bep,'*r')

%Plots lines of constant guide-vane opening
% plot(Ned(1:12),Qed(1:12),'-k');      % GV 1 deg
% plot(Ned(13:28),Qed(13:28),'-k')      % GV 2 deg
% plot(Ned(29:45),Qed(29:45),'-k')      % GV 3 deg
```

```
% plot(Ned(46:63),Qed(46:63),'-k')      % GV 4 deg
% plot(Ned(64:82),Qed(64:82),'-k')      % GV 5 deg
% plot(Ned(83:102),Qed(83:102),'-k')    % GV 6 deg
% plot(Ned(103:122),Qed(103:122),'-k')  % GV 7 deg
% plot(Ned(123:143),Qed(123:143),'-k')  % GV 8 deg
% plot(Ned(144:164),Qed(144:164),'-k')  % GV 9 deg
% plot(Ned(165:185),Qed(165:185),'-k') % GV 10 deg
% plot(Ned(186:206),Qed(186:206),'-k') % GV 11 deg
% plot(Ned(207:227),Qed(207:227),'-k') % GV 12 deg
% plot(Ned(228:248),Qed(228:248),'-k') % GV 13 deg
% plot(Ned(249:269),Qed(249:269),'-k') % GV 14 deg
```

Published with MATLAB® R2017a

```
%frequency analysis;

numb = 175; %11=SNL, 56=ML, 113=PL, 175=BEP, 217=HL, 259=FL

%Removing mean values from pressure data.
%pressureData. is a struc with all the filtered pressure data
p = zeros(60*10240,7);
p(:,1) = detrend(pressureData.fPTR1(numb,:));
p(:,2) = detrend(pressureData.fPTR2(numb,:));
p(:,3) = detrend(pressureData.fPTR3(numb,:));
p(:,4) = detrend(pressureData.fPTR4(numb,:));
p(:,5) = detrend(pressureData.fPTGV4(numb,:));
p(:,6) = detrend(pressureData.fPTDT13(numb,:));
p(:,7) = detrend(pressureData.fPTDT17(numb,:));
%p(:,8) = detrend(hillChart.PTSC1(numb,:));

pxx = zeros(801,7); f = pxx;
for i = 1:7
    [pxx(:,i), f(:,i)]=quickFFT(p(:,i),10240,1,500, 0); %welch method
    fn(:,i)=f(:,i)./(hillChart.RPM(numb)./60); %normalize speed.
   figure(1)
   hold on
   grid on
   plot3(i.*ones(1,801),fn(:,i),pxx(:,i)) %plotting the freq plot
end
legend('1=PTR1','2=PTR2','3=PTR3','4=PTR4','5=PTGV4','6=PTDT13','7=PTDT17','Locati
set(gca,'TickLabelInterpreter','latex')
xlabel('Sensor','interpreter','latex')
ylabel('Reduced frequency $f_n$ [Hz]','interpreter','latex')
zlabel('Relative Amplitude','interpreter','latex')
set(gca, 'Fontsize', 11)
set(gcf, 'Units', 'centimeters', 'Position', [1, 2, 12.6, 8])
grid minor
axis([1 7 0 80 0 2.5])
legend('boxoff')
view([110,25])
%print(gcf, ('Figures\ppPT.png'), '-dpng', '-r200' );

%quickFFT function, is a function that uses MatLabs pwelch built-in
%function to calculate the frequency spectrum.
function [pxxnew, Fnew] =
 quickFFT(DePTX1,Fs,f_res,max_freq,numberofwindow)
if numberofwindow == 1  %Option to get one Hann-window for the whole
 series
L = length(DePTX1);
H=hann(L);
overlap=0;
nfft=L;
else
N=Fs/f_res;
nfft = 2^nextpow2(N);
fres = Fs/nfft;
```

```
H = hann(nfft);
overlap = floor(nfft/2); %50percent overlap
end
[pxx1, F] = pwelch(DePTX1,H,overlap,nfft,Fs,'power'); %power spectrum
pxx = sqrt(2)*sqrt(pxx1); %normalizing the signal

for i=1:length(F)
    if F(i)>=max_freq  %max freq intersted in
        break;
    end
end
Fnew = F(1:i);
pxxnew = pxx(1:i);
end
```

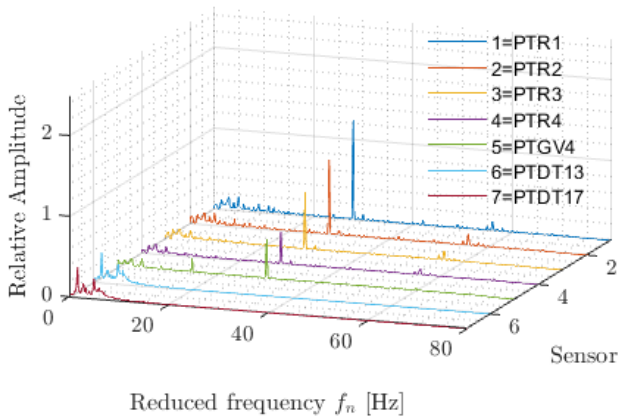

Published with MATLAB® R2017a

```
numb=175; %Choose which operation point you want
dataset = pressureData.fPTR1(numb,:); %Choose which sensor
level=0.97; % Confidence level of 97%
plotting=0; %0=no plots, 1=histogram plot + pressure-time plot with
 limits

[lower, upper]=cpf(dataset,level,plotting); %Running the funtion

%The function gives out an upper and lower limit. The differences in
 these
%two values are the peak-peak value
function [lower,upper] = cpf(dataset,level,plotting)
[N,e] = histcounts(dataset,1000);
        Me = mean(dataset);
        NumberOfPoints = sum(N);

            temp=0;
        for i = 1:length(N)
            temp = temp+N(i);  value = temp/NumberOfPoints;
            if value >= (1-level)/2
                lower = e(i);
                break;
            end
        end
            temp=0;
        for j = 1:length(N)
            temp = temp+N(j);  value = temp/NumberOfPoints;
            if value >= level+(1-level)/2
                upper = e(j);
                break;
            end
        end
        if plotting == 1
            time = [0:1/10240:60-1/10240];
            figure(1)
            plot(time,dataset,'b');  hold on
            plot([0, 60-1/10240],[lower, lower],'r','LineWidth',1.5)
            plot([0, 60-1/10240],[upper, upper],'r','LineWidth',1.5)
            hold off
            figure(2)
            hist(dataset,1000);  hold on
            plot([lower, lower],[0, max(N)],'r','LineWidth',1.5)
            plot([upper, upper], [0, max(N)],'r','LineWidth',1.5)
            hold off
        end
end
```

Published with MATLAB® R2017a